The Horizontal Pre-Support in Tunnels

by

Shu-Sheng Chen

B.S. Civil and Environmental Engineering
National Central University, Taiwan, 1991

Submitted to the
Department of Civil and Environmental Engineering
in Partial Fulfillment of the Requirements
for the Degree of

Master of Science
in Civil and Environmental Engineering
at the

Massachusetts Institute of Technology

May 1995

Signature of Author_____
Department of Civil and Environmental Engineering
May 12, 1995

Certified by_____
H. H. Einstein
Thesis Supervisor

Accepted by_____
Joseph M. Sussman
Chairman, Departmental Committee on Graduate Studies

THE HORIZONTAL PRE-SUPPORT IN TUNNELS

by

Shu-Sheng Chen (Tony)

Submitted to the Department of Civil and Environmental Engineering
May 12, 1995 in partial fulfillment of the requirement for the Degree
of Master of Science in Civil and Environmental Engineering

ABSTRACT

This thesis provides a theoretical and analytical framework regarding the arching effects of tunnels. It gives a new explanation for the development of arching, develops a new method to estimate the area of yield zones, and introduces a new technique of using triangular pre-support tubes to reduce the ground surface settlement.

The approach that the author employs consists of two parts. First, by analyzing in detail the past empirical results and analytical frameworks, different stages of arching are obtained. The soil has maximum strength when the triangular prism just forms. The triangular prism transforms into a combination of two triangular prisms later with increasing trapdoor downward movement. The different stages of the triangular prism are then examined with the Mohr Failure Envelope and the Mohr-Coulomb Failure Envelope.

Second, based on the observed results of crack formation (Heuer and Hendron, 1971), there could be an inward movement of triangular failed wedges appearing around the springline during the last stages of failure. By incoporating this result and the theory of triangular prisms, the author presents a new method of estimating the yield zones of maximum soil strength for circular and triangular tubes. It should be noted that this method is somewhat conservative because inward moving triangular wedges are assumed to have formed.

Finally, a comparison between the traditional circular pre-support tubes and triangular pre-support tubes is made using both Peck's Error Curve and the finite element analysis.

Thesis Supervisor: Herbert H. Einstein

Title: Professor, Department of Civil and Environmental Engineering

Acknowledgments

My thesis gratitude is hereby expressed to the following people who have helped bring this thesis into function:

* Professor Herbert H. Einstein, for his intellectual insights and consistent encouragement throughout the writing of this thesis. Without his support and help, the thesis would not have come into being. Therefore, I owe my greatest thanks to him.

* Professor Charles C. Ladd and Professor Robert V. Whitman for their wonderful classes and patient instructions, which laid a solid foundation for this paper.

* My classmates - Boonchi Ukritchon (Lek), Twarath Sutabutr (John), and Achilles Papadimitriou for their support and help during my first year of graduate study at M.I.T. Especially, I thank Lek for his enthusiastic, great friendship; I give him and John my best wishes for their future study at M.I.T.

* My senior consultants - Shun-Ming Lee for his help on the application of the Finite Element Method (FEM), Patrick G Kinnicutt for his help in correcting my thesis, Samir Chauhan, and Dante Legaspi for their help in answering many challenging questions.

* Ms. Mary, our dear administrative assistant of Geotechnics group,.for her lovely and friendly correction of my oral English, and for always giving me new energy by making the freshest coffee.

* Mr. Hsien-Jen Tien and Ms. Lucy Jen for their patience in teaching me how to get used to M.I.T. Marika Santagata, Mike Geer, and Mike Whelan, for making my daily life more colorful.

* Rebecca W. Xiang for her taking a lot of time to teach me how to run a computer. She was the real T.A. for the C language class. Without her, the programming would have been much harder for me.

* Kathy Wenyun Liu, who is a big helper and sometimes a big trouble maker, for the lovely moments I spent with her. We sat through numerous nights in front of the computer, supported and carried each other through the challenges of M.I.T.

* My parents, who always stand by my side, and whose love and support gave me the courage to complete the rigorous graduate program at M.I.T. I hope I did not disappoint them.

TABLE OF CONTENTS

LIST OF FIGURES

LIST OF TABLES

Chapter 1. INTRODUCTION

1.1 The General Behavior of Arching

Arching can be defined as the transfer of stresses over a buried structure due to differences in the deformation properties of the structure and the soil (Einstein, et.al., 1980). Active arching results in the reduction of load on the underground structural support, which is like the trap door in a trap door test, and often occurs either when the structure is more compressible, or when it is the opening of the tunnel. In a simple elastic soil model, the basic ideas of active arching are presented in Figures 1-1 (a), (b), (c), (d), which consecutively show that the stress distribution for structure and surrounding soil when the structure is more compressible than the surrounding soil (active arching).

Passive arching, however, will increase the load on the underground structural support, and is frequently found when the structure is less compressible than the surrounding soil. Cut-and-cover underground structures are often good examples of passive arching. Figures 1-2 (a), (b), (c), (d) consecutively show that the stress distribution for structure and surrounding soil when the structure is more compressive than the soil (passive arching).

In the trapdoor test, a few general phenomena can be observed when a symmetric condition is concerned. In active arching, the vertical stresses on the trap door are reduced after the trapdoor is moved downward. In Figure 1-3, which presents the general behavior during active arching, Evans (1983) showed that a triangular zone above the door expands vertically with noticeable dilation, while there is also some lateral contraction, which is largely compensated for by the dilation. Those areas of soil on either side of the trapdoor act like abutments, receiving the stresses transferred from the load above the trapdoor; these areas undergo vertical contraction with some lateral expansion toward the door, and the major principal stress is vertical. However, his measurement of the vertical and horizontal stresses indicates that the major principal stresses directly above the door are approximately horizontal (see Figure 1-4).

Passive arching is shown in Figure 1-5. When the trap door moves upward, the vertical stresses increase on the trap door, and arching will also be mobilized. A trapezoidal prism of soil above the trap door moves upward with some vertical contraction and lateral expansion. This is

similar to the Rankine passive earth pressure zone, and the major principal stresses above the trapdoor are vertical. The areas of soil on either side of the trapdoor undergo horizontal contraction, and some vertical expansion; the major principal stress is vertical in theses areas (see Figure 1-6).

This thesis will focus primarily on active arching which is particularly important regarding surface displacement over shallow tunnels.

1.2 Objectives of Research

Ground surface settlement is the most important consideration in design and construction of a shallow tunnel, especially when the tunnel is built in modern cities.

Construction of a driven tunnel results in a changed state of stress in the surrounding soil. Since no soil material is perfectly rigid, construction must produce some strains and ground movement. Many papers have been written proving that most ground movements occurring around shallow soft ground tunnels are produced during construction. This doesn't mean that ground movement is definitely harmful to a tunnels. On the contrary, some deformation may be beneficial if the shear stress mobilized in the soils were to reduce the load on the lining.

Ground settlement can be reduced by using a steel rib or permanent concrete support around the surface of the opening; however, there could be large variations between settlements if different construction methods are used. For the horizontal pre-support of tunnels, circular tubes are one of the popular ways to reduce the surface settlement of shallow tunnels. Figure 1-7 shows the configuration of the circular pre-support tubes, which are used parallel to the longitudinal direction of the tunnel. In Milan, a so-called Cellular Arch Method has been developed. It is a composite structure of semicircular section similar to a framed structure, in which the longitudinal elements (cells) are represented by pipes in reinforced concrete rendered functional by a series of large transverse ribs (arches). This method can minimize the ground surface settlement for shallow tunnels (Lunardi, 1991).

The purpose of this thesis to present a method of decreasing the ground surface settlement by minimizing the deformation around the pre-supporting tubes, and by further exploring the development of arching. To simplify the research, uniform sand is the only soil material considered. Finally, a suggested design for the pre-supporting tubes is presented.

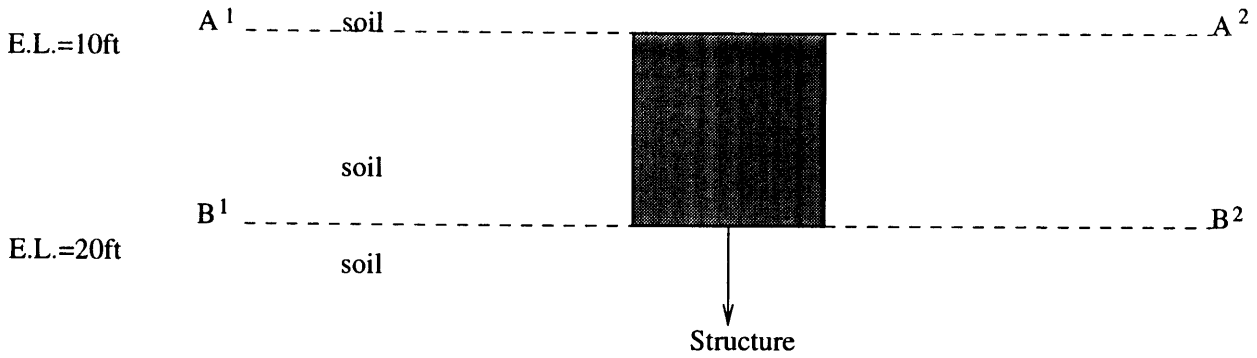

A. Structure within Soil Mass (No Force Present)

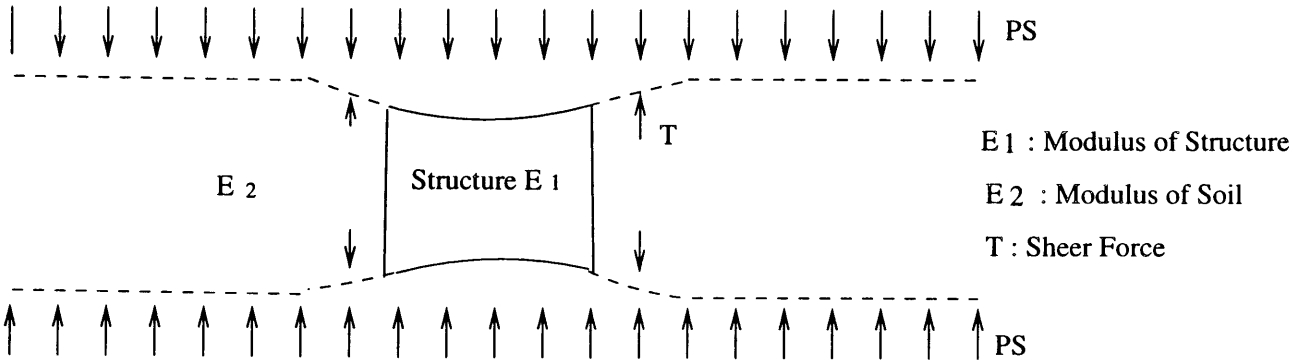

B. Displacement under Pressure PS When Structure
Is More Compressible than Surrounding Soil (E1<E2)

Figure 1-1 (a) Stress Distribution for a Structure and Surrounding Soil
(Active Arching)

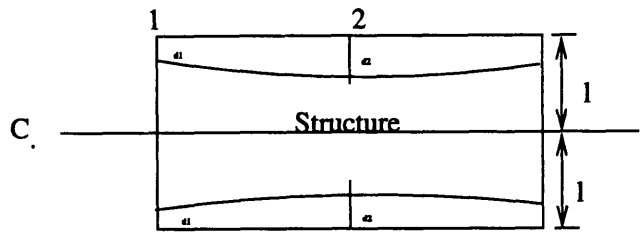

Assumptions:

1. 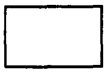 is the structure with no force present.

2.  is the structure when the pressure PS is present.

3. Both structure and soil are homogenous, elastic materials.

4. Due to the plane strain, $\sigma = E\ (\varepsilon 1 - \nu\, \varepsilon 2)$ where ν is the Poisson ratio

5. $\varepsilon_{x,y}$ where x is the point, and y is the axis.

$\sigma 1 - \sigma 2 = E(\varepsilon 11 - \nu\varepsilon 12) - E(\varepsilon 21 - \nu\, \varepsilon 22) = E(\varepsilon 11 - \varepsilon 21) =$ E(d1-d2) ,

Because & d1 < d2 therefore, $\sigma 1 < \sigma 2$

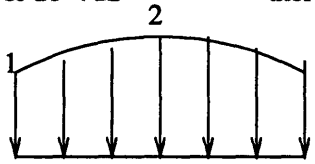

Stress Distribution

Figure 1-1 (b) Stress Distribution for Structure and Surrounding Soil (Active Arching)

D. For the soil on A1A2 and B1B2

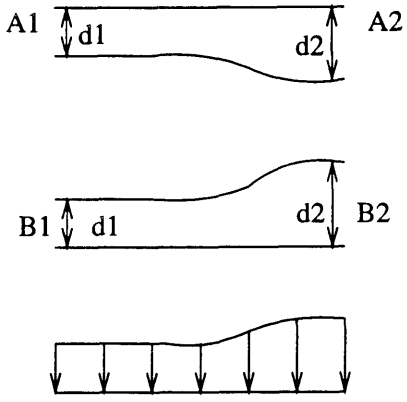

Normal Stress Distribution

Under the same assumptions and calculations as in Figure 1-1(a), we obtain:

$d2 > d1$, and

$\sigma 2 > \sigma 1$

E. Compare soil and structure.

$E2 > E1$

$\varepsilon_{soil} = \varepsilon_{structure}$,

therefore,

$\sigma_{soil} > \sigma_{structure}$

Figure 1-1 (c) Stress Distribution for Structure and Surrounding Soil (Active Arching)

From A, B, C, D, and E, we can draw following conclusions:

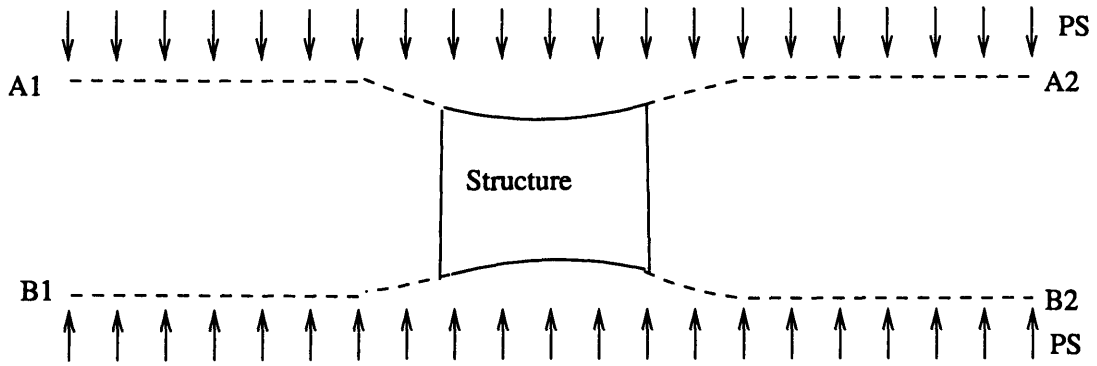

Displacement under Pressure PS When Structure
Is More Compressible than Surrounding Soil

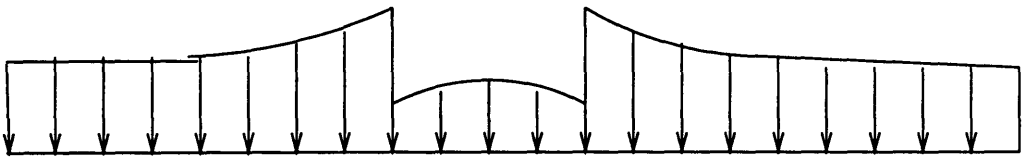

Normal Stress Distribution across Upper Curve Plane A1A2 or Lower Plane B1B2

Figure 1-1(d) Active Arching.

Figure 1-1 (d) Stress Distribution for Structure and Surrounding Soil
(Active Arching)

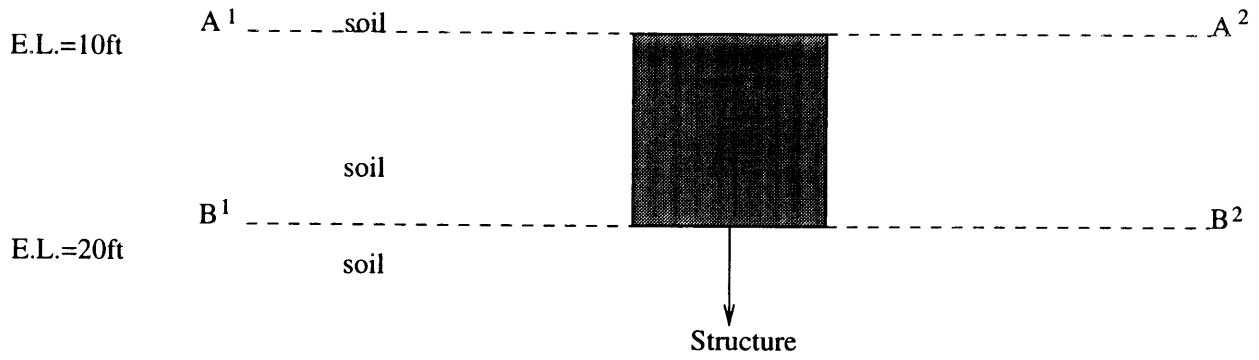

A. Structure within Soil Mass (No Force Present)

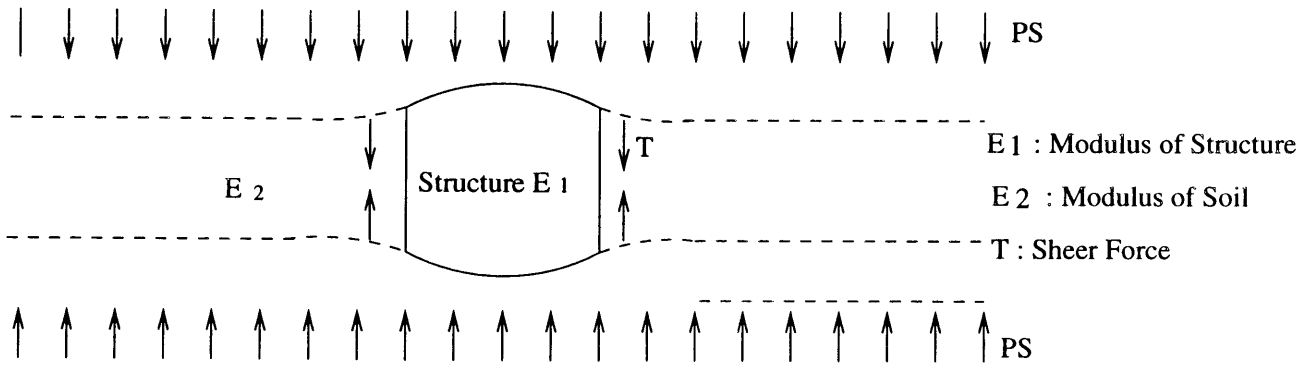

B. Displacement under Pressure PS When Structure
Is Less Compressible than Surrounding Soil (E1>E2)

Figure 1-2 (a) Stress Distribution for Structure and Surrounding Soil
(Passive Arching)

C.

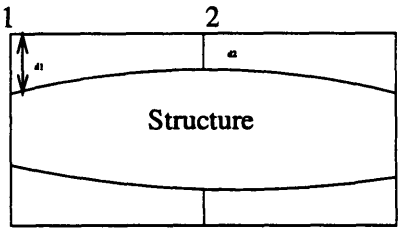

Assumptions:

1.  is the structure with no force present.

2. 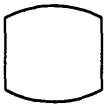 is the structure when the pressure PS is present.

3. Both structure and soil are homogenous, elastic materials.

4. Due to the plane strain, $\sigma = E(\varepsilon 1 - \nu\ \varepsilon 2)$ where ν is the Poisson ratio

5. $\varepsilon_{x,y}$ where x is the point, and y is the axis.

$\sigma 1-\sigma 2=E(\varepsilon 11-\nu\ \varepsilon 12)- E(\ \varepsilon 21-\ \nu\varepsilon 22)=E(\varepsilon 11-\varepsilon 21)=$ E (d1-d2)

Because & d1> d2 therefore, $\sigma 1>\sigma 2$

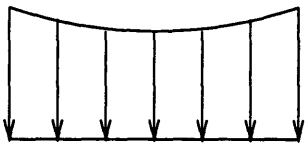

Stress Distribution

Figure 1-2 (b) Stress Distribution for Structure and Surrounding Soil

(Passive Arching)

D. For the soil between A1A2 and B1B2

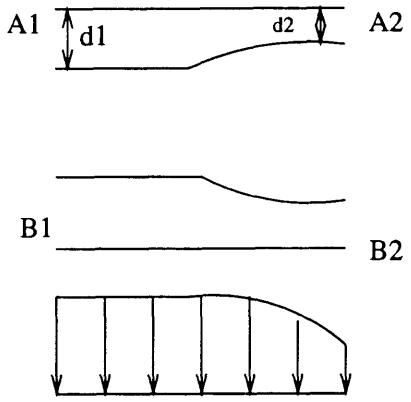

Normal Stress Distribution

Under the same assumptions and calculations as in Figure 1-1(a), we obtain:

d2<d1, and

$\sigma 2 < \sigma 1$

E. Compare soil and structure.

E2 < E1

$\varepsilon_{soil} = \varepsilon_{structure}$, at the connecting point of the materials

therefore,

$\sigma_{soil} < \sigma_{structure}$

Figure 1-2(c) Passive Arching.

Figure 1-2 (c) Stress Distribution for Structure and Surrounding Soil (Passive Arching)

From A, B, C, D, and E, we can draw following conclusion:

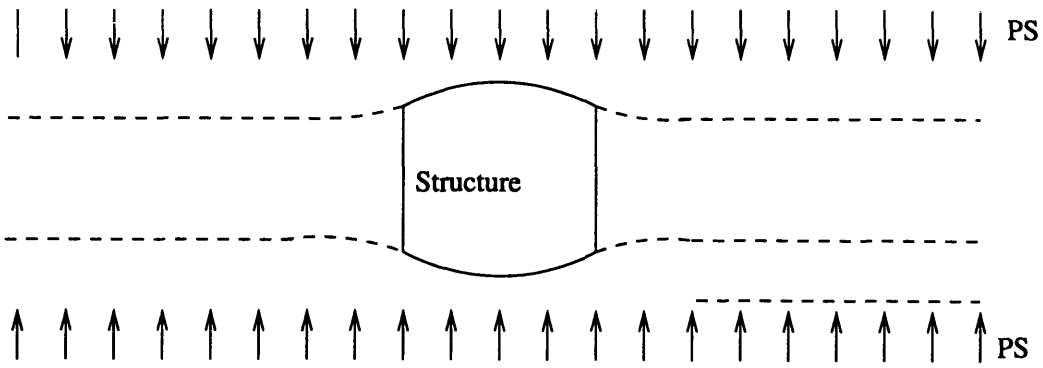

Displacement under Pressure PS When Structure
Is Less Compressible than the Surrounding Soil

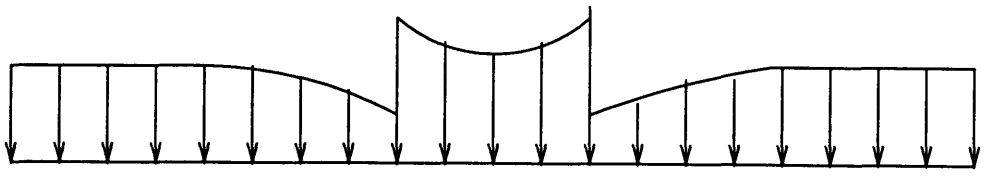

Stress Distribution across Upper Curve Plane A1A2 or Lower Plane B1B2

Figure 1-2(d) Passive Arching

Figure 1-2 (d) Stress Distribution for Structure and Surrounding Soil
(Passive Arching)

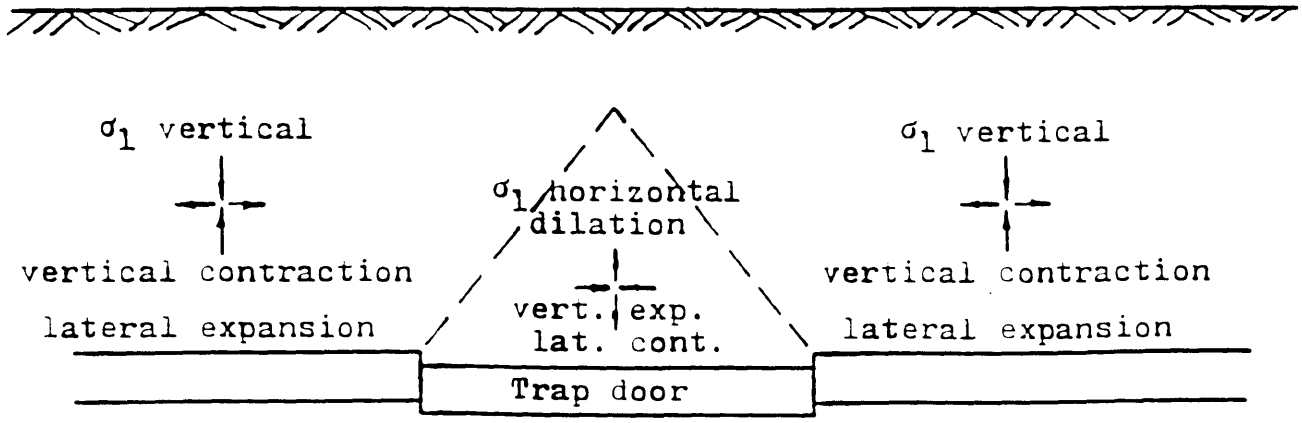

Figure 1.3 General Soil Behavior-- Active Arching (Evans, 1983)

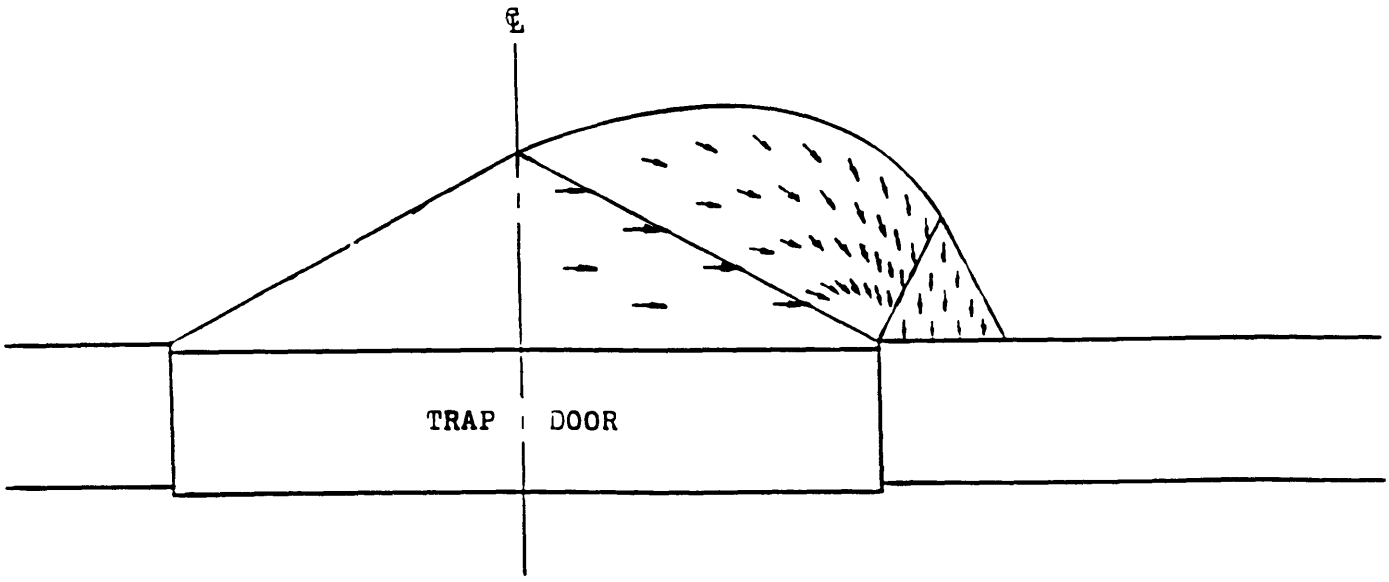

Figure 1-4 Direction of Major Principal Stress - Active Arching (Evans, 1983)

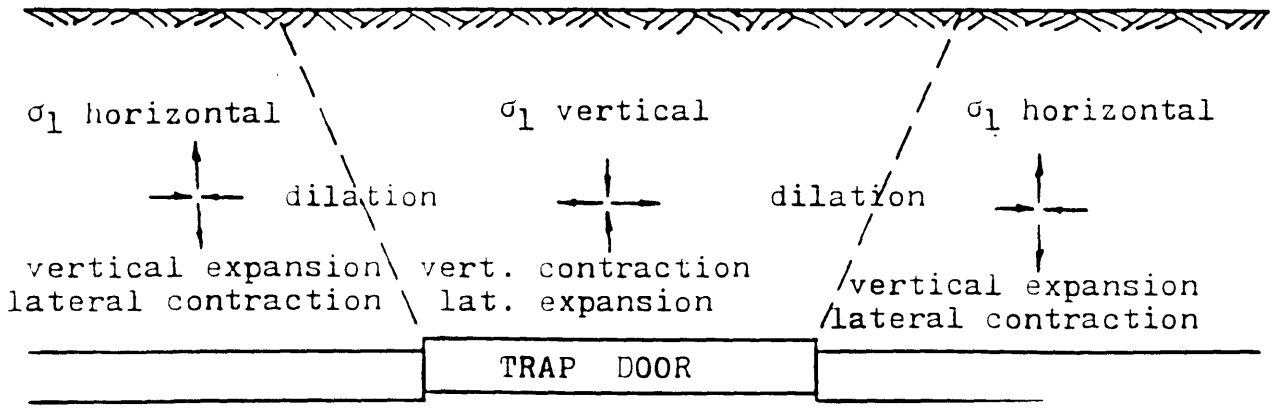

Figure 1-5 General Soil Behavior-- Passive Arching (Evans, 1983)

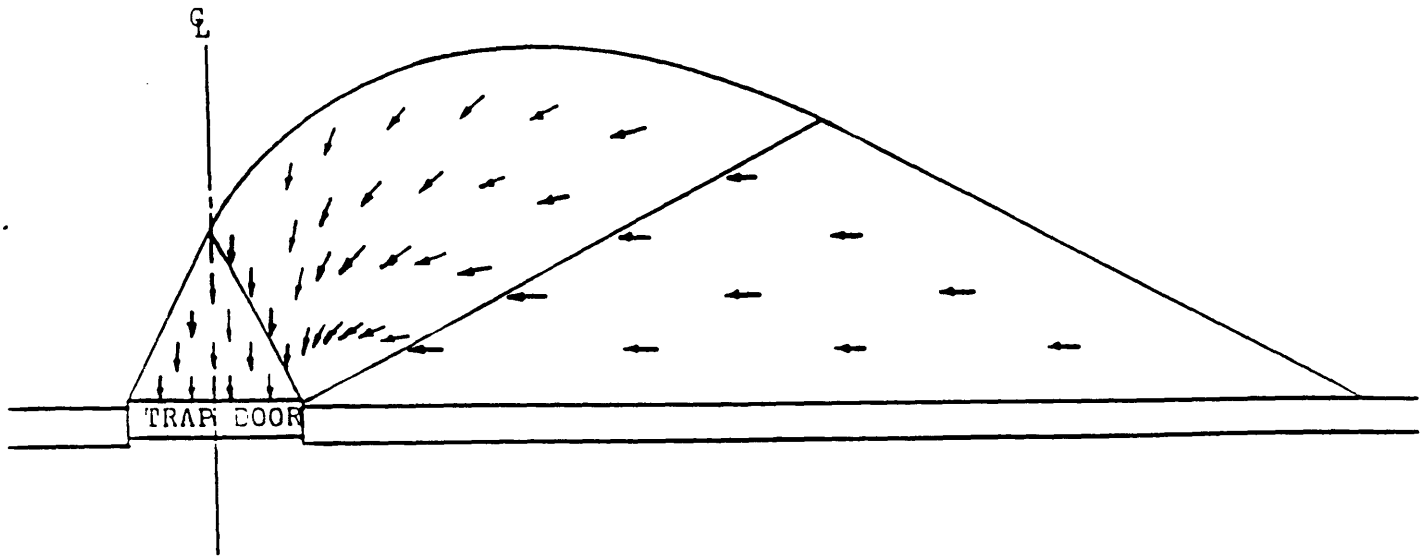

Figure 1.6 Direction of Major Principal Stress - Passive Arching (Evans, 1983)

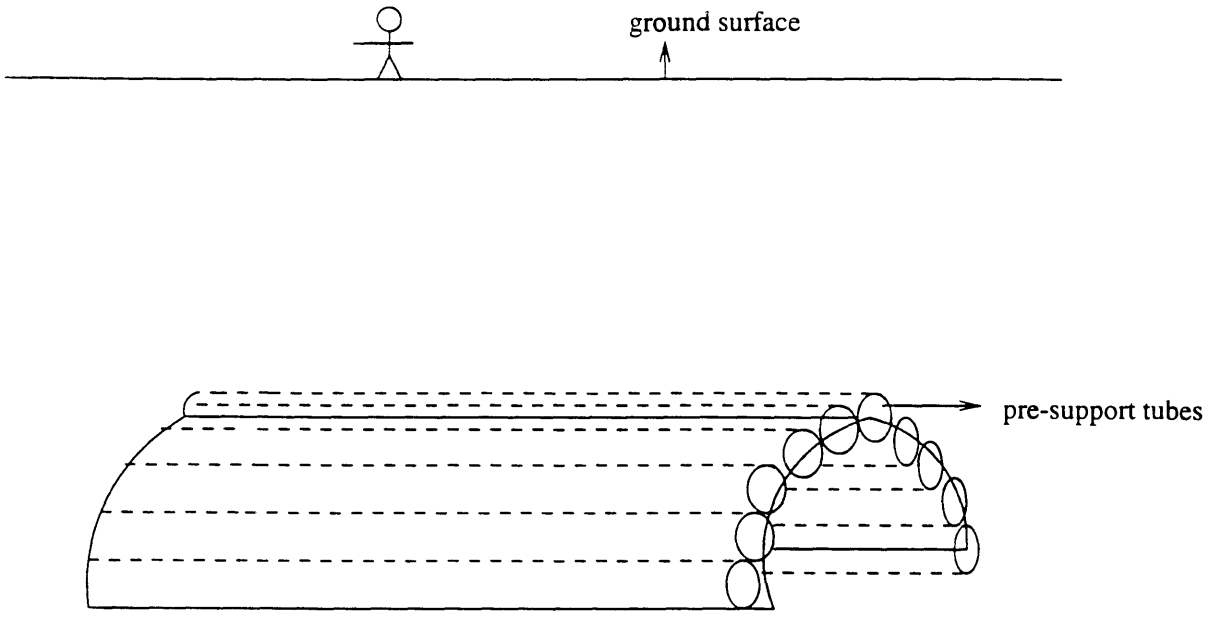

Figure 1-7. The Configuration of the Circular Pre-Support Tube.

Chapter 2. THE HISTORICAL REVIEW OF ARCHING THEORY

2.1 Terzaghi's Investigations of Arching(1936)

Terzaghi, who is the father of soil mechanics, conducted the most widely known experimental and theoretical investigations of arching. In his plain strain tests, a trapdoor initially mounted flush with the base of a box containing sand (Figure 2-1(a)) was moved downward. The total load on the trapdoor and the displacement of trapdoor were monitored at the same time. Figure 2-2 shows the actual and assumed sliding surface in Terzaghi analysis.

Figure 2-1 (b), (c), (d), (e) show results of Terzaghi's tests. The force on the trapdoor decreases rapidly as the displacement begins, with minimum values occurring at a displacement of about 1% of the trapdoor width. These minimum values were less than 10% of the overburden, and could be even less if a dense sand is used. The load on the trapdoor will increase to 13% of the overburden while the displacement of the trapdoor is increased to 10% of the trapdoor width.

In addition, the results of Terzaghi's tests indicated that the soil stresses above the trapdoor at a distance more than 2 times of the width of the trapdoor won't be affected by the displacement of the trapdoor (See Figure 2-1 (d)). Therefore, Terzaghi assumed that shearing resistance is only mobilized in the region, which is smaller than 2 times of the width of the trapdoor, while the remaining overburden acts as a surcharge. His equation is:

$$F = \frac{B^2(\Upsilon - 2\frac{c}{B})}{2K\tan\phi}\left(1 - e^{-2K\tan\phi(\frac{H}{B})}\right) + Bqe^{-2K\tan\phi(\frac{H}{B})} \tag{2.1}$$

Where

F is the total force on the trap door.

H is the distance between the trap door and the surface of the overlying soil.

B is the width of the trap door.

Υ is the unit weight of the soil.

ϕ is the friction angle of the soil.

q is the surcharge which acts on the soil.

c is the cohesion of the soil.

K is the coefficient of lateral stress, recommended to be taken as 1.0 by Terzaghi.

Terzaghi assumes that the shearing resistance is mobilized along the lower 2B of the sliding surface while the remaining overburden acts as a surcharge. Then, the surcharge is equal to $q+\Upsilon(H-2B)$ when the soil cover H is 2B or greater, and the above equation can be modified as:

$$F = \frac{B^2(\Upsilon - 2\frac{C}{B})}{2K\tan\phi}(1-e^{-4K\tan\phi}) + B[q+\Upsilon(H-2B)]e^{-4K\tan\phi} \qquad (2.2)$$

2.2 McCutcheon (1949) & Heuer and Hendron (1971)

In classical plasticity theory, the slip planes are assumed to be oriented in the directions of the maximum shearing stresses; the plastic state is defined as the entire region where slip occurs.

Unfortunately, the actual slip line fields are very difficult to get for most problems.A commonly used simplifying approximation, offered by McCutcheon, assumed that slip lines are oriented at $\pm(45-\frac{\phi}{2})^\circ$ to elastically determined principal stress trajectories. This approximation ignores the redistribution of stresses which accompanies the slip. Heuer and Hendron did some model tests and assumed that the slip line boundaries of the radial shear zone correspond to the experimentally observed sliding surfaces. The test results showed that the observed sliding surfaces and the predicted solution are similar in the orientation of their sliding surfaces (see Figure 2-3 and Figure 2-4). Any discrepancy may be largely attributed to the difficulty of observing micro-cracking and to the deviation of the modeling material's behavior from the ideal elasto-plasticity (Einstein, et.al., 1980). Furthermore, the observed crack formation for a non-uniform stress condition (Figure 2-5) agrees well with the prediction of slip-line theory and with the shear-wedge theory of Rabcewicz (1973). Failed wedges form at the springlines and gradually move into the cavity while the soil above the tunnel slides down to fill the resulting void.

2.3 The Tests of Atkinson et. al.(1975)

Atkinson et. al. designed a simple but repeatable and reliable test (see Figure 2-6). Leighton Buzzard sand was poured in the direction of the assumed tunnel axis, the direction parallel to the tube, to a void ratio of 0.52 while a grid of lead was placed in a plane normal to the tunnel axis. A 32 mm radius tunnel (tube) consisting of two cylindrical rubber membranes, one membrane is constructed inside the other. Both membranes were attached to cylindrical extension pieces fixed to the sides of the sample box to minimize the end effects during collapse.

The tunnel was also filled with sand to the same level of sand which was outside the tunnel. After the pouring was finished, the annulus between the two membranes was pressured with air with the magnitude of the overburden pressure at the crown (i.e. $\sigma_T = \gamma c$, where γ is the unit weight of soil, and c is the depth of the cover). The sand in the tunnel was excavated by using a vacuum cleaner. During this process, the inner membrane collapsed, and the outer membrane became the tunnel lining supported by air pressure.

The tests were conducted by reducing the tunnel pressure in stages until the collapse occurred. A radiograph of the apparatus was taken after every decrement in tunnel pressure, such as the one shown in Figure 2-7. Additional radiographs of the apparatus were taken before the sand was excavated and after the tunnel had collapsed. Before and after the excavation of sand, the lead shot images on radiographs revealed no discernible deformation.

The results of these tests showed that the first movements occurred just above the crown long before the tunnel collapsed; Figure 2-8 indicates that such a movement was initially restricted to a very small zone (which appeared to be the wedge ABC, whose sides were tangent to the circle). Planes AB and BC make an angle 2ν at B, where ν is the angle of dilation. As the tunnel pressure decreased further, this zone of movement grew upward toward the surface but it still was restricted by two planes DE, FG, projected upward from the points close to the tunnel springlines (see Figure 2-9).

Collapse was sudden and occurred at a well defined tunnel pressure for each test, and resulted in a sudden large movement of sand into the tunnel causing a compression of the air and a consequent increase in the tunnel pressure to a new equilibrium value. The pressures at both collapse and final equilibrium state were recorded in Figure 2-10 where R is the radius of model

tunnel, and the dimensionless parameter $\frac{\sigma_t}{\gamma C}$ has been plotted against $\frac{C}{R}$; The lower line represented the initial collapse, and the upper line indicated the final equilibrium state. From this figure 2-10, Atkinson found the tunnel pressure at initial collapse is almost independent of the cover to radius ratio. The equilibrium tunnel pressure after collapse exceeds that required just to prevent collapse by a factor about 3 at $\frac{C}{R} = 1$ and a factor of about 7 at $\frac{C}{R} = 4$.

2.4 Evans' Plastic Model (1983)

Evans tried to describe the non-recoverable deformation that occurs in soils. The theory of plasticity, therefore, was used to predict the flow rule, which relates the incremental plastic shear strain to the incremental plastic volumetric strains. The plastic potential is defined as a curve, which is perpendicular to all the plastic strain increment vectors. The angle of dilation ν is defined as the angle between the direction of plastic potential and the horizontal (see Figure 2-11).

To simplify the mathematics in solving the problem, the associated flow rule, in which ν is assumed to be equal to the friction angle ϕ, was used, and the major principal strain rate direction was assumed to coincide with the direction of the major principal stress. The Coulomb failure criterion was also used to define the direction of the failure surface.

Evans's trapdoor test is a plane strain active arching test, in which a triangular zone is formed first. As the displacement increases, the triangular shaped zone expands vertically with noticeable dilation (See Figure 2-12). Therefore, a free body diagram of a triangular section (see Figure 2-13) is drawn with the sloping sides forming an angle ν with the vertical. A state of so-called "maximum arching "occurred, i.e., the load on the trap door is a minimum, or the soil has the maximum strength (Einstein, 1980), when the dilation angle ν approaches the friction angle ϕ. Later, Iglesia found that the shape of Evans's assumption is exactly the same as Bierbaumer's (1913). For the same configuration, the resultant of the forces due to the normal and shear stresses at both sides of the triangle are horizontal, therefore, they do not contribute to the vertical load. The minimum force P_{min} (per unit length) on the trapdoor is only due to the weight of triangular prism, and occurs when the displacements are 1~2% of the width of the trap door.

Evans presented the following two equation:

When H/B is smaller than $1/(2\tan\phi)$, the equation is:

$$F = \Upsilon HB\left(1 - \frac{H}{B}\tan\phi\right) \tag{2.3}$$

When H/B is larger than or equal to $1/(2\tan\phi)$, the equation is:

$$F = \frac{\Upsilon B^2}{4\tan\phi} \tag{2.4}$$

F is the total force on the trap door.

H is the distance between the trap door and the surface of the overlying soil.

B is the size of the trap door.

Υ is the unit weight of the soil.

ϕ is the friction angle of the soil.

The purpose of the limit value for H/B ratios is to consider whether a triangular zone can be formed. A trapezoidal prism can be formed when the depth of the soil is not sufficient to contain a triangular prism.

2.5 Stone's Experiments (1988, 1992)

Stone was the first to conduct the plain strain trap door test on the centrifuge. Leighton Buzzard sand in different sets of particle sizes was used to observe the development of rupture in soils as well as scale effects. Stone arranged the geomaterial into horizontal sand layers of different colors. By observing the films taken while the centrifuge was turning, deformation patterns were monitored.

A few pictures are presented from the results of Stone's centrifuge tests. Figure 2-14 shows the contours of maximum shear strain for different increments of trap door base translation; and Figure 2-15 shows the vertical displacement for various base translations. The clearer pictures are in Figure 2-16. These three pictures show that inclined shapes of yield zones are formed at the initial stages of the experiment when the displacement is small. During this phase, the maximum shear strain and vertical displacement contours change from a triangle to an arch-like shape. With an increase in the displacement, the reorientation of the failure surface approaches the vertical.

Stone also considered the effects of scale. When the tests were run by using finer particle sizes, more complex and more detailed patterns of localized deformation would also be observed. The results show that the finer the sand, the smaller the displacement forming the localization. Therefore, one can expect that the fine sands will show deformation patterns similar to those of coarse sands only at the earliest stages of the experiments.

2.6 Iglesia's Theory (1991)

Iglesia suggested that the minimum load at relatively small trapdoor displacements can probably be explained by considering a parabolic arch oriented at an angle of $\theta = 90 - \phi$ (See Figure 2-17) at the edge, consistent with Evans's condition of the dilation angle $\nu = \phi$. Actually, this shape is the same as Engesser's parabolic derivation, but the angle is different. Besides, by using the Mohr-Coulomb failure criterion, and the assumption that the surfaces of the arch are the failure surfaces, the relation between the horizontal and vertical stress at the level of the trap door can be obtained.

From the geometric relationship in Figure 2-17, Iglesia obtained:

$$\sigma_v = \frac{\cos^2\phi}{1+\sin^2\phi} \times \sigma_h \tag{2.5}$$

Iglesia tried to use the Engesser's (1882) equation

$$P = B^2\Upsilon\left(\frac{HK_a}{BK_a + 2H\tan\phi} + \frac{\tan\phi}{6}\right) \tag{2.6}$$

by assuming

$$K' = \frac{\sigma v}{\sigma h} = \frac{\cos\phi^2}{1+\sin\phi^2} \tag{2.7}$$

and replacing K_a by K', he got

$$P_{min} = B^2 \Upsilon \left(\frac{HK'}{BK' + 2H\tan\phi} + \frac{\tan\phi}{6} \right). \tag{2.8}$$

He wanted to keep in line with Engesser's formulation, but the angle of Engesser's equation and that of Iglesia's equation are complementary. Therefore, a modified expression for the minimum load can be obtained as below:

$$P_{min} = B^2 \Upsilon \left(\frac{HK'}{BK' + 2H\cot\phi} + \frac{\cot\phi}{6} \right) \tag{2.9}$$

normalizing this with the geostatic force (per unit length) $P_0 = \Upsilon$ HB, one obtains

$$\left(\frac{P}{P_0} \right)_{min} = \frac{B}{H} \left(\frac{K'}{\frac{BK'}{H} + 2\cot\phi} + \frac{\cot\phi}{6} \right) \tag{2.10}$$

By applying this equation to centrifuge tests, he concluded from Table 2-1 that his proposed Engesser-Bierbaumer-Evans hybrid scheme provides a very good prediction of the minimum trapdoor load.

Finally, he found that the computed load for parabolic yield zones are almost the same as the computed load for the triangular yield zone; this could possibly explain why the load tends to be at a low level for quite a while as the triangular arch slowly transforms into the curved arch. Eventually, the soil will collapse, and the failure surface will become vertical.

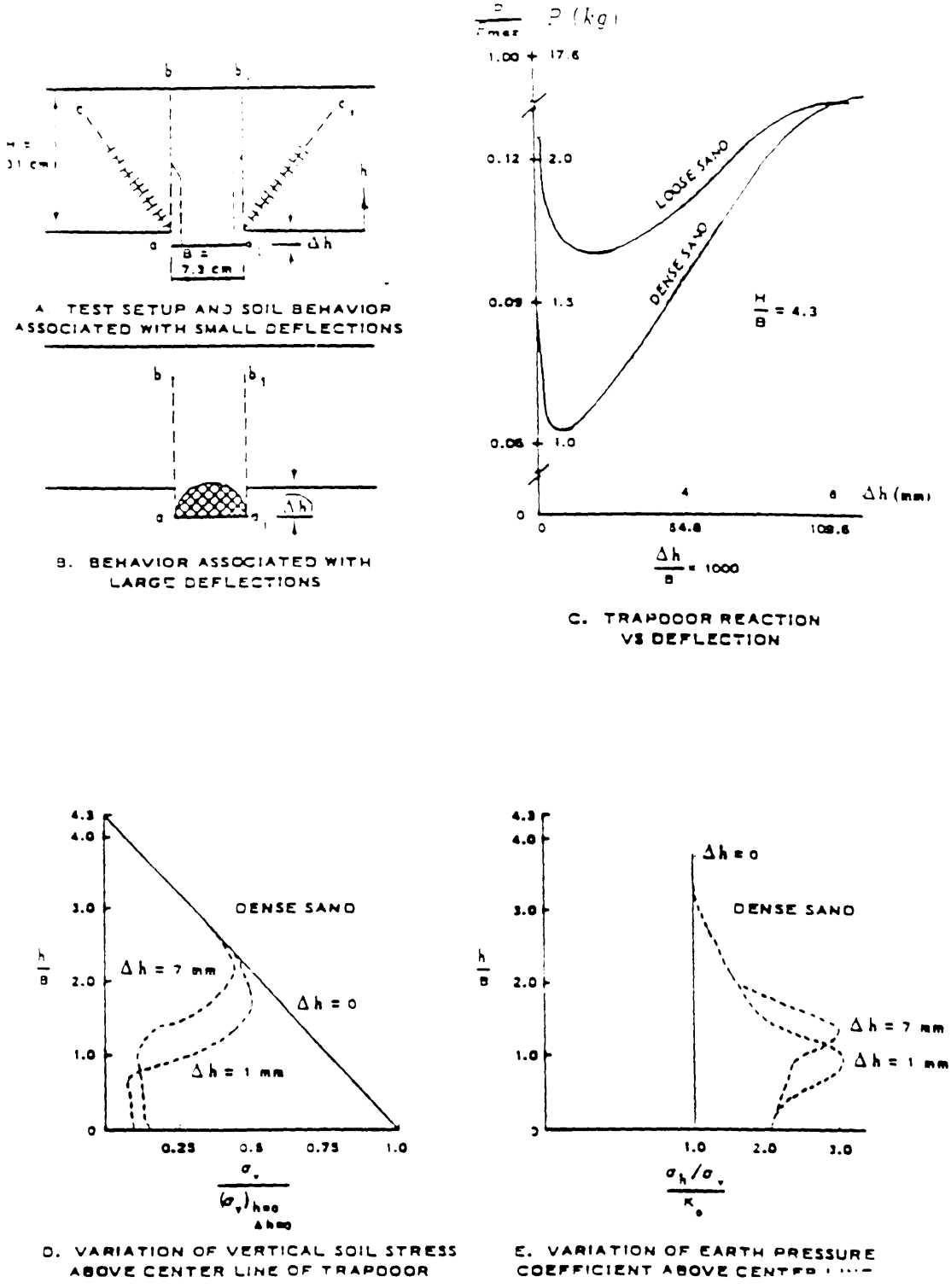

Figure 2-1 Terzaghi's (1936) Trapdoor Experiments (from McNulty, 1965)

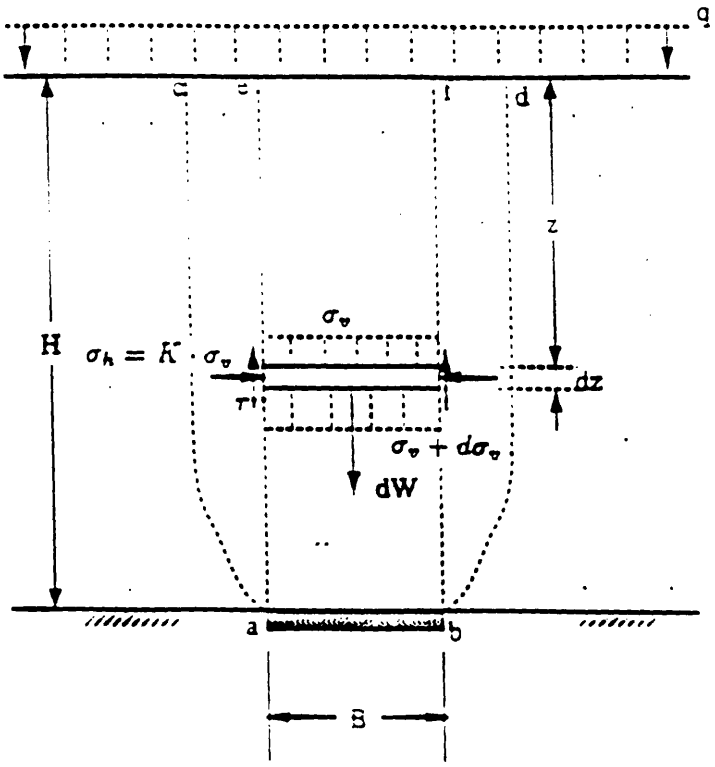

Figure 2-2 Actual and Assumed Sliding Surface in Terzaghi's Analysis

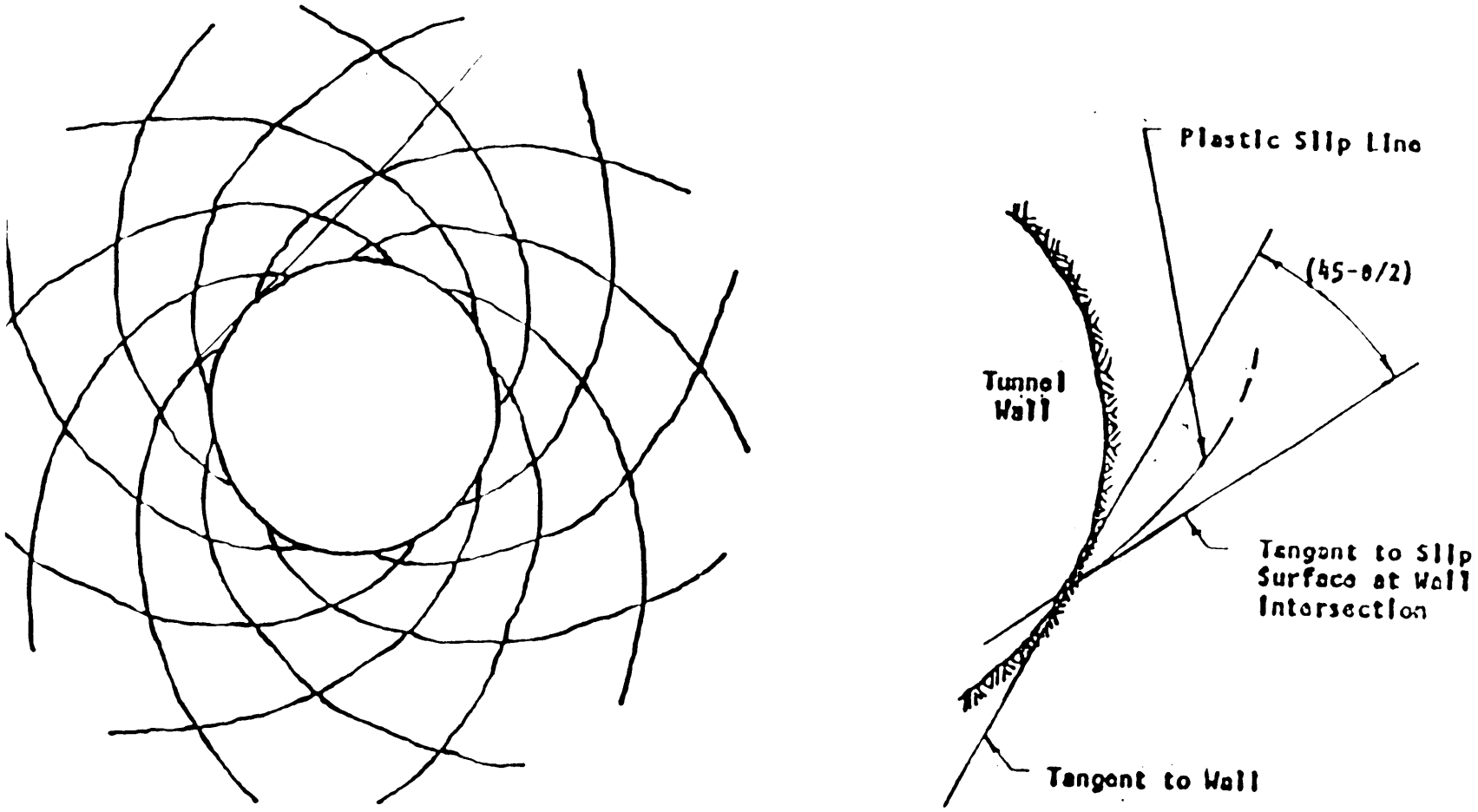

2.3 Theoretical Plastic Sliplines around a Circular Opening in Frictional Material - K=1 (Heuer and Hendron, 1971)

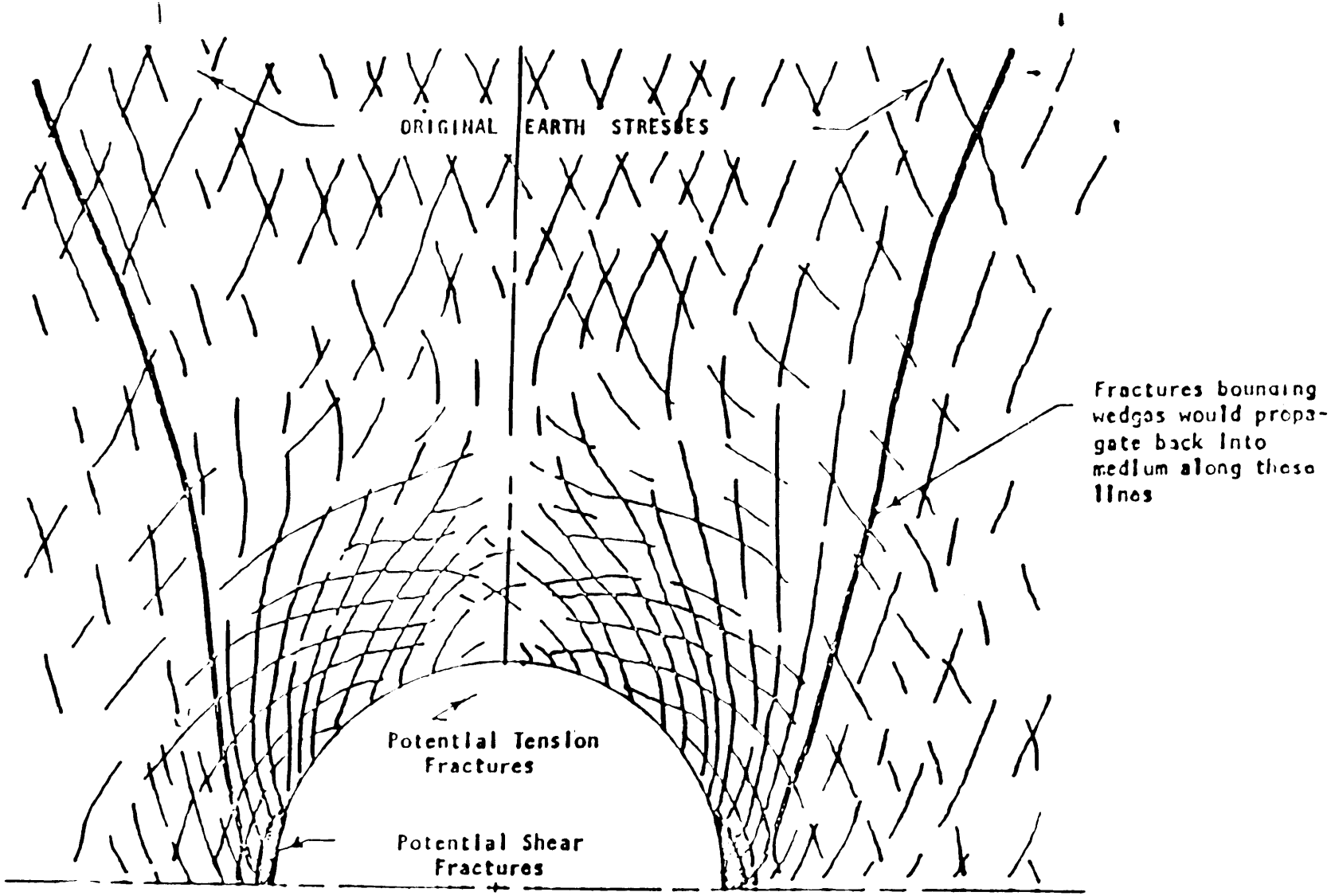

2.4 Potential Shear Planes about a Circular Opening Assuming An Elastic Stress Distribution (Heuer and Hendron, 1971)

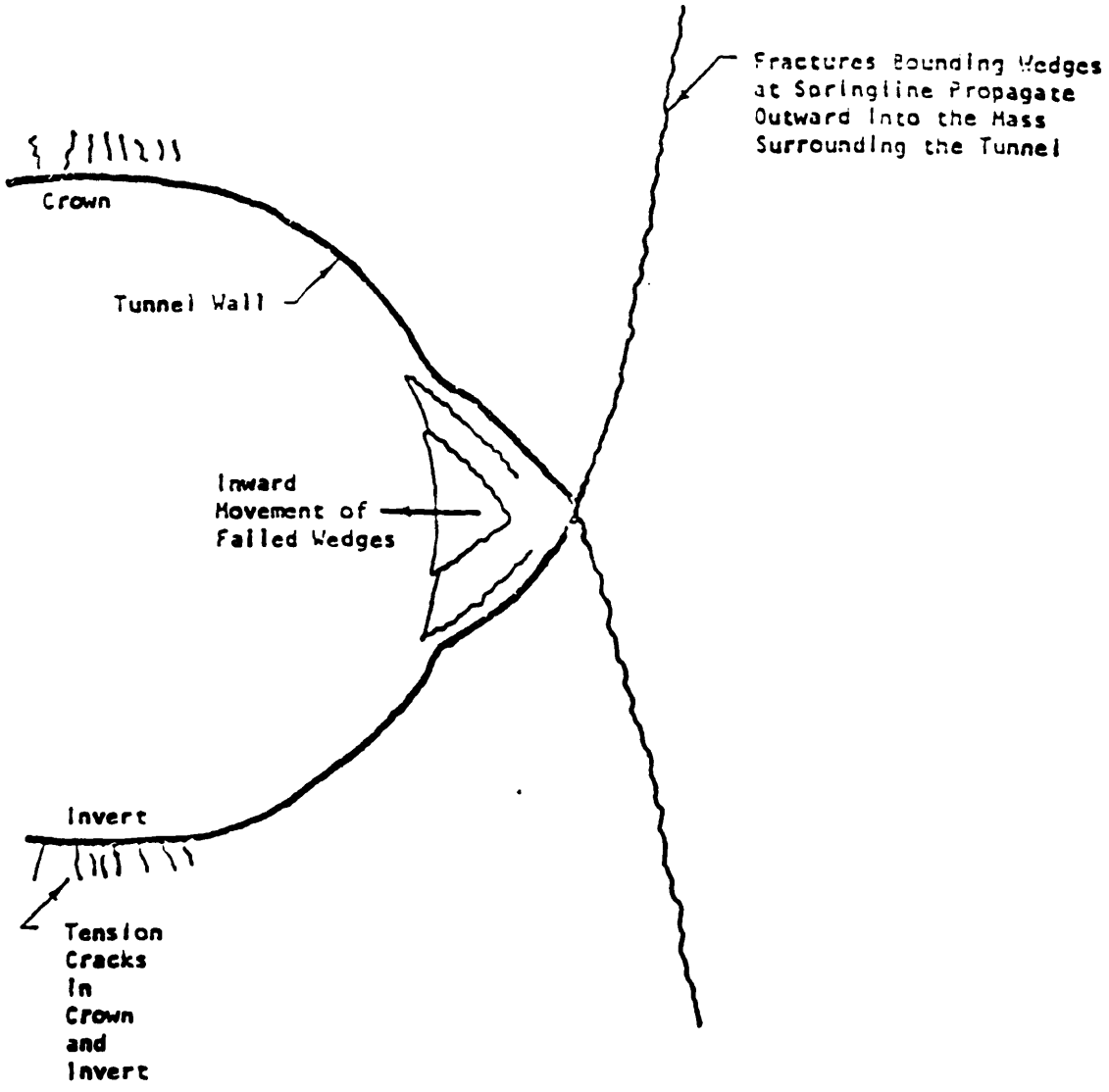

Figure 2-5 Significant Features of the Behavior Around a Circular Opening during the last Stage of Failure -- K=1/4 (Heuer and Hendron, 1971)

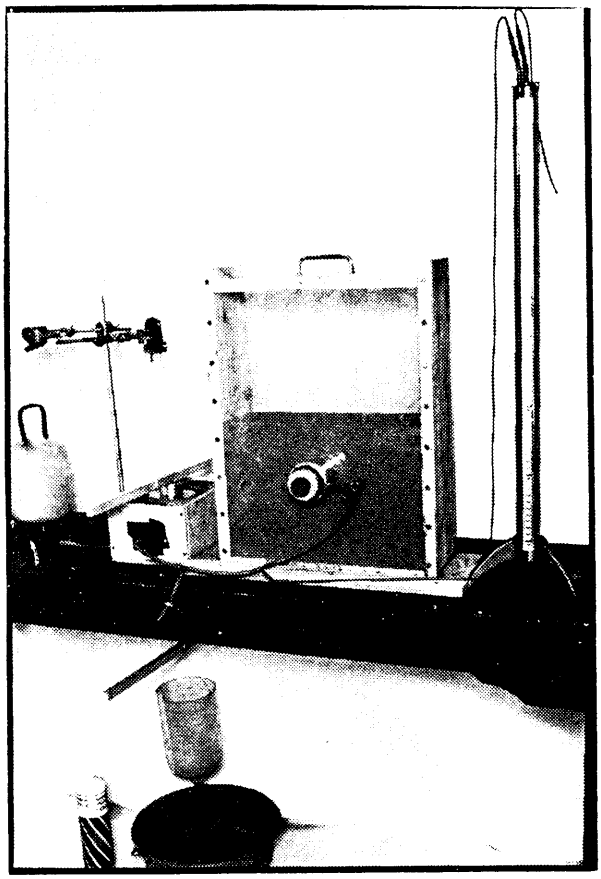

Figure 2-6 The Model Tunnel Test Apparatus (Atkinson et. al., 1975)

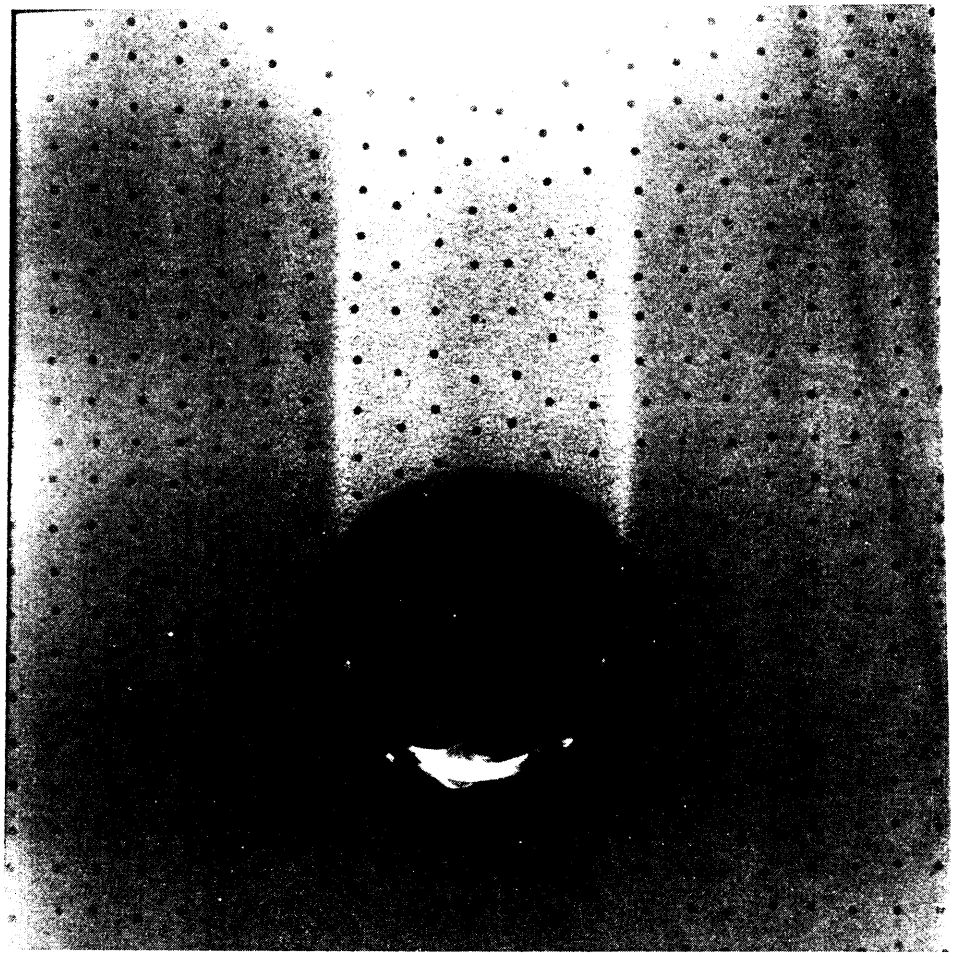

Figure 2-7 A Radiograph of the Model Tunnel Test (Atkinson et. al., 1975)

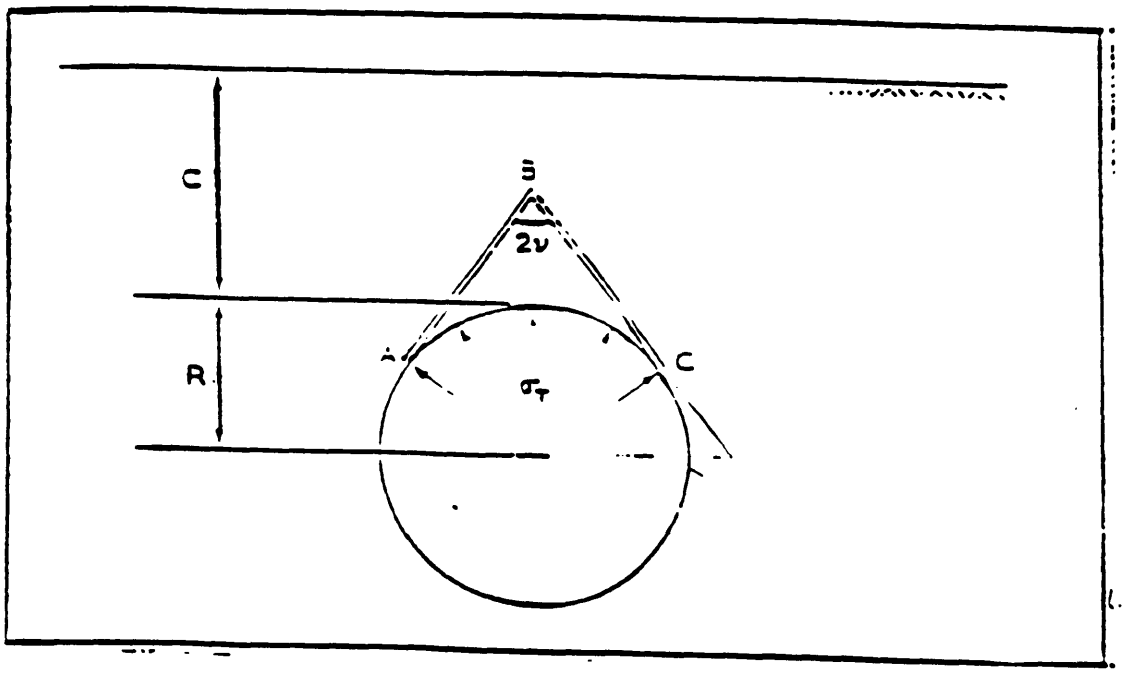

Figure 2-8 Collapse Mechanism of the Model Tunnel Test for Initial Failure (Atkinson et. al., 1975)

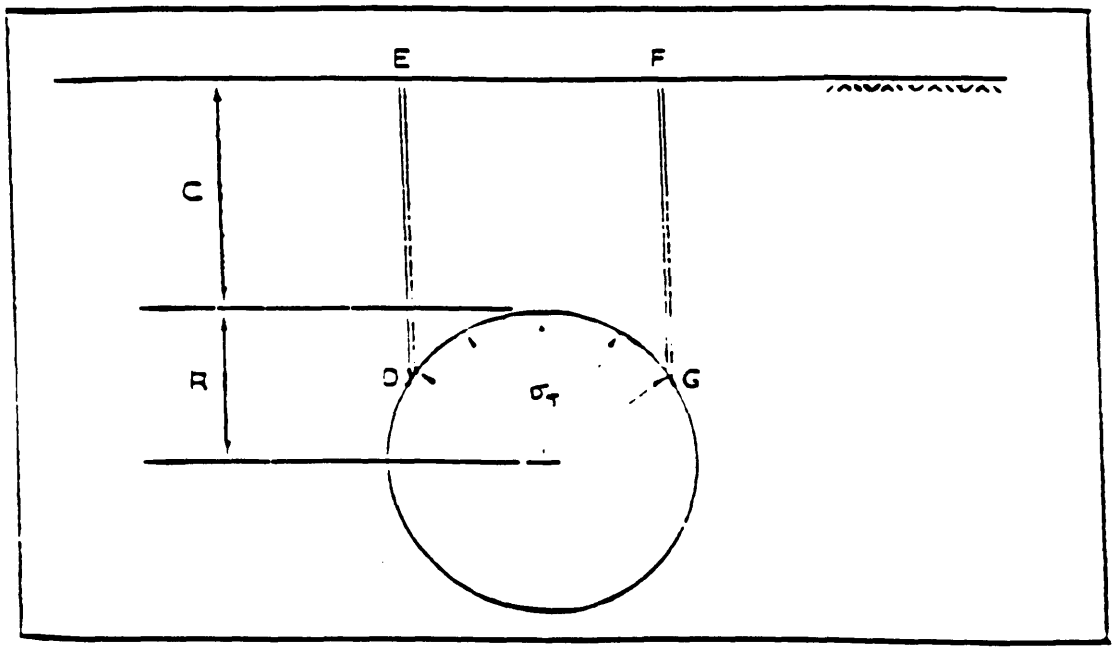

Figure 2-9 Collapse Mechanism of the Model Tunnel Test for Final Equilibrium (Atkinson et. al., 1975)

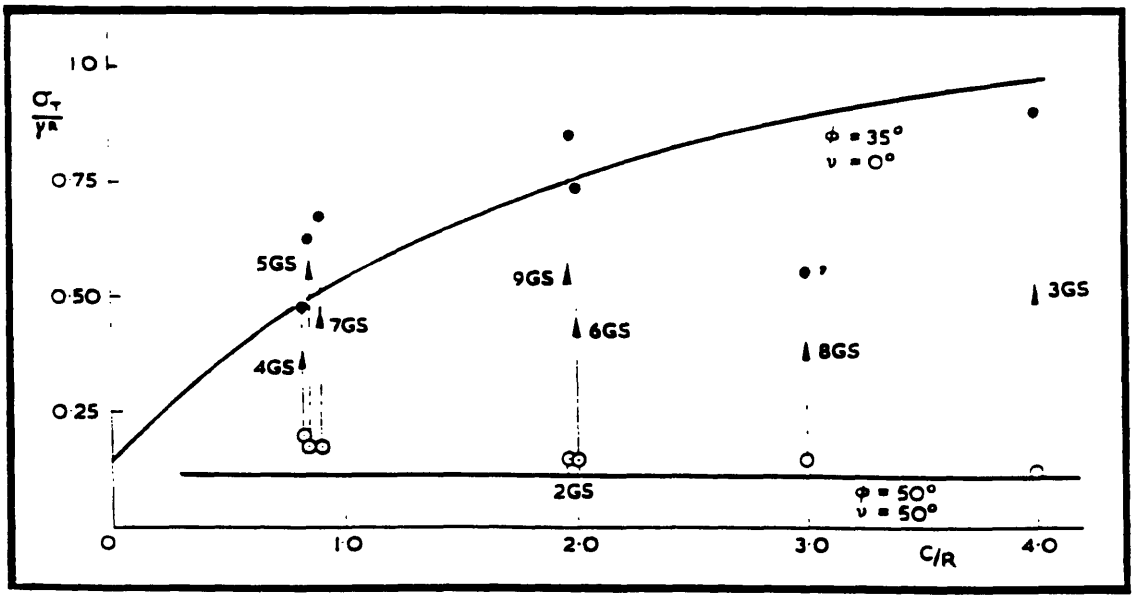

Figure 2-10 The Results of the Model Tunnel Test (Atkinson et. al., 1975)

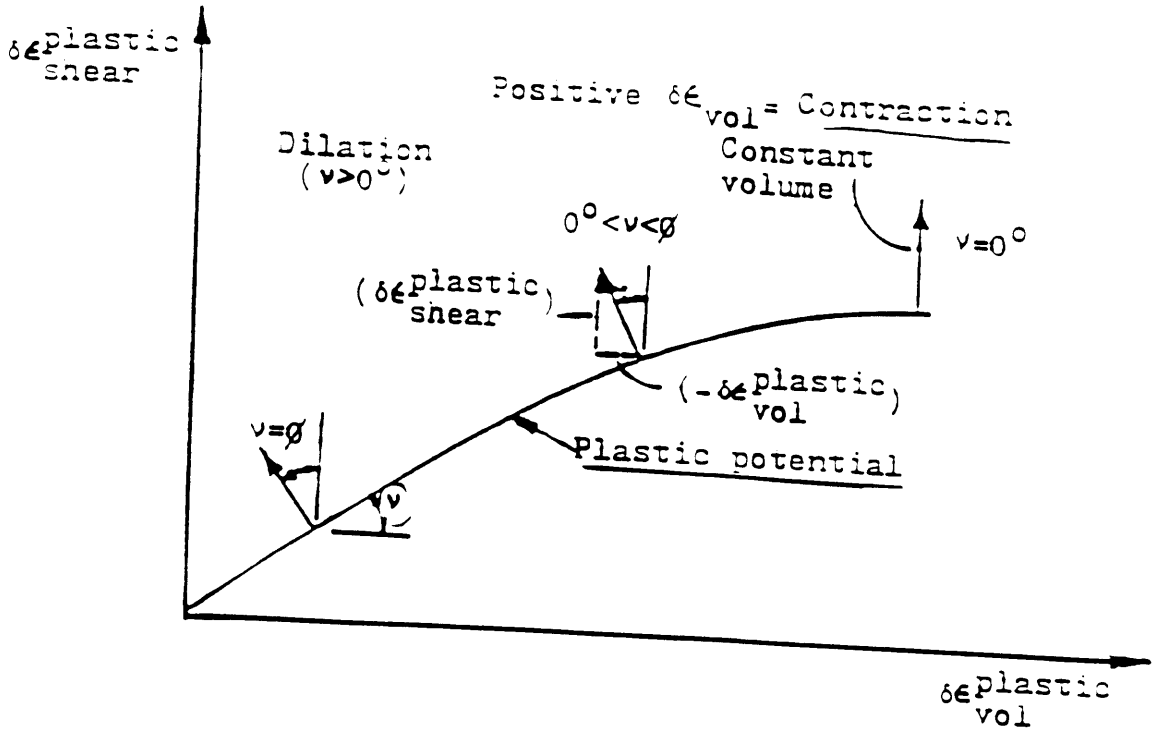

Figure 2-11 Plastic Flow Rule (Evans, 1983)

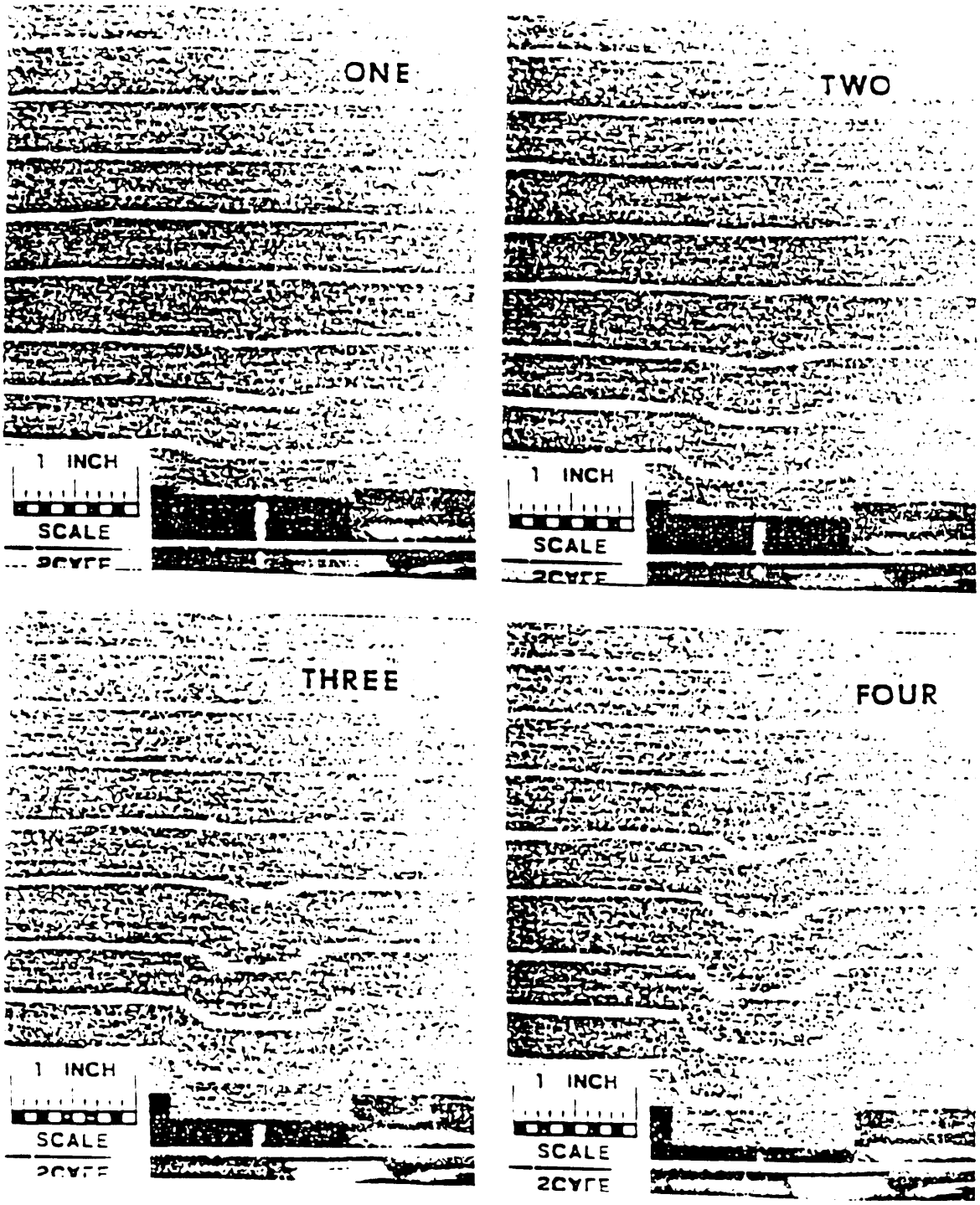

Figure 2-12 Variation of Soil Displacement Pattern with Increasing Trapdoor Displacement during an Active Arching (Evans, 1983)

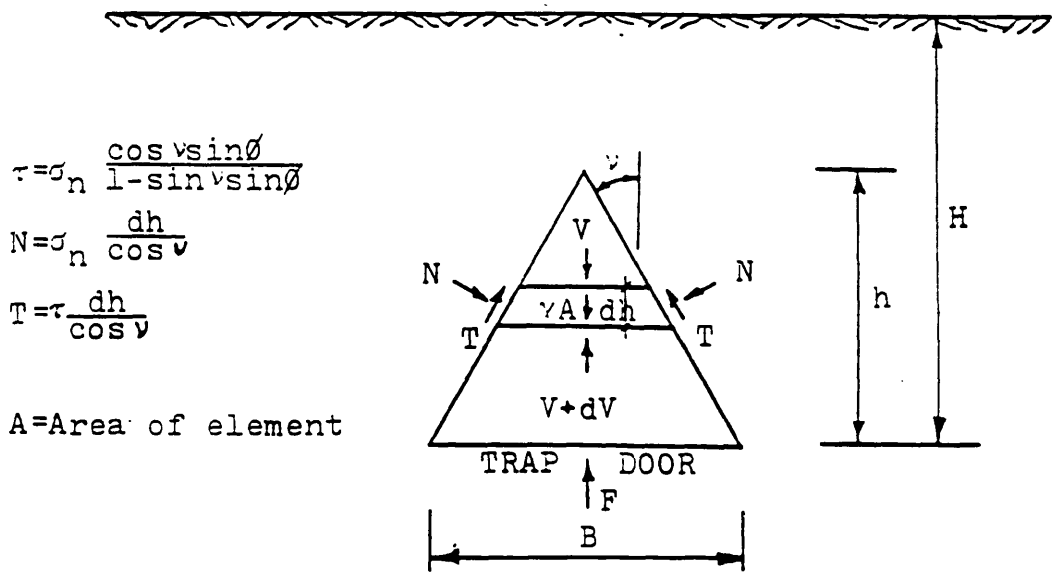

A. Free Body Diagram for $\nu>0^o$

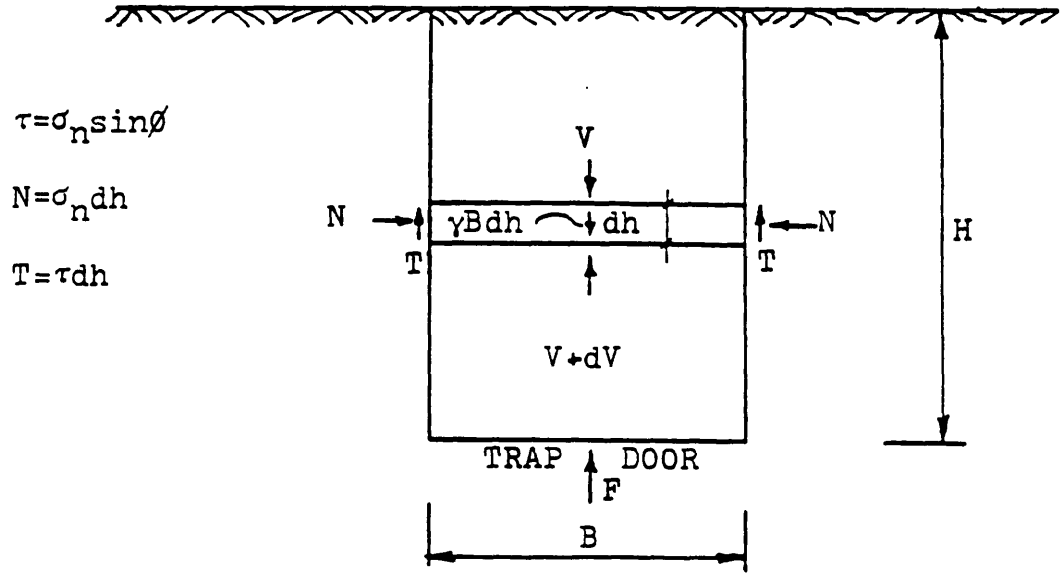

B. Free Body Diagram for $\nu=0^o$

Figure 2-13 Free Body Diagram for Active Arching (Evans, 1983)

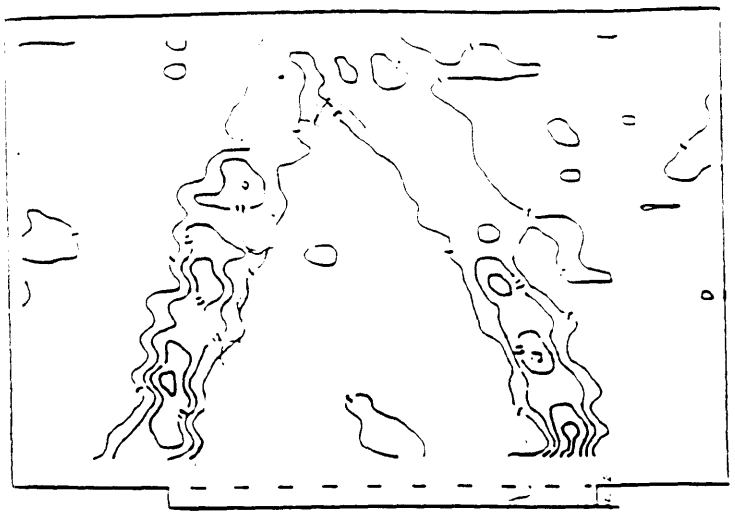

a) Test KS10, 14/25 sand; Δ_B=4.6 to 8.6 mm.

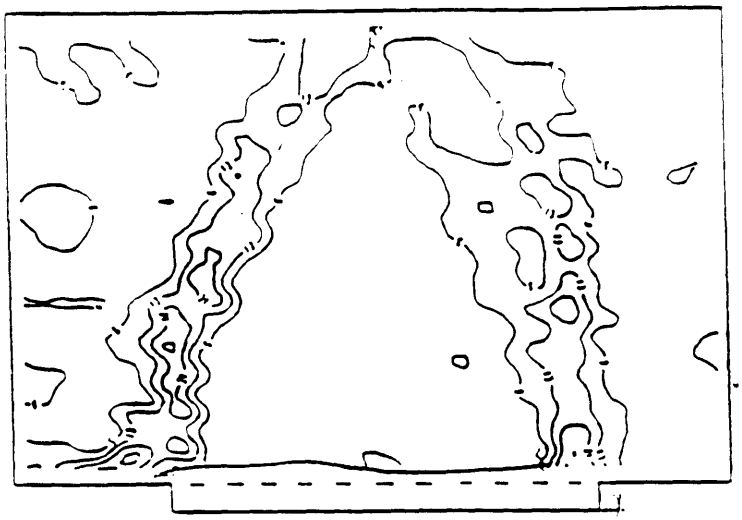

b) Test KS10, 14/25 sand; Δ_B=8.6 to 13.1 mm.

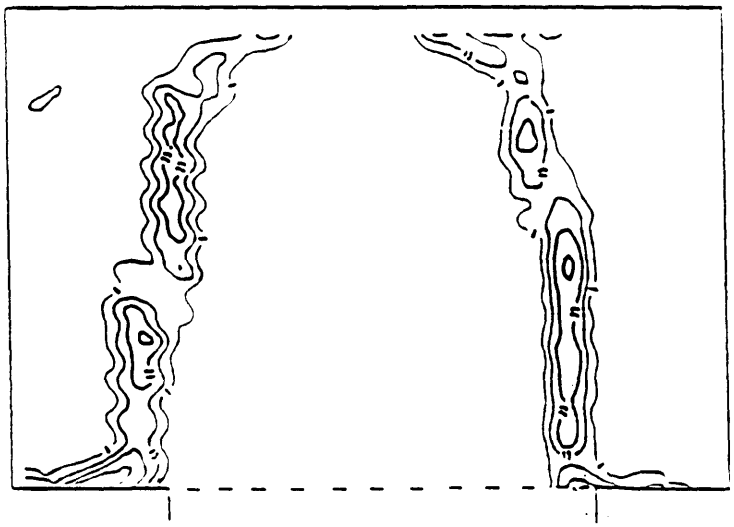

c) Test KS10, 14/25 sand; Δ_B=20.9 to 25.0 mm.

Figure 2-14 Maximum Shear Strain Contours (Stone, 1988)

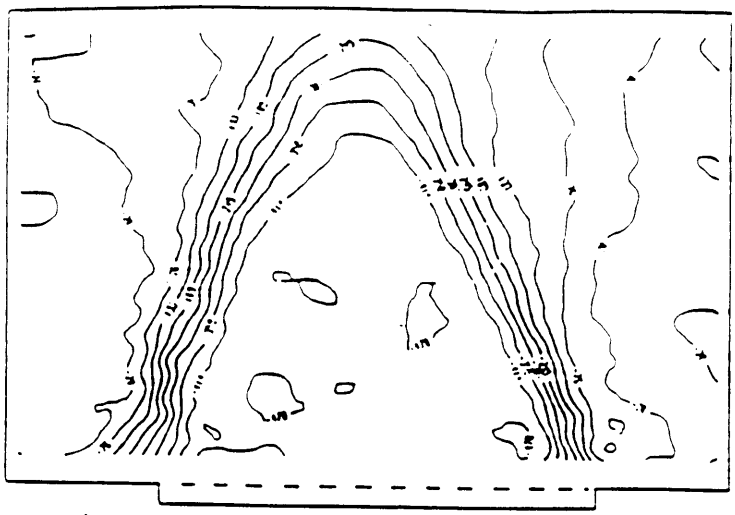

a) Test KS10, 14/25 sand; Δ_B=4.6 to 8.6 mm.

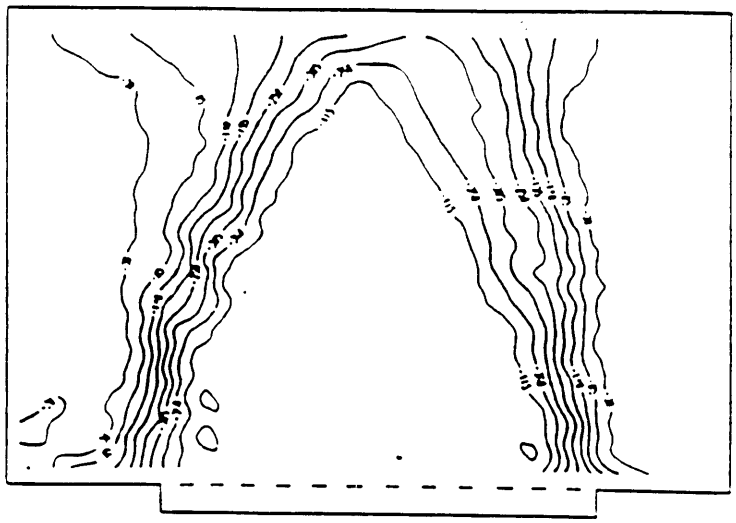

b) Test KS10, 14/25 sand; Δ_B=8.6 to 13.1 mm.

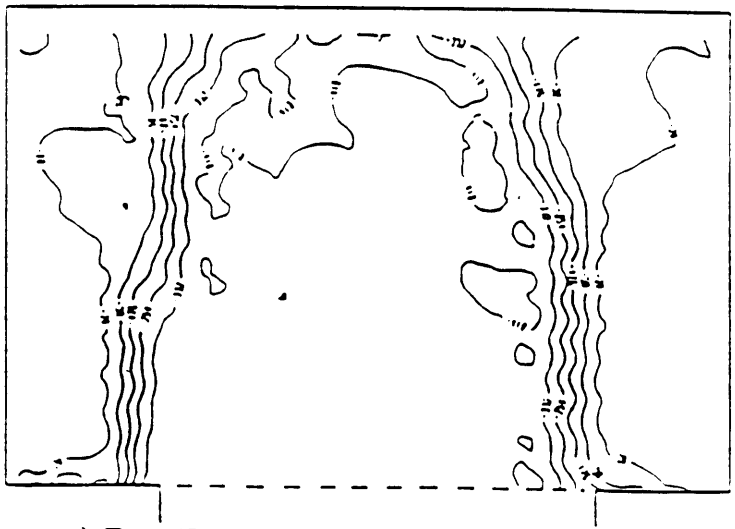

c) Test KS10, 14/25 sand; Δ_B=20.9 to 25.0 mm.

Figure 2-15 Vertical Displacement Contours (Stone, 1988)

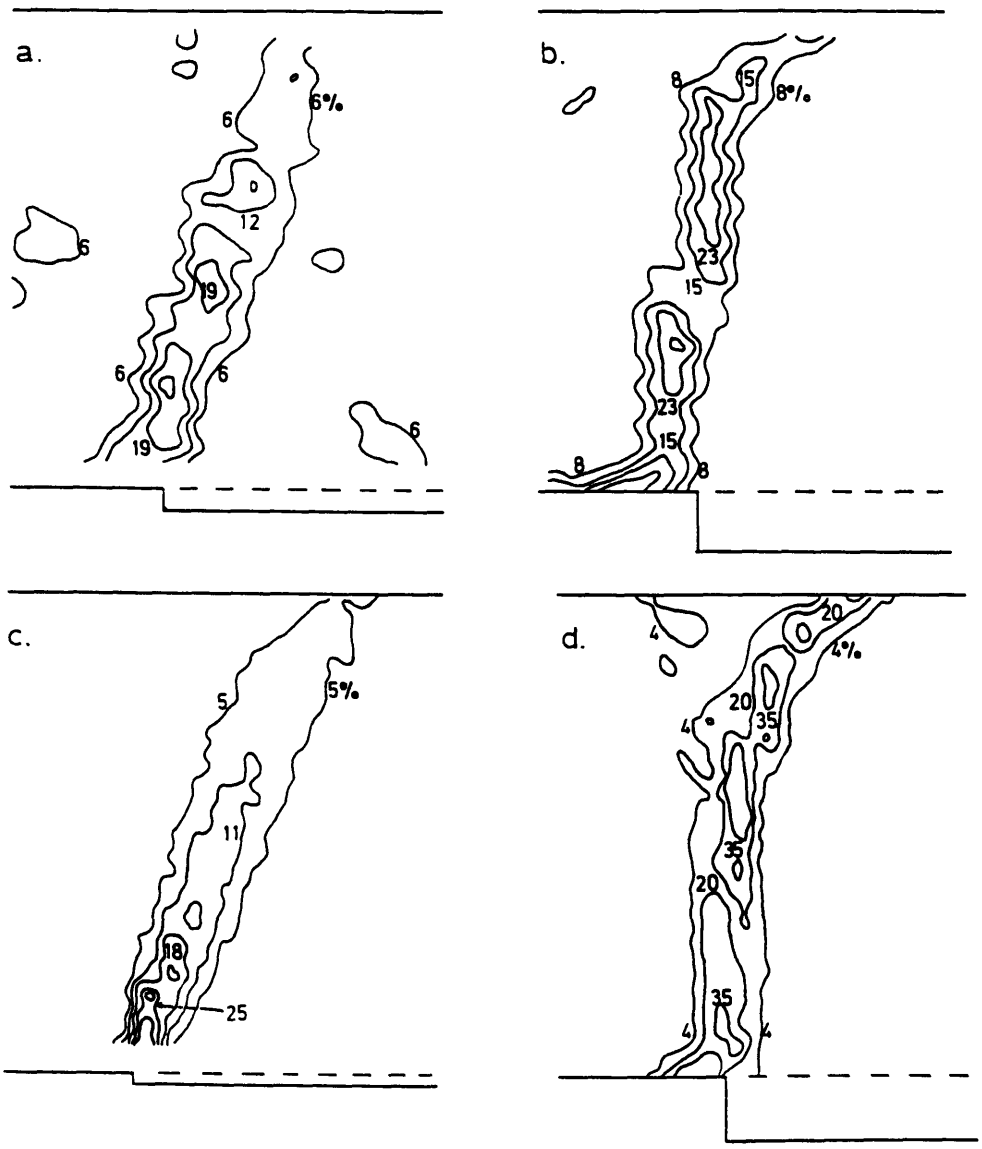

Figure 2-16 The Development of Initial and Secondary Localizations

(a), (b) tested in 100 g, (c), (d), tested in 1 g (Stone, 1992)

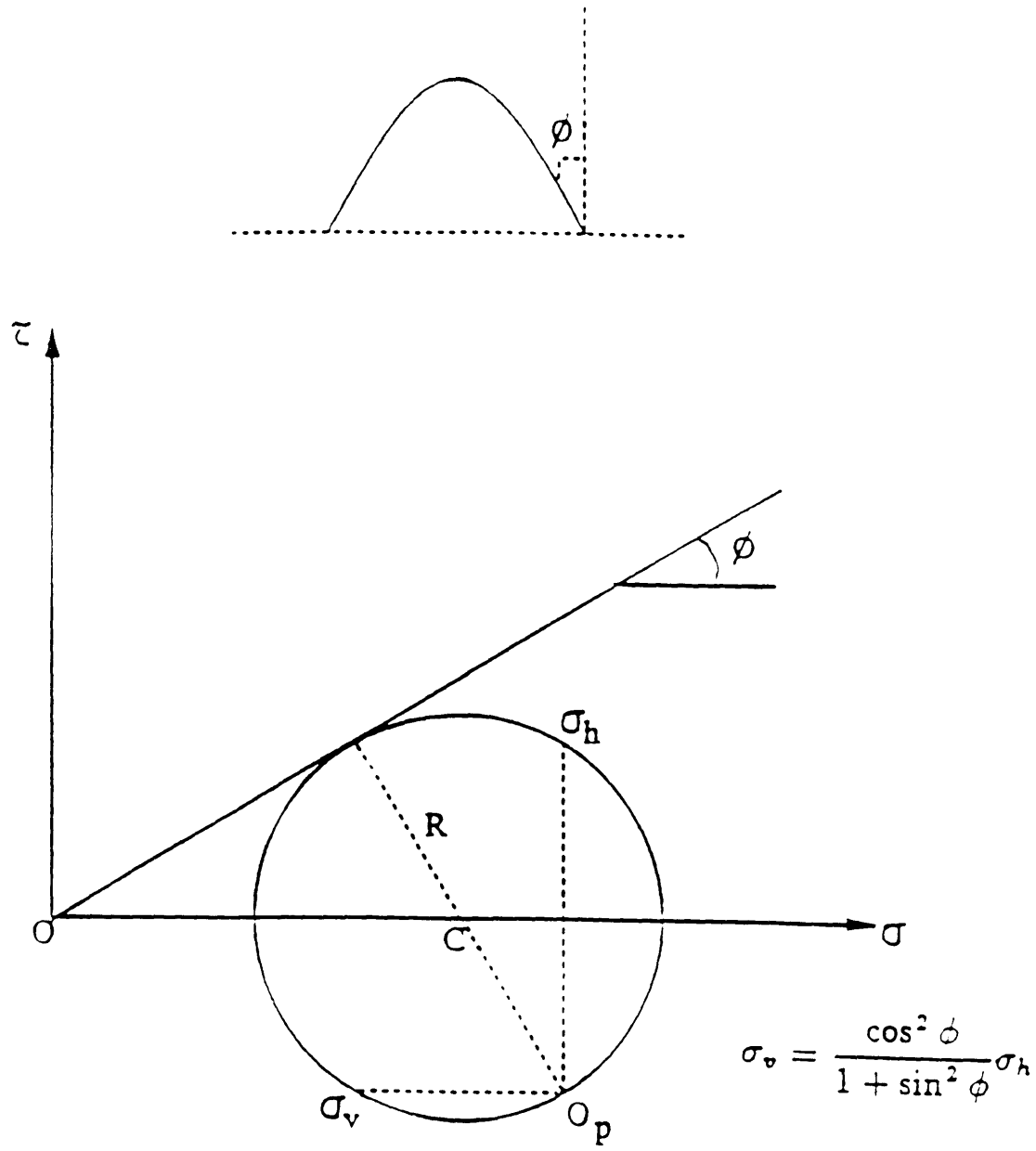

Figure 2-17 Proposed Theory of Iglesia (Iglesia, 1991)

Table 2-1 Predicted Values of $(P/P_0)_{min}$ with Proposed Theory (Iglesia, 1991)

H/B	$P/P_{0\,min}$	
	Predicted	Measured
	Tests with sand	
1	0.355	0.36
2	0.183	0.18
3	0.093	0.09
	Tests with glass beads	
1	0.453	
2	0.232	0.21-0.25

Chapter 3. New Explanations for the Development of the Triangular Prisms

3.1 Introduction

The development of triangular prisms are not clearly understood. In this chapter, the Mohr-Coulomb failure envelope and Mohr failure envelope are used to explain the development of triangular prisms.

After the triangular prism has already formed, the shapes of the yield zone will change with the increment in the downward trapdoor displacement. This change can be divided roughly into four stages which are shown in the pictures of Evans' experiment (see Figure 2-11), and the pictures of Stone's tests (see Figure 2-13, and Figure 2-14). Figure 3-1 shows the first stage when the triangular prism has just formed. Figure 3-2 indicates that the previous triangle has changed into a combination of two triangles. One has a steeper slope than the initial triangle had, and the slope of the other is flatter. Figure 3-3 shows that the lower triangle develops upward, and the slope of upper triangle decreases continually (It seems that the development is very similar to that of a circular arch in this stage). The final state is plotted in Figure 3-4, in which the upper triangle has an approximately horizontal slope, and reaches a new equilibrium state.

Two kinds of failure envelopes are used for analysis. They are the Mohr Failure Envelope and the Mohr-Coulomb Failure Envelope. The difference between these two types of envelopes is that the Mohr Failure Envelope is a curve, while the Mohr-Coulomb Failure Envelope is a straight line.

3.2 Assumptions

The analysis is based on the following assumptions:

1. Both sides of the triangular prism are assumed to be failure surfaces.
2. After the stresses are redistributed, the sides of the prism are still failure surfaces even though their shapes have changed.
3. For active arching, the major principal stress is approximately horizontal in the triangular prism (Evans' and Engesser's theories).
4. The Mohr failure envelope and the Mohr-Coulomb failure envelope are used for analysis.
5. Only one Mohr failure envelope is assumed, but more than one Mohr-Coulomb failure envelopes are assumed for the following reasons: Since the Mohr-Coulomb failure envelope is a straight line, the corresponding slope of the failure surface is unique. A unique failure surface slope cannot explain the actual situation. To solve this problem, more than one Mohr-Coulomb failure envelopes have to be assumed. The Mohr failure envelope, however, has different slopes at different stress levels which corresponds to the actual observation. Details will be explained in section 3-3 and 3-4.
6. The term "i" is defined as the initial stage, and the term "l" is defined as the latter stage.
7. The term "m" is a constant, and is defined as $(\Delta \sigma_1)/(\Delta \sigma_3)$. "m" will be used to decide whether the particles, which have new stress states, are still on the same Mohr- Coulomb Failure Envelope by comparing the old "m" with the magnitude of the new "m".

3-3 The Explanation of Triangular Arching by Using the Mohr-Coulomb Failure Envelope

3.3.1 The Relationship between Different Stress States on the Same Failure Envelope

After the stresses redistribute in the soil, the Mohr-Coulomb failure envelope can be changed. There is a relationship between stresses if the soil still has the same Mohr- Coulomb failure envelope. i.e. the same slope of slip lines exit as before the stress redistribution. This rela-

tionship is explained below.

The basic assumptions are: (See Figure 3-5)

$$\sigma_{1l} = \sigma_{1i} - \Delta\sigma_1, \tag{3.1}$$

$$\sigma_{3l} = \sigma_{3i} - \Delta\sigma_3, \tag{3.2}$$

$$\frac{\Delta\sigma_1}{\Delta\sigma_3} = m, \tag{3.3}$$

$$p = \frac{\sigma_1 + \sigma_3}{2}, \tag{3.4}$$

$$q = \frac{\sigma_1 - \sigma_3}{2}, \tag{3.5}$$

Where the point "e" is the center of the original Mohr Circle, and "f" is the center of the Mohr Circle after the stresses are redistributed.

The first equation is

$$\frac{\overline{af}}{\overline{be}} = \frac{\frac{(\sigma_1 - \Delta\sigma_1) - (\sigma_3 - \Delta\sigma_3)}{2}}{\frac{(\sigma_1 - \sigma_3)}{2}} = \frac{\sigma_1 - \sigma_3 - (m-1)\Delta\sigma_3}{\sigma_1 - \sigma_3} = \frac{2q - (m-1)\Delta\sigma_3}{2q}. \tag{3.6}$$

Because the triangle o-a-f ~ the triangle o-b-e, the second equation is

$$\frac{\overline{af}}{\overline{be}} = \frac{\overline{of}}{\overline{oe}} = \frac{\frac{(\sigma_1 - \Delta\sigma_1) + (\sigma_3 - \Delta\sigma_3)}{2}}{\frac{(\sigma_1 + \sigma_3)}{2}} = \frac{2p - (m+1)\Delta\sigma_3}{2p}. \tag{3.7}$$

From the above two equations, we can get

$$\frac{2q-(m-1)\Delta\sigma_3}{2q} = \frac{2p-(m+1)\Delta\sigma_3}{2p} \tag{3.8}$$

$$m = \frac{p+q}{p-q} = \frac{\frac{\sigma_1+\sigma_3}{2}+\frac{\sigma_1-\sigma_3}{2}}{\frac{\sigma_1+\sigma_3}{2}-\frac{\sigma_1-\sigma_3}{2}} = \frac{\sigma_1}{\sigma_3}. \tag{3.9}$$

Because

$$m = \frac{\Delta\sigma_1}{\Delta\sigma_3}, \tag{3.10}$$

then

$$m = \frac{\Delta\sigma_1}{\Delta\sigma_3} = \frac{\sigma_1}{\sigma_3}. \tag{3.11}$$

Therefore, after the stresses are redistributed, a new 'm' can be obtained according to the above conclusion. The "m", therefore, will allow one to determine the new slope of the Mohr-Coulomb Failure Envelope. The new slope will become steeper if the new 'm' is greater than the old 'm', and vice versa.

Two variables are defined as below:

$$m_1 = \frac{\sigma_{1i}}{\sigma_{3i}} \tag{3.12}$$

$$m_2 = \frac{\sigma_{1l}}{\sigma_{3l}}. \tag{3.13}$$

The definitions of m_1 and m_2 will be used in the following section.

3.3.2 The Explanation for the Development of Triangular Prisms

There are three different regions with which we are concerned (see Figure 3-2). Region 'A', which is at the edge of top triangle, is getting a flatter failure slope (see Figures (3-1, 3-2, 3-3, and 3-4). Point 'B', which is at the intersection point of the upper and the lower triangles, is moving upward while region 'C' retains almost the same slope. It is noted that all these parts of the prism are at relative and not absolute positions.

Because major principal stresses are approximately horizontal in the triangular prism, the pole point of the Mohr Circle is at the σ_1 point. The direction of the failure surface can be obtained from the straight line that passes the pole and the point where the failure envelope is tangent to the Mohr circle.

Region 'A' will expand vertically when the trapdoor moves downward. Because the vertical support is released; the vertical stress σ_{3i} will therefore decrease by $\Delta\,\sigma_3$. Because the slope of the failure surface is getting flatter in region 'A', the Mohr-Coulomb Failure Envelope shifts to a steeper slope. In other words, this part of the soil develops a bigger friction angle, and can keep the upper triangle flatter (See Figure 3-6).

From the above conclusion of Section 3.3.1,

$$\frac{\sigma_{1l}}{\sigma_{3l}} = \frac{\sigma_{1i} - \Delta\,\sigma_1}{\sigma_{3i} - \Delta\,\sigma_3} = m_2 > m_1 = \frac{\sigma_{1i}}{\sigma_{3i}}. \tag{3.14}$$

Therefore,

$$\sigma_{3i}(\sigma_{1i}-\Delta\sigma_1) > \sigma_{1i}(\sigma_{3i}-\Delta\sigma_3) \tag{3.15}$$

$$\sigma_{3i}\cdot\Delta\sigma_1 < \sigma_{1i}\cdot\Delta\sigma_3 \tag{3.16}$$

$$\frac{\Delta\sigma_1}{\Delta\sigma_3} < \frac{\sigma_{1i}}{\sigma_{3i}} = m_1. \tag{3.17}$$

The change in horizontal stress will be smaller than 'm_1' times the change in the vertical stress. The value of 'm_1' will be different when different kinds of sand are concerned.

Region 'C', seems to keep the original slope of the failure surface while the other regions are changing the slopes of the failure surface (see Figures 3-2, 3-3, and 3-4). This means that those on the edge of the lower triangle will have almost the same Mohr-Coulomb Failure Envelope, whose ratio of change in major principal stress to the change in minor principal stress is m_1, too. Actually, from Figure 2-14, one can see that the maximum shear strain remain almost unchanged in magnitude at the innermost edge of the lower triangle. For a specific Mohr-Coulomb Failure Envelope whose slope is not zero, those points which have the same maximum shear stress on the failure surface should be on the same Mohr Circle. This means that there are no changes, or only slight changes in the major and minor principal stresses (see Figure 3-8).

3.4 Explanation of Triangular Arching by Using the Mohr Failure Envelope

The Mohr Failure Envelope is a curve, unlike the Mohr-Coulomb failure envelope which is a straight line. The reason that most scientists use the Mohr-Coulomb Failure Envelope is because the Mohr-Coulomb failure envelope is simple and easy to use. However, the Mohr Fail-

ure Envelope is closer to the test result (Halts, & Kovacs, 1981).

The pole point of the Mohr Circle is still at the σ_1 point, and the direction of failure surface can also be obtained from the straight line that passes through the pole and the point where the failure envelope is tangent to the Mohr Circle.

Only two regions 'A', and 'C' can be explained by using the Mohr Failure Envelope:

Region 'A' will expand vertically when the trapdoor moves downward, and the horizontal stress σ_1 will decrease with respect to the decrease in vertical stress σ_3. The Mohr Circle, therefore, moves left. Because the slope of the Mohr failure envelope gets steeper when the stresses get smaller. Then, the slope of the failure surface gets flatter until the Mohr failure envelope is tangent to the point of origin. It means that the slope of the failure surface cannot be flattened anymore (see Figure 3-9).

Region 'C' again seems to keep the same slope of the failure surface. This means that those points on the edge of the lower triangle (See Figures 3-2, 3-3, and 3-4) will have the same, or almost the same, stresses. On the other hand, Figure 2-14 shows us that there are the same maximum shear stress in the innermost triangle. For a specific Mohr Failure Envelope, every Mohr circles tangent to the failure envelope, has exact only one maximum shear stress. So those points which have the same maximum shear stress on the failure surface have the same Mohr Circle, which means that there are no changes, or only slight changes in the major and minor principal stresses (see Figure 3-10).

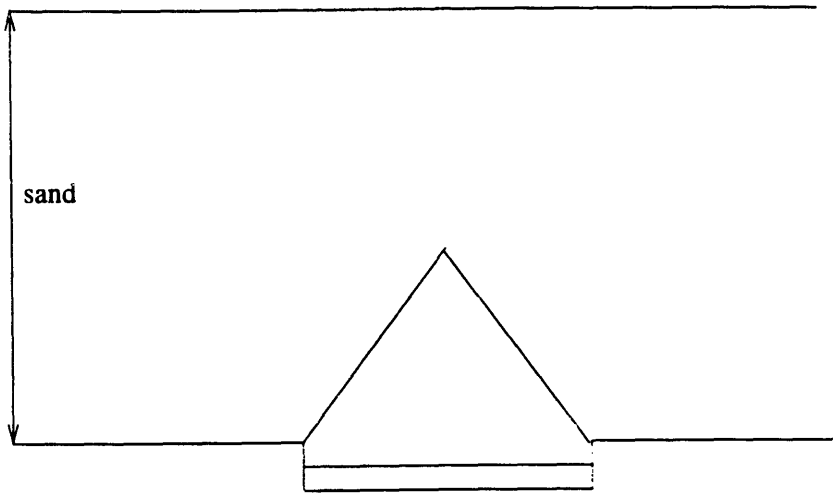

Figure3-1. the First Stage of the Triangular Prism.

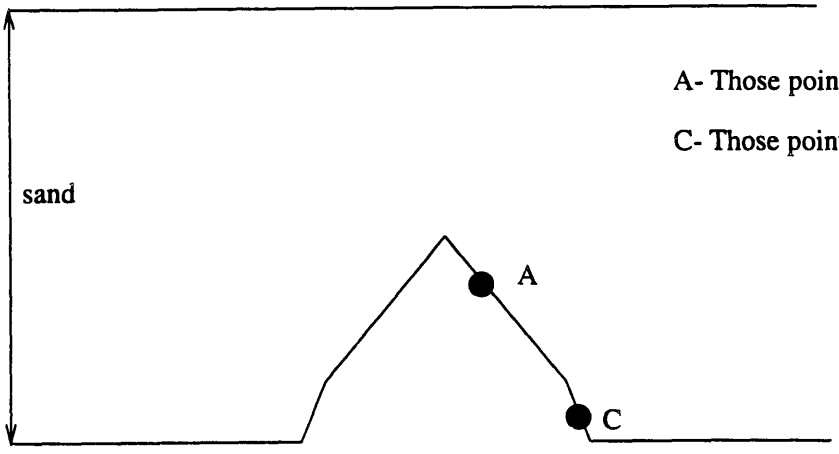

A- Those points on the edges of upper triangle

C- Those points on the edges of lower triangle.

Figure 3-2. The Second Stage of the Triangular Prism.

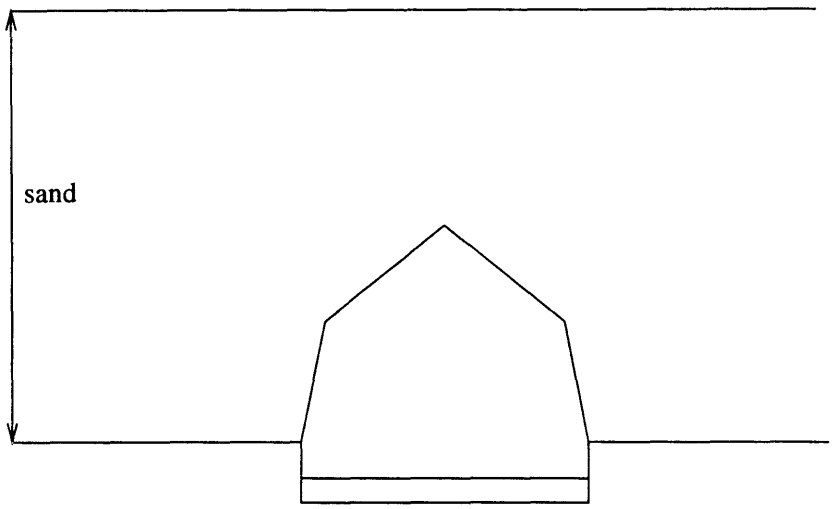

Figure 3-3. The Third Stage of the Triangular Prism.

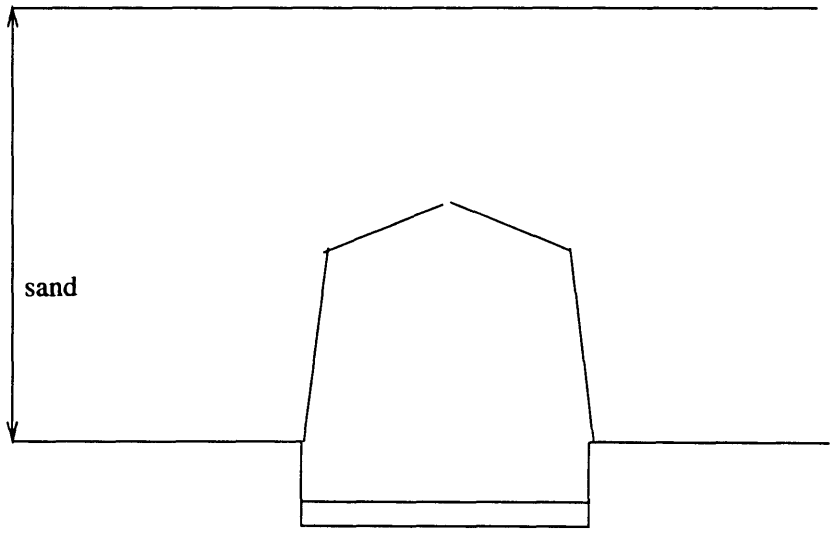

Figure 3-4. The Fourth Stage of the Triangular Prism.

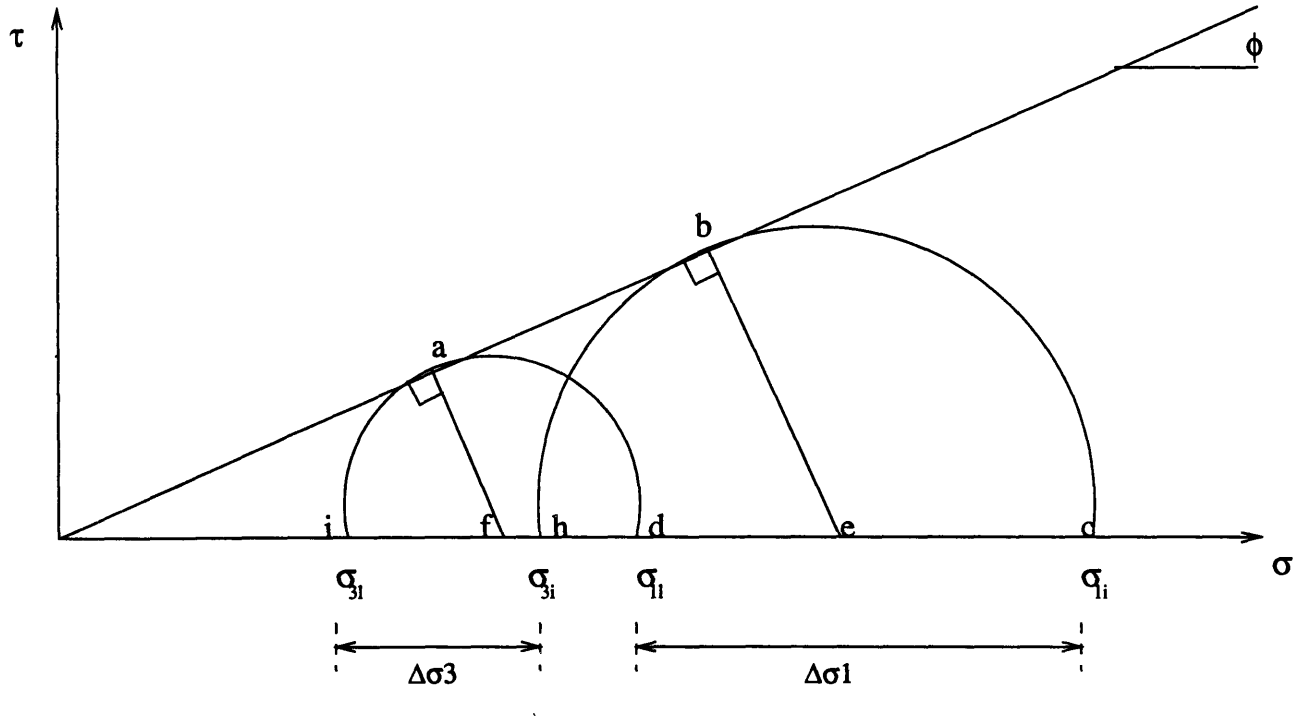

Figure 3-5. The Mohr-Coulomb Failure Envelope and Mohr Circles.

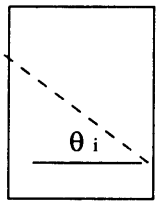

The Initial Failure Surface

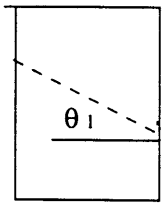

The Later Failure Surface

$$\frac{\sigma_{1i}}{\sigma_{3i}} = m_1 \qquad \theta = 45^{o} - \frac{\phi}{2}$$

$$\frac{\sigma_{1l}}{\sigma_{3l}} = m_2$$

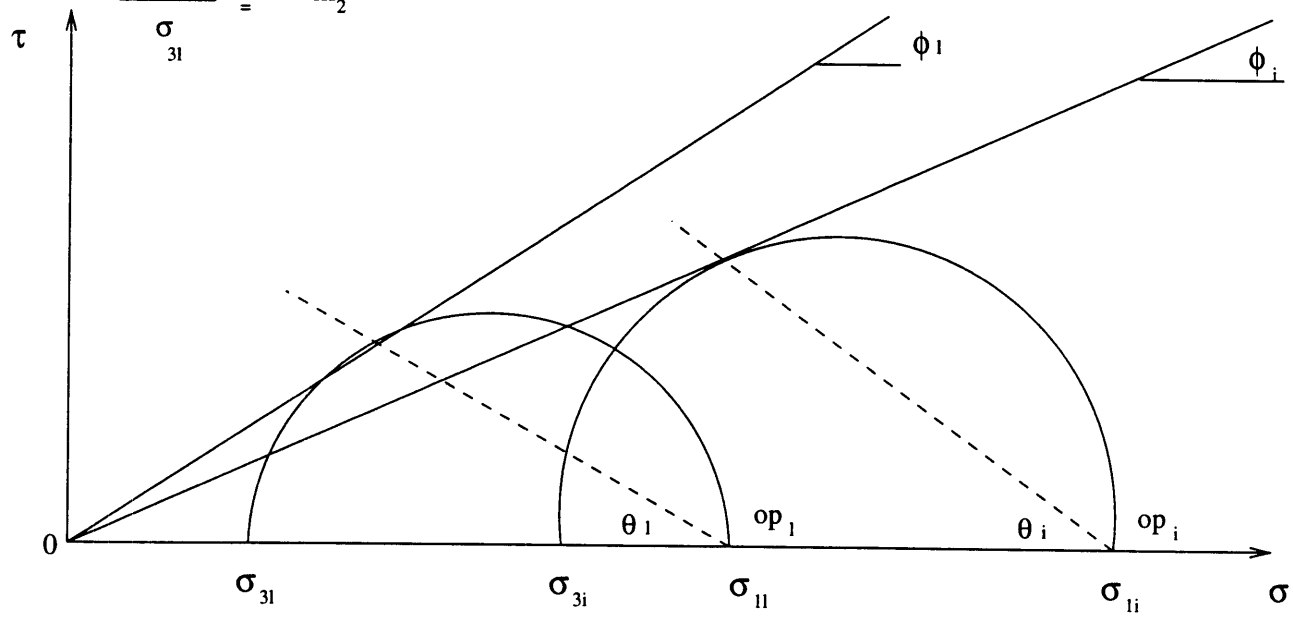

Figure 3-6. The Development of the Failure Surface in Region 'A'.

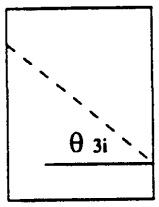

The Initial Failure Surface

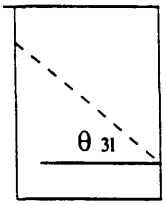

The Latter Failure Surface

$$\frac{\sigma_{1i}}{\sigma_{3i}} = m_1$$

$$\frac{\sigma_{1l}}{\sigma_{3l}} = m_2$$

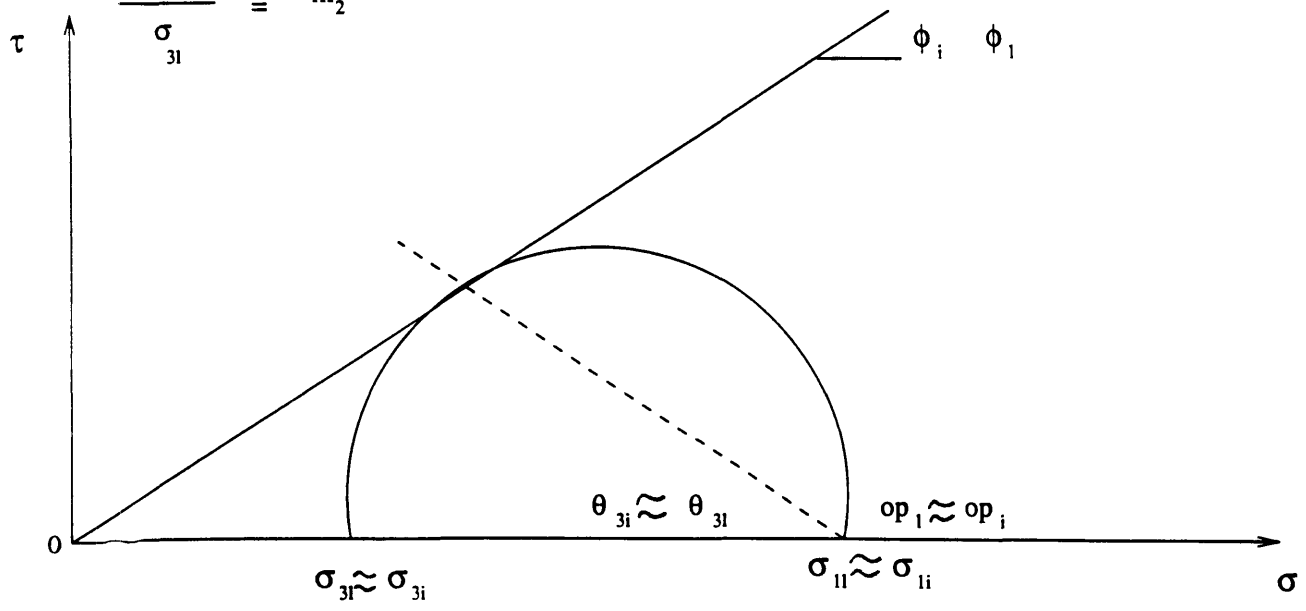

Figure 3-7. The Development of the Failure Surface in Region 'C'.

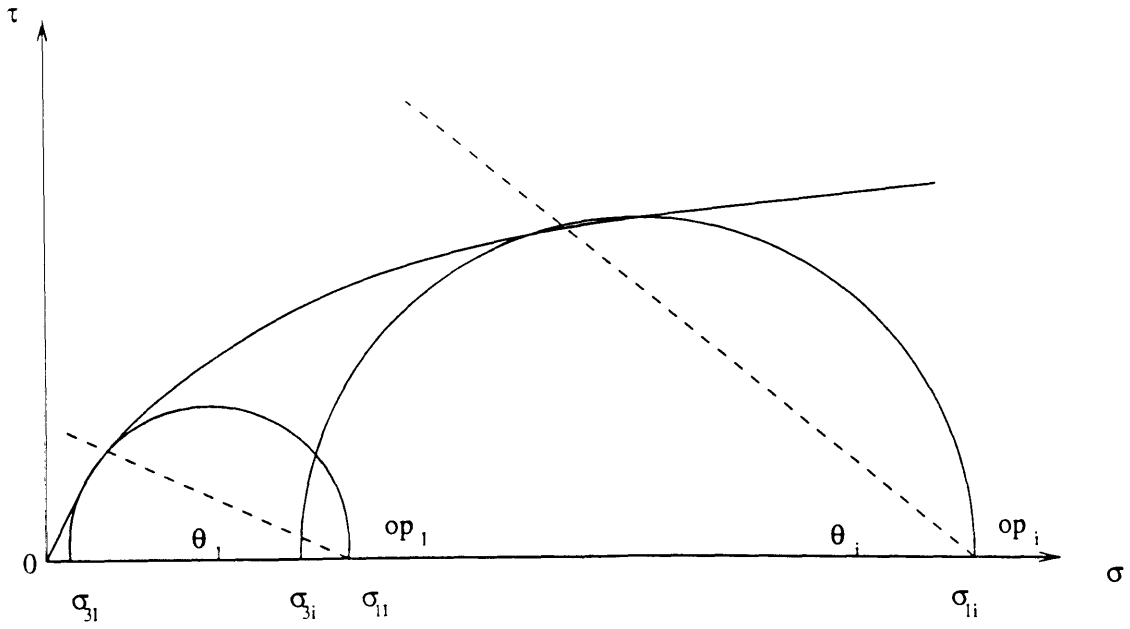

Figure 3-8. The Developement of the Failure Surface in Region 'A' Explained by the Mohr Failure Envelope.

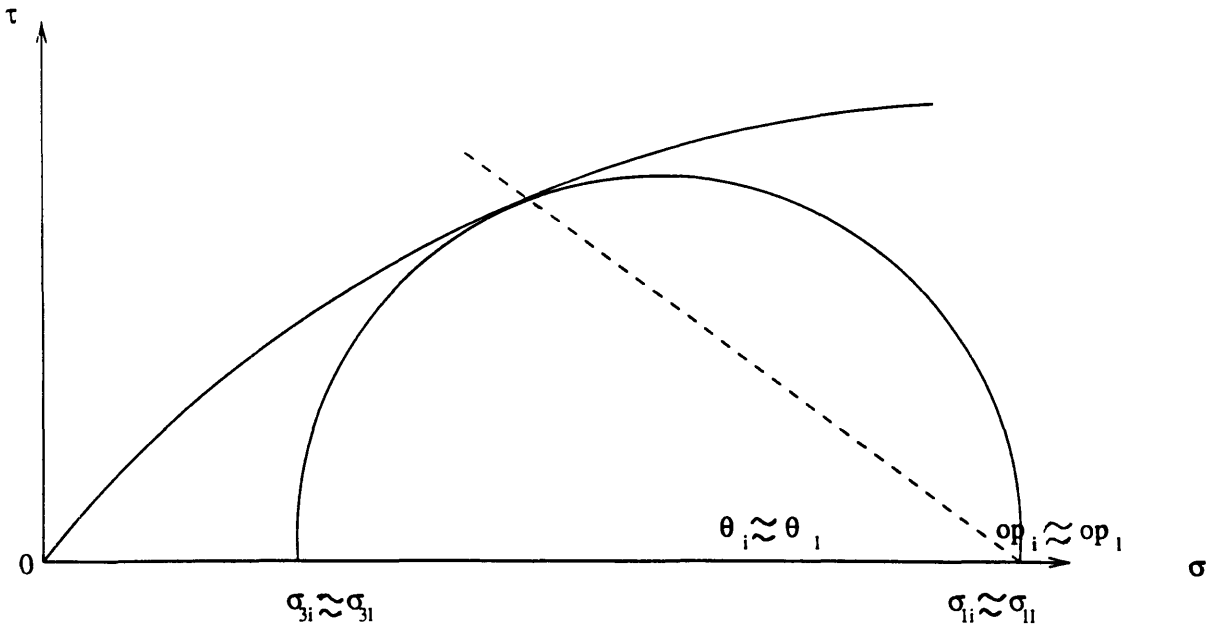

Figure 3-9 The Developement of Failure Surface in Region 'C'

Explained by the Mohr Failure Envelope

Chapter 4. Application of Triangular Arching in the PreSupport Tubes

4.1 Introduction

From the results of Evans' and Stone's research (see Figures 2-11, 2-13, 2-14), several phenomena can be observed. For example, the sand samples always try to form a triangular prism in the early stage. After the trapdoor effect starts, the shapes of the yield zone changes with the downward movement of the trapdoor. In real cases, the time period between the completion of driving a micro-tunnels and the completion of installing the pre-supporting tubes is a major concern. The longer the time period that leaves the opening unsupported, the greater the downward the movement of the crown (See Figure 4-1). Larger downward movements of the upper half of the tunnel face will produce the same effect as the downward movement of a trapdoor.

Second, after the width and location of the trapdoor are decided, the shape of the yield zone can be a parabola (Iglesia, 1991), or triangle (Evans, 1983), and have an angle of $\theta = 90° - \phi$ at the edges when the minimum load is reached (See Figure 2-15). Therefore, the width and location of the trapdoor becomes a major concern in deciding the failure zone.

Bulson (1985) did a series of model tests using non-circular pipes, closed cylinders and shells under static loads. He found that the stress distribution is totally different from that of the circular tubes, and the surface settlement is therefore different. For example, thin-walled square tubes have similar inward deflections between the roof and sides at deep cover, but have only a small inward deflection of the sides at shallow cover. He also maintained that he monitored results for different shapes of the pipe such as the elliptic culverts used in Canada.

In this chapter, the idea of a triangular prism is extended into the open face of a tunnel or a pre-support tube, by assuming that the open face can be divided into a combination of many horizontal trapdoors, and assuming that those trapdoors have a very small height. Furthermore, the assumption is extended to compare the different tube shapes. The circular tube and the triangular tube, will be used for analysis by employing empirical methods, and by using a finite element analysis to compare different ground surface settlements induced by different tube shapes.

4.2 Comparisons between the Circular Tube and the Triangular Tube

4.2.1 The Possible Width of the Failure Base

All circular tubes can be roughly divided into two groups. thick-walled pipe, and thin-walled pipe. In general, the thin-walled pipe is more flexible than the thick-walled pipe. A useful experimental program was reported by Allgood and Herrmann(1969), who examined reinforced model cylinders buried in dry sands with their longitudinal axis parallel to the surface. According to this procedure, twelve cylinders were tested with varying thicknesses, reinforcements, and cover depths.

The outcome of the tests shows that the thick-walled cylinders have a small deflection at a low surface load. However, a thick-walled cylinder can develop longitudinal cracks, lose stiffness, and, therefore, have higher deflections than a thin-walled pipe at a higher load. In real cases, if longitudinal cracks occur, the thick-walled concrete pipe will produce more soil loss than the thin-walled pipe. The cracks could extend to the springline (see Figure 4-2).

Bulson (1985) did some collapse model tests using thin-walled cylinders and pipes (see Figures 4-2 & 4-3). In his tests, twelve cylinders were tested, with varying thicknesses, reinforcements and cover depths. The results of his tests indicate that, regardless of the depth of cover, the pipes will eventually end up with the same forms, yielding from the points close to the springlines, which are at the position of the maximum cross-section. From the results of thin-walled and thick-walled pipe tests, it seems to be reasonable to assume that the horizontal maximum cross-section is the preferred location to assume an equivalent trapdoor base; because the crack, or yielding, will finally extend from springline to springline.

There are different opinions about the location and width of the trapdoor base. Munn et al (1970), for example, have suggested the width of the base should match the points of possible crown failure of the tube (see Fig 4-5). Most people choose the diameter of the tube as the width of the base, however, since it seems more reasonable to use the diameter as the width of the trapdoor base when the shield tunnel, or micro-tunnel, is excavated in clay soils. This is so since clay has a higher strength due to cohesion, which possibly allows workmen to finish the support before the clay yields.

For sand, most of the deformation takes place immediately after the excavation. The sand will soon reach the maximum soil strength state, which requires little deformation. It is reasonable to assume that the triangular prism still forms even if there is good workmanship. Therefore, the analytical method used for sand will be different from the one for clay. The assumed width of the trapdoor base with sand changes with location, which will be discussed in section 4.2.2.

4.2.2 The Base Location during the Occurrence of the Trapdoor Effect

Again, there have been many different assumptions regarding the location of the trapdoor base. Placing the base at the crown of the tunnel seems too conservative when the diameter of the tube is still assumed to be the width of the trapdoor. However, the assumption of Munn et al (1970), who performed the tests on circular arches and presented the idealized failure mode (see Figure 4-5), seems to be overly optimistic about the location of the crown failure. In the same year, Meyerhof (1970) did some interesting model tests and found that the crown failure is not limited to the two points of Munn's, but can extend from one springline to the other when a relatively shallow cover is concerned. However, it is conservative to use the biggest slipline, which tangent to the opening, for design.

Figures 2-4 and 2-5 show an important fact that the yield triangle can propagate along its sliplines, which are tangent to the opening in a horizontal plane at the elevation of the tunnel center, which is also the maximum horizontal section of the opening. The directions of crack propagation are almost the same as those of the sliplines (see the connected straight lines in Figure 2-4). To be conservative, in the comparison of the circular tube and triangular tube in sand, the width of the trapdoor's base is, therefore, assumed to be the distance between the two points where the two tangent sliplines intersect the horizontal plane of the maximum section.

4.2.3 Assumptions Used for the Empirical Comparison

Einstein, et. al. (1980) presented a way to optimize the performance of supports (see Figure 4-7). They argue that the optimization requires that the support system be designed so that the maximum strength of the ground mass is mobilized. i.e. the soil itself sustains most of the redis-

tributed load resulting from the excavation, and leaves only a small load to be carried by the support. So they try to intersect the ground characteristic curve at its lowest point by adjusting the stiffness and location of support. However, we must also notice that different sizes of openings will produce different maximum strengths. The bigger the opening is, the larger the minimum force is required to be supported.

Peck and Schmidt (1969) presented an empirical method to calculate the ground surface settlement. In their method, one of the parameters used for analysis is the amount of ground loss V_0, which is defined as the volume per unit tunnel length enclosed between the final excavation line and the initial position of these points prior to excavation (see Figure 4-8). They determine this value as a percentage of the cross-section.

However, when the different shapes of openings are analyzed, the yield zones shall follow the sliplines. The circular tube will, therefore, have a larger ground settlement. The reason is explained below (see also Figure 4-9):

1. The geometry of the half circular tube can be defined as half circle a-b-d-e.
2. The geometry of the triangular tube can be defined as triangle a-c-e.
3. The method mentioned in Section 4-2-2 is used to decide the width and location of the trapdoor effect for the two different kinds of tubes.
4. Only the upper parts of the tubes are used in the analysis of the trapdoor effect.
5. When the triangular tubes a-c-e-is concerned, the maximum possible sliplines, which pass the tube, are $\overline{ac}$ and $\overline{ce}$. So the upper yield zone should be triangle a-c-e.
6. When the circular tube is considered, the maximum possible sliplines for the tubes are $\overline{hf}$ and $\overline{hj}$, which are the tangent lines of the tube. So the upper yield zone should be the triangle f-h-j. The top angle of this triangle will be maintained in the following section.

4.2.4 Quantitative Comparison Using the Empirical Method

"Prediction of ground loss is very difficult because of the influence of many factors not only of the soil (non-linear behavior, delayed deformation), but also details of the construction procedure (type of excavation and support systems, advance rate, etc.), and the 3-dimensional character of the problem. As a consequence, the theoretical methods by themselves are not suitable, and only the experience gained from measurements in actual cases gives a basis for reliable predictions." (Sagaseta, 1992).

The most successful empirical method has been the "Error Curve" method (Peck, 1969; Schmidt, 1969). By using the following equation. Figure 4-8 shows the transverse settlement profile fitted by Gauss curve:

$$\delta_v = \delta_{max} \cdot exp\left(\frac{-x^2}{2i^2}\right) \tag{4.1}$$

where δ_v is the transverse settlement, δ_{max} is the maximum settlement (at the tunnel centerline, i.e. x=0), and "i" is the abscissa of the point of inflection. A property of the error curve is the volume of settlements enclosed by the error curve and the horizontal axis:

$$V_s = (2\pi)^{0.5} \cdot i \cdot \delta_{max} = 2.5 \cdot i \cdot \delta_{max} \tag{4.2}$$

where V_{s_s} is the volume of settlements enclosed by the error curve and the horizontal axis, and is related to the amount of ground loss V_0. V_0 is generally given as k percentage of the cross-section area of the tunnel. Attewell et. al. (1986) suggested that the value k is usually between 0.5 percent and 2.5 percent when cohesive soils are considered, and ranges from 2 percent to 5 percent when the tunneling is done in granular soils above the water table. After comparison with cohesive soils, Attewell et. al. (1986) found that the granular soils are more dependent on operators' expe-

rience and skills. They also mentioned that the k value should be adjusted to 2-10 percent when the granular soils are below the water table, and be appropriately chosen as 5 percent for preliminary calculations. V_s is generally chosen as a fraction "α_v" of the ground loss at the tunnel ($V_s = \alpha_v \cdot V_0$), where the factor α_v is defined as "1" when incompressible soil (clay) is concerned, and is $0 \le \alpha_v \le 1$ when drained soil is involved.

Peck (1969) also suggested that the ratio "i/D" depends on the relative depth "H/D" and the soil types, where 'D' is the diameter of the tunnel, and 'H' is the length of the cover above the crown of the tunnel. The further revision reduces the influence of the soil types, and a unique relation between "i/D" and "H/D" is proposed for any type of soil:

$$\frac{i}{D} = \frac{1}{2} \cdot \left(\frac{H}{D}\right)^n \tag{4.3}$$

where the "n" is 1.0 (Attewell, 1977) or 0.8 (Clough & Schmidt, 1981; Schmidt, 1988)(see Figure 4-11).

My assumptions for the empirical analyses are:

1. The triangular yield zones are used to estimate V_o, not the cross sections of the tunnel.
2. The ground loss V_o is equal to "K" percentage of the yield zone. i.e. $V_o = K \cdot A$.
3. The factor α_v is taken as the mean value of the drained case where $0 \le \alpha_v \le 1$ (Attewell et.al., 1977). i.e. α_v is 0.5.
4. The factor 'n' is equal to 1 (Attewell's assumption, 1977).

Hence:

i/D=1/2 * (H/D); thus, i=1/2 * H

$$V_o = K \cdot A \tag{4.4}$$

where A is the area of the triangular yield zone, and K is a constant.

$$V_s = \alpha_v \cdot V_o = 0.5 \cdot V_o = 2.5 \cdot i \cdot \delta_{max} = 1.25 \cdot H \cdot \delta_{max} \tag{4.5}$$

$$0.5 \cdot K \cdot A = 1.25 \cdot H \cdot \delta_{max} \tag{4.6}$$

thus

$$\frac{\delta_{max}}{K} = 0.4 \cdot \frac{A}{H} \tag{4.7}$$

As long as we get the internal friction angle ϕ of the soil, the area of the yield zone can be obtained by using 2ϕ as the top angle of the triangle; The triangle d-e-f is tangent to the circular tube, and the triangle a-b-c is a similar, and smaller triangle with d-e-f; the calculation for A is discussed below (see Figure 4-12).

The estimated yield zones of circular and triangular tubes at the friction angle is ϕ, where the radius $\overline{ob}$ is chosen as an unit length "1 m", which is a common size for horizontal pre-supporting pipe, and the angles $\hat{cab}$ and $\hat{fde}$ are equal to twice the frictional angle ϕ. Thus,

from the Figure 4-12,

$$\overline{oe} = \sec\phi \tag{4.8}$$

$$\overline{od} = \overline{oe} \cdot \tan\left(\frac{\pi}{2} - \phi\right) = \sec\phi \cdot \cot\phi = \csc\phi \tag{4.9}$$

$$\overline{oa} = \cot\phi \tag{4.10}$$

$$A_{abc} = \frac{2.\cot\phi}{2} = \cot\phi \tag{4.11}$$

where the triangular tubes are used.

$$A_{def} = \frac{2\sec\phi \cdot \csc\phi}{2} = \sec\phi \cdot \csc\phi \tag{4.12}$$

where the circular tubes are used.

$$\frac{\delta_{max\,(abc)}}{K} = \frac{0.4}{H} \times \cot\phi \tag{4.13}$$

$$\frac{\delta_{max\,(def)}}{K} = \frac{0.4 \cdot \sec\phi \cdot \csc\phi}{H} \tag{4.14}$$

$$\frac{\delta_{max\,(def)}}{\delta_{max\,(abc)}} = \frac{0.4 \cdot \sec\phi \cdot \csc\phi}{0.4 \cdot \cot\phi} = \frac{1}{\cos\phi^2} \tag{4.15}$$

In general, the friction angles of sand range from 30° for loose sand to 45° for dense sand (Lambe and Whitman, 1979). Therefore, the biggest difference in ground surface settlement occurs between the triangular and circular tube when ϕ is close to 45°(dense sand). The ratio of ground surface settlement induced by a circular tube to the one induced by a triangular tube is about 2 for ϕ = 45° (dense sand). This ratio of ground surface settlement is 1.33 when ϕ is close to 30°(loose sand).

A program written for the calculation of the settlement at the ground surface is listed in Appendix A. This program is based on the "Error Curve". The only difference between my program and the "Error Curve" is that the yield zones are used to estimate the ground loss, not the tunnel cross-section. For the purpose of simplicity, there are some assumptions presented below (see Figure 4-12):

1. When the horizontal distance between the vertical center line and the pre-support tube, x, is between one sixth of the radii of the tunnel (see Figure 4-12, section A), the pre-supporting tubes are arranged with a midpoint distance equal to one full diameter in the x direction. The vertical positions can then be obtained by the Pythagorean Theorem.

2. The rest of pre-support tubes (see Figure 4-12, section B) are arranged with an space at midpoint distance equal to one full diameter in the vertical direction. The x positions can also be obtained by the Pythagorean Theory
3. The "Error Curve" is based on natural openings, or caverns. It does not include the effect of reinforcement, temporary or permanent support. So the results of calculations are higher than the field settlement using modern technologies; the results should multiplied by a reduction factor, which will be different for different methods, or technologies used to reduce the settlements.

4.3 The Numerical Comparisons between the Circular and Triangular Tubes

4.3.1 Introduction

In this section, the finite element method (FEM) is used to compare the difference between the traditional circular pre-support tube and the proposed triangular pre-support tube. To simplify the comparison, the influence on the neighboring tubes is neglected. In my analysis, a circular and a triangular tube are placed in the same environment, in which they have 200 Kpa uniform surface loading, and have no pressure on the inside surface of the opening; it means that there is no support.

The influence of the depth of cover is determined by using different depths of cover while the ground surface bears the same uniform loading. Therefore, the different ground surface settlements, due to the different depths of cover are obtained.

4.3.2 The Material Models

There are many material models that can be used in the analysis. Even for the same type of soil, different material characteristics can be obtained from various tests. However, the differences between soils are not part of our consideration. To simplify the scope of the problem, the following material models are chosen for this analysis.

Larson (1989) presented the Automated Plane Strain Reinforcement (ASPR) cell (see Figures 4-13, & 4-14), which measures the tensile stresses induced in a planar reinforcement due to the shearing of the surrounding soil. The ASPR cell applies uniform boundary tractions (σ_1, σ_3) to deform the soil compression and can contain a single reinforcement with depth. The results of his five plain strain tests showed that for dense Ticino sand, the soil stiffness modulus ranges from 18,000 to 19,000 kpa; the dry unit weight is about 1.64 g/cm^3; the initial yielding stresses are between 210 to 270 kpa (see Figure 4-15), and the mobilized friction angle is about 52°.

In the present analysis, the stiffness modulus is assumed to be 18,500 kpa, γ_d is assumed to be 1.64 g/, and the initial yielding stress is 240 kpa. However, the friction angle in his model seems too high for practical cases. The reason why he got higher friction angles in ASPR tests is that ASPR tests using low confining stresses. In the real case, the confining stress is larger than ASPR tests. So lower value should be used. 45° is used as the friction angle in my comparison (dense sand). The Poisson ratio is assumed to be 0.3 for analyzing the influence induced by different depths of cover. The perfect elasto-plastic model is used, i.e. the stiffness modulus is zero after the soil yields.

4.3.3 The Geometry of Models

There are two different kinds of tubes used for comparison (see Figure 4-17).The circular pre-support tube has a radius of 1 m. The triangular pre-support pipe has the same circular shape in its lower half potion to reduce the stress concentration. The upper half, however, is a triangular prism. The top angle of the prism is equal to 2ϕ. The angle is the same as assumed by Evans and Iglesia.

Figures 4-18 to 4-20 show the geometry and FEM meshes for the circular tubes with different depths of cover. Figures 4-21 to 4-23 show the geometry and FEM meshes for the triangular tubes with different depths of cover. The boundary conditions are similar in all cases. For example, Figure 18 has the following boundary conditions:

1. Planes EF and FG having a fixity in y direction while there is no fixity in the z direction.

2. Plane HG has a fixity in z direction while there is no fixity in the x direction.

3. Plane EF bears a 200 Kpa uniform vertical load.

4. The circular opening is excavated first, then the gravity is added.

5. There is no load applied on the inner surface of tube.

6. Points G and H are fixed in both y and z directions.

4.3.4 The Finite Element Method (ADINA)

ADINA is a finite element program for two dimensional and three dimensional analysis. Both static and dynamic analysis of structural systems can be analyzed. Its library of material models permits us to analyze both linear and nonlinear materials. There is one limitation for analyzing the soil model. The limitation is that ADINA does not offer a strain softening model for analysis, because ADINA is primarily designed for analyzing structural problems.

4.3.5 The Results of the Numerical Method

Figures 4-23 to 4-25 show the results of ground surface settlements vs. different depths of cover for circular tubes. Figures 4-26 to 4-28 show the results of ground surface settlements vs. different depth of cover for triangular tubes. The above results are summarized in Figure 4-29, and Table 4-1. The results show us that the shallower the cover, the greater the difference between ground surface settlement; the settlement difference is 0.6 mm when the cover is 9m, and is 4.8 mm when the cover is 2 m.

Figures 4-30 to 4-32 show the results of maximum shear stress vs. different depths of cover for circular tubes. Figures 4-33 to 4-35 show the results of maximum shear stress vs. different depth of cover for triangular tubes. The above results are summarized in Figure 4-36, and Table 4-2.

In real design (see Figure 4-16), the triangular pre-support tubes have arc shapes in all

connection points (the top of the triangular prism and the spring line), possibly reducing the stress concentration.

An additional FEM analysis is employed (see Figures 4-37, 4-38, 4-39) to compare different settlements induced by a circular opening and by a larger modified opening. This is one of the possible methods to include the yield zone of the circular tube. The results show that the circular opening a-b-l-k has almost the same ground surface settlements as the Polygon f-b-d-l-k-i (Figure 4-24 and Figure 4-39).

It is possible that the procedures of construction are more complicated when triangular tubes are used instead of circular tubes. However, the above results of the numerical analyses show that the triangular pre-support tubes may be better when the ground surface settlement is a very important consideration, such as in constructing shallow tunnels in cities.

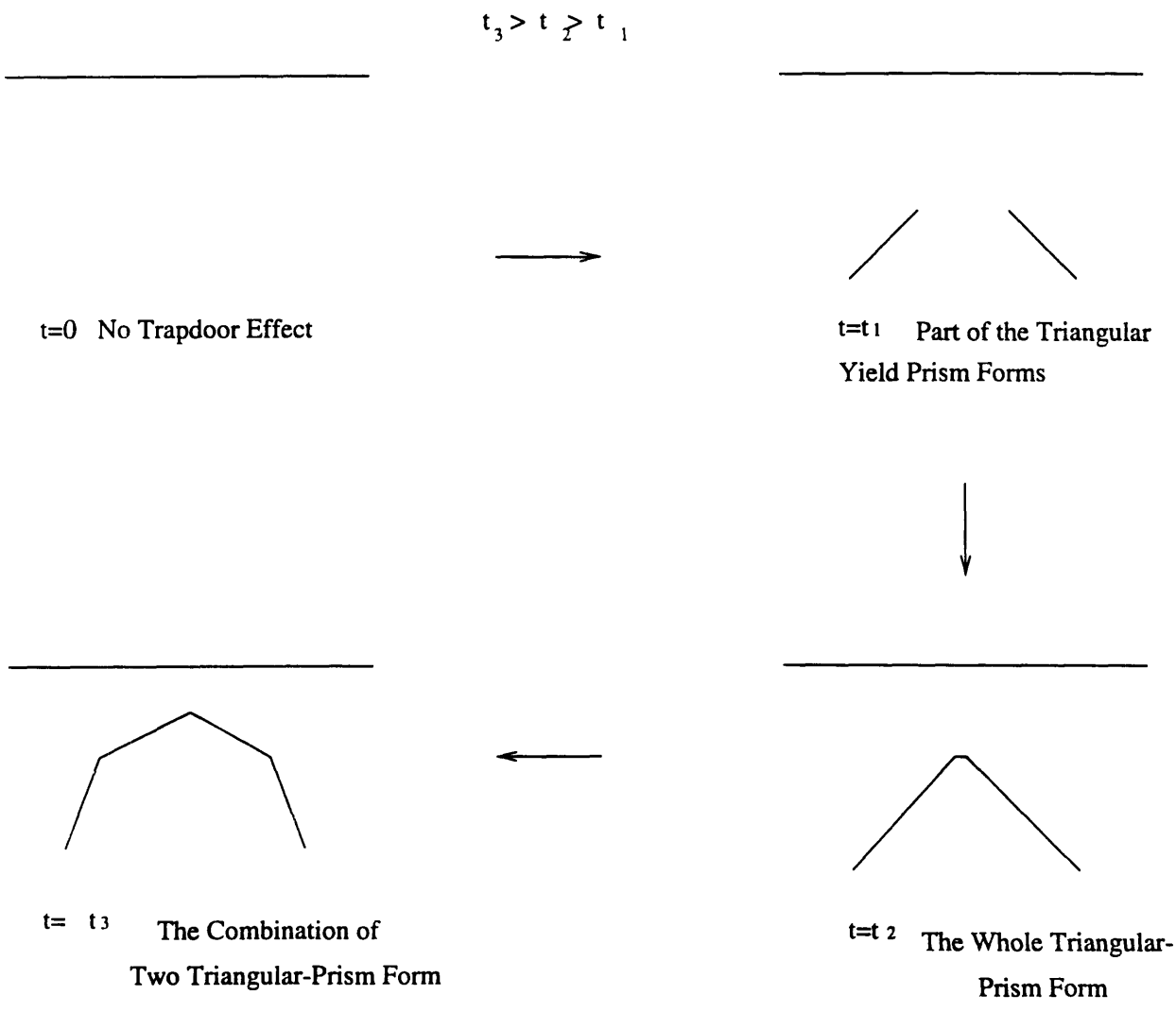

Figure 4-1. The Transformation of the Triangular Arch at Different Unsupport Time Periods after the Tunnel is Excavated.

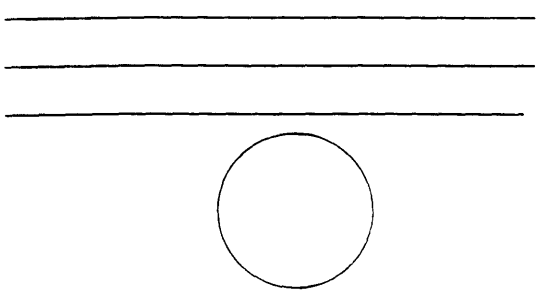

(a) Before Longitudinal Cracking.

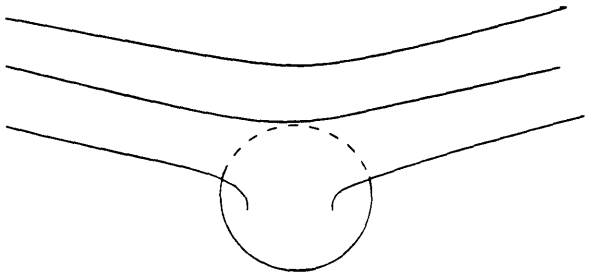

(b) After Longitudinal Cracking.

Figure 4-2. Cracking of Thick-Walled Concrete Tubes.

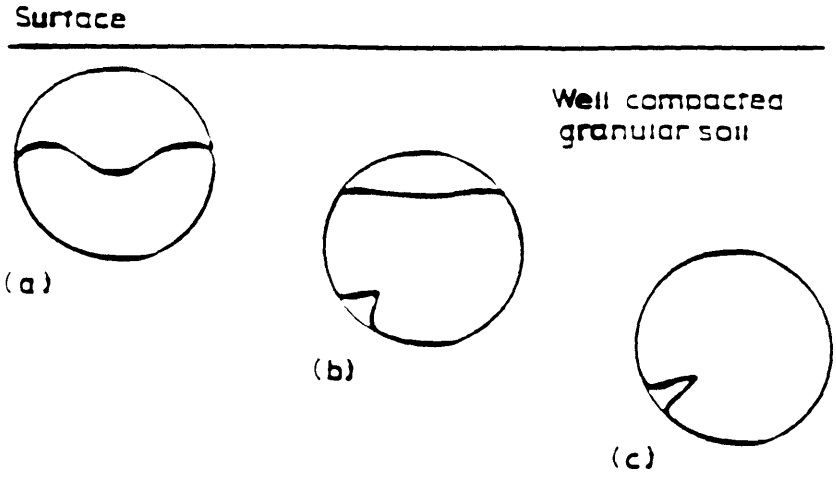

Figure 4-3 Collapse Modes of Thin-walled Buried Cylinders.
(a) Shallow Cover (b) Intermediate Cover (c) Deep Cover.
(Bulson, 1985)

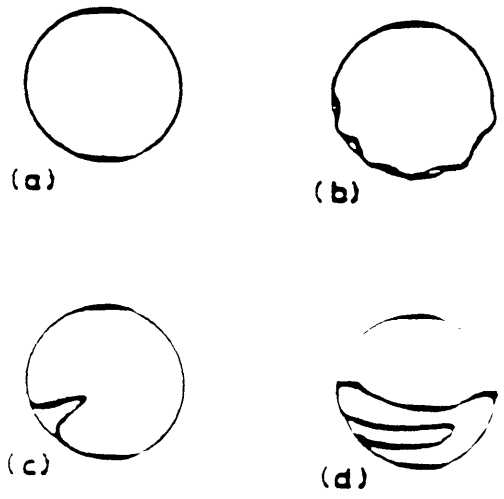

Figure 4-4 Collapse Sequence at Deep Covers (a) Original Shape (b) Lower Rim Buckles (c) One Buckle Grow (d) Final Shape (Bulson, 1985)

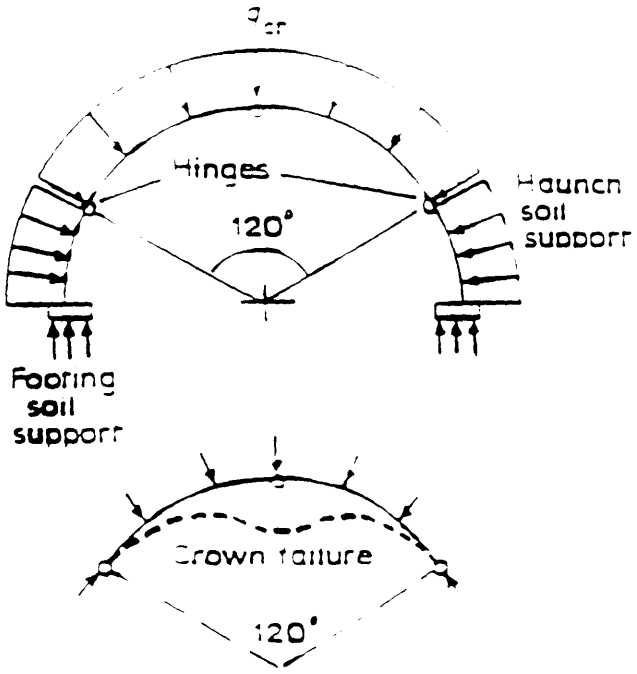

Figure 4-5 Idealized Failure Modes (Munn et. al., 1970)

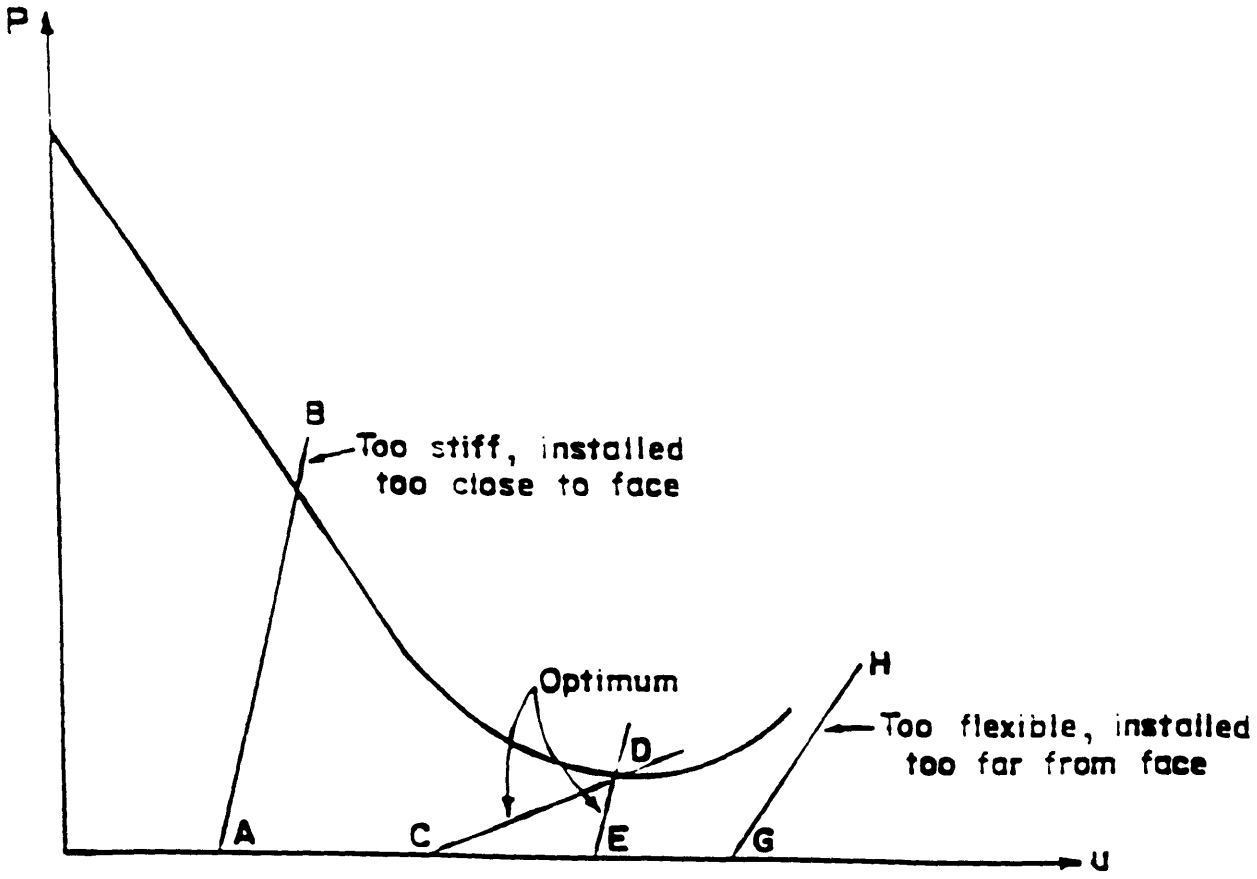

Figure 4-6 Optimization of the Support System (Einstein et. al., 1980)

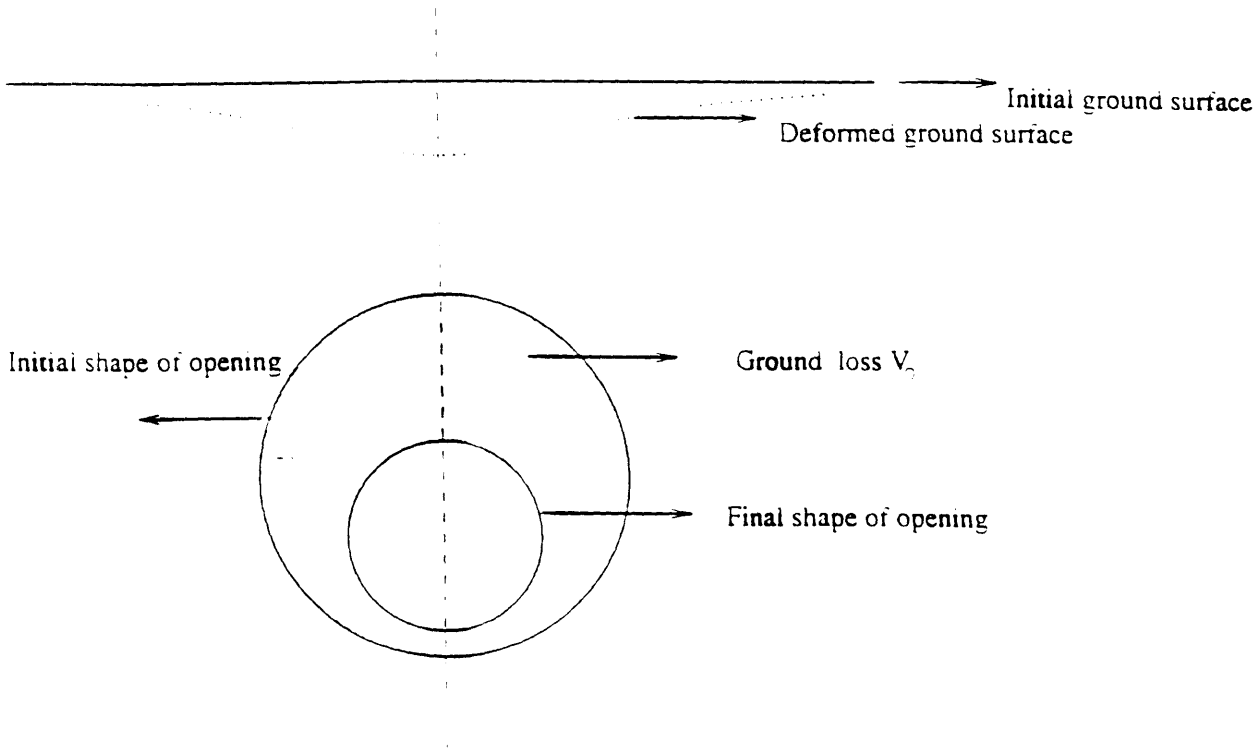

Figure 4-7 The Error Curve and Ground Loss

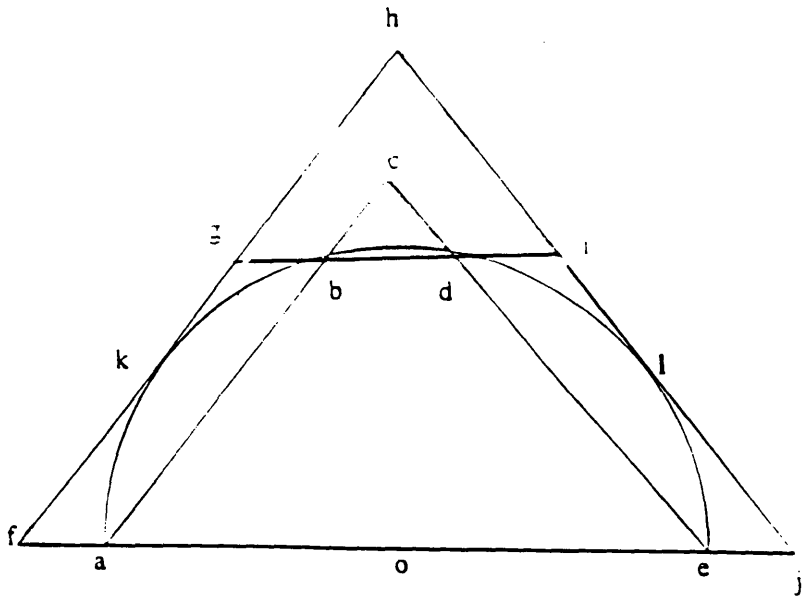

Figure 4-8 The Yield Zones of Circular and Triangular Tubes

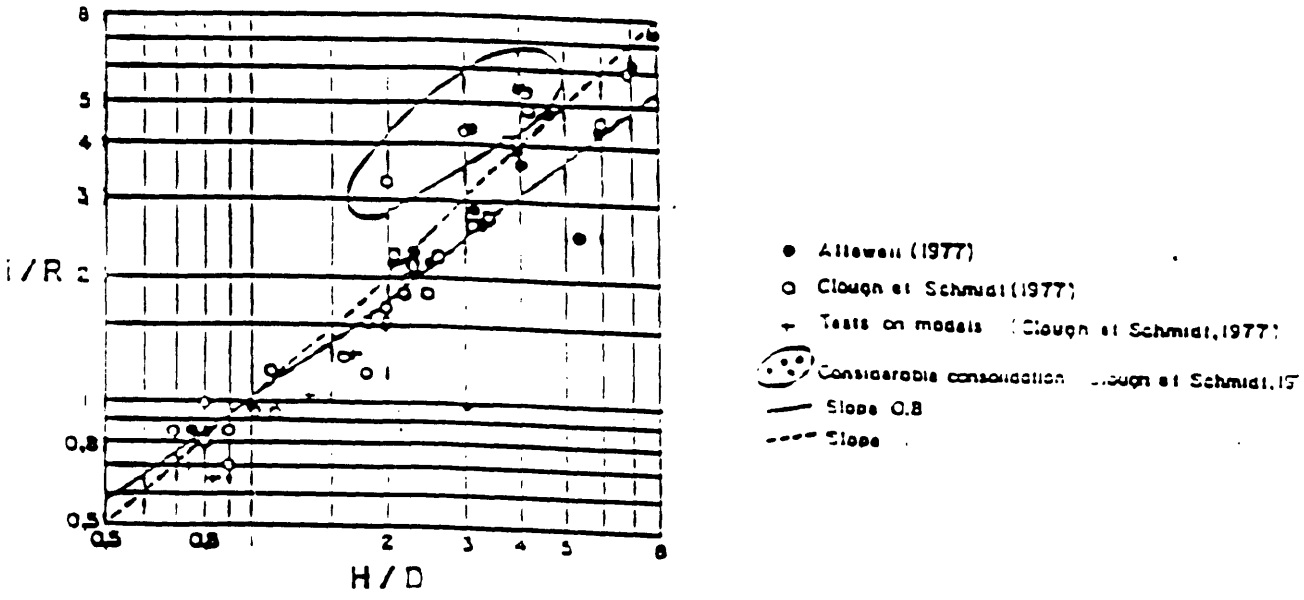

Figure 4-9 Abscissa of the Inflection Point (Schlosser et. al., 1985)

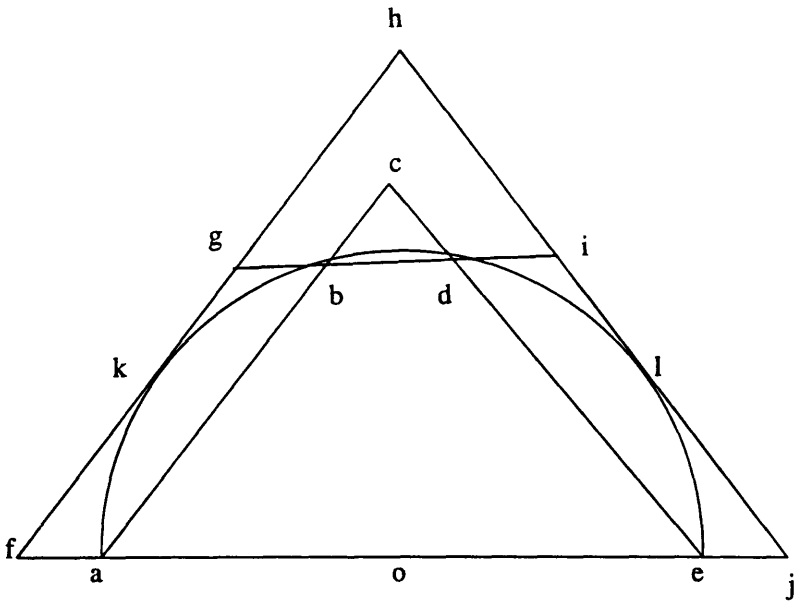

Figure 4-10. The Assumed Yield Zones for Calculating A.

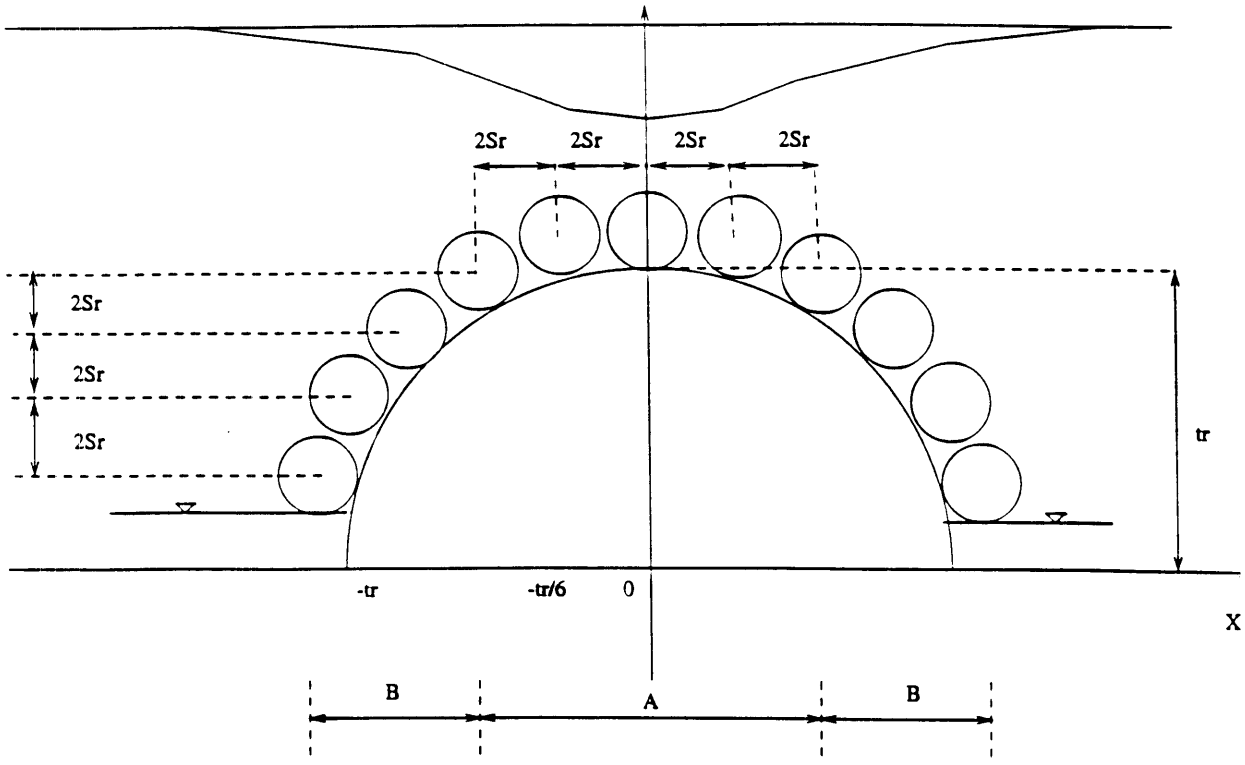

Figure 4-11. The Model for the Settlement Program.

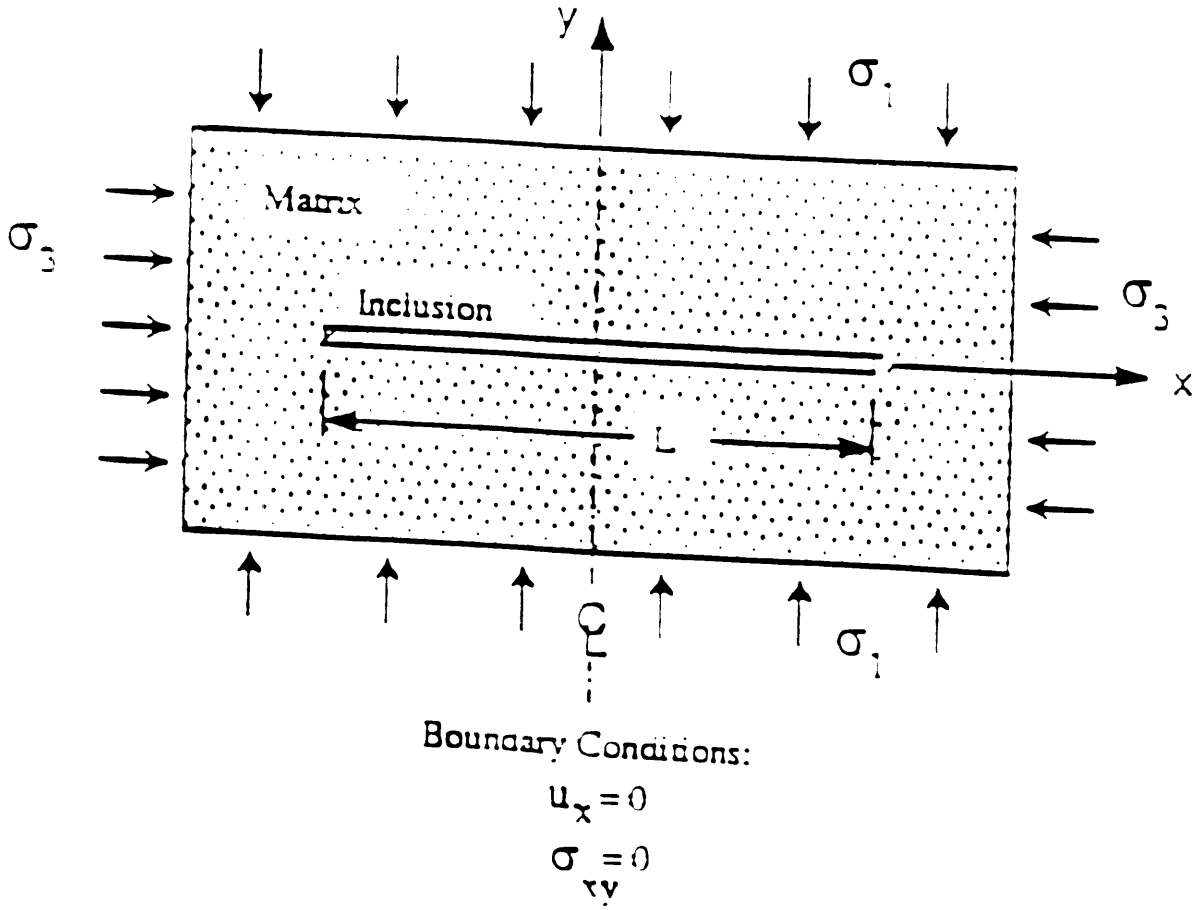

Figure 4-12 Geometry of the ASPR Ideal Plane Strain Reinforced Composite Soil Element (Larson, 1992)

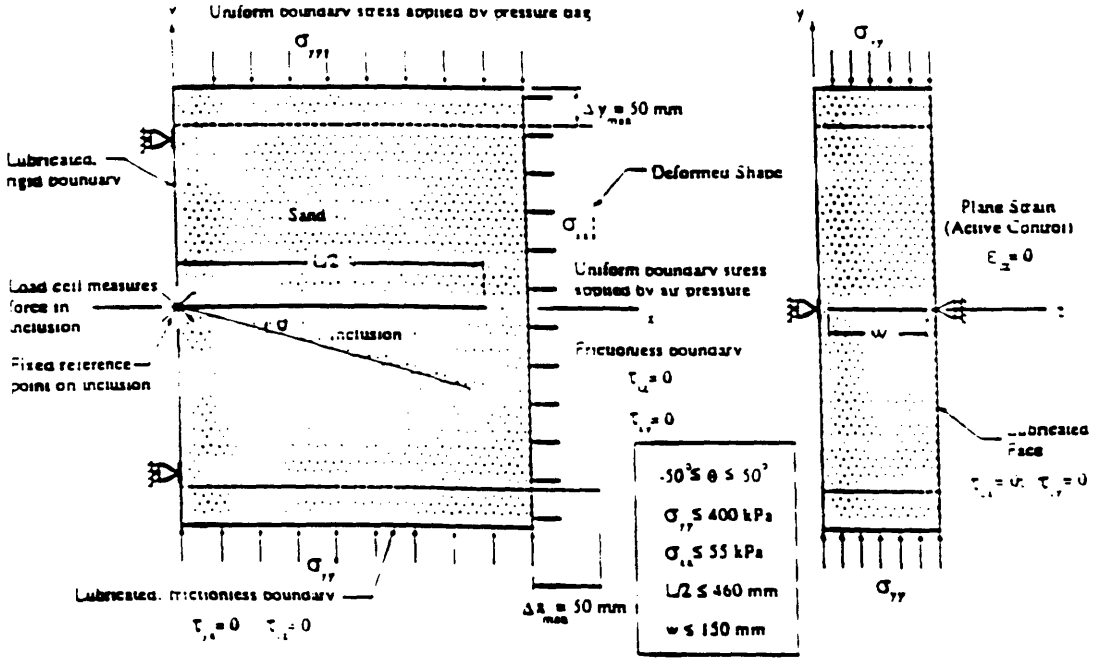

Figure 4-13 Conceptional Design of the ASPR Cell (Larson,1992)

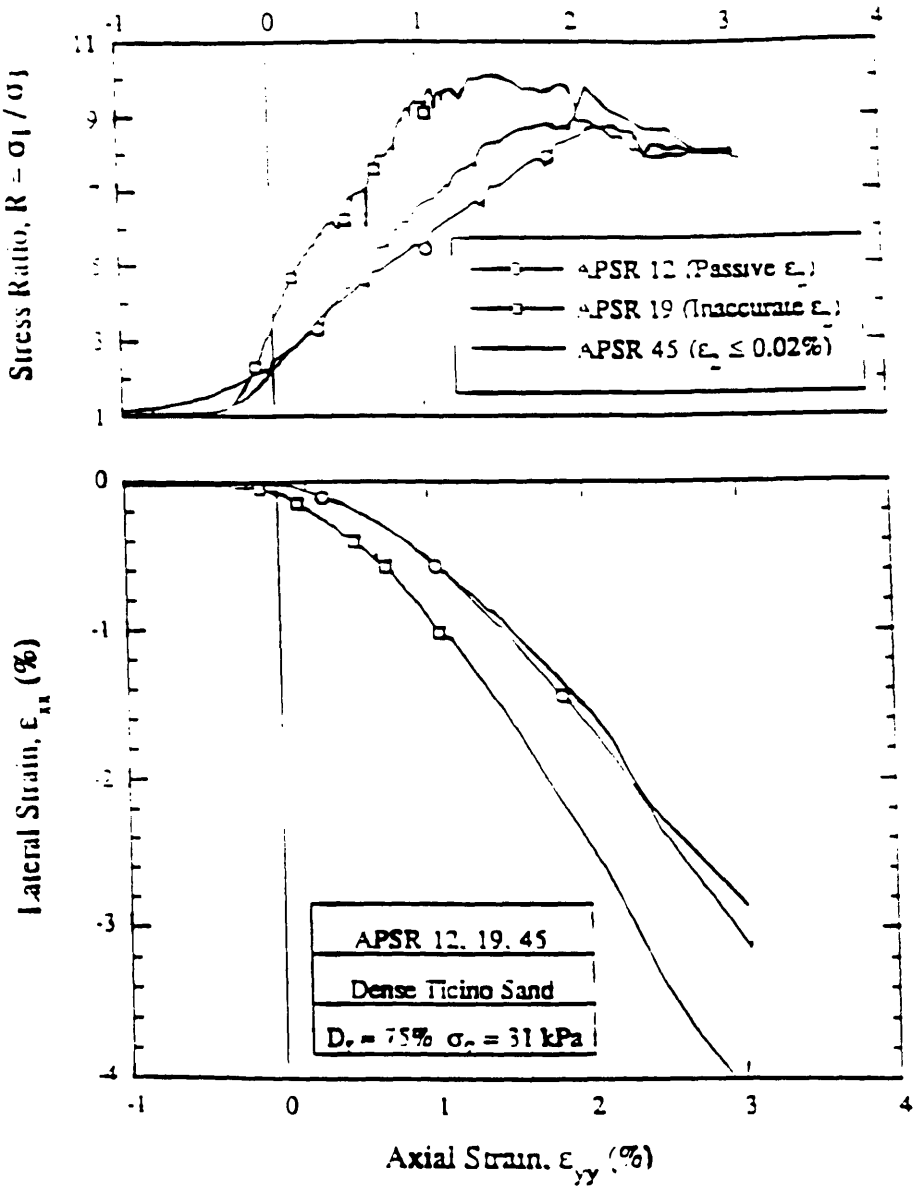

Figure 4-14 The Results of Plane Strain Condition on the Shear Behavior of Dense Ticino Sand (Larson, 1992)

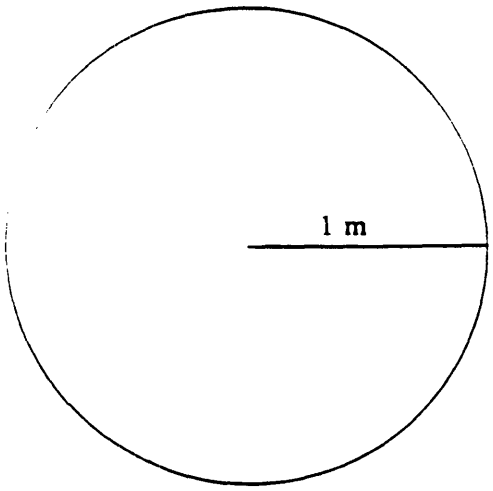

The Cross-Section of Circular Pre-Support Tube.

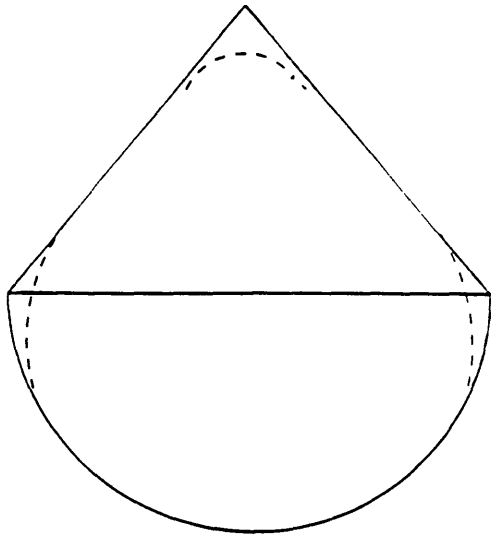

The Cross-Section of Triangular Pre-Support Tube.

——— Used for Analysis

- - - - Used in Real Design

Figure 4-15 The Geometries of Circular and Triangular Pre-support Pipes

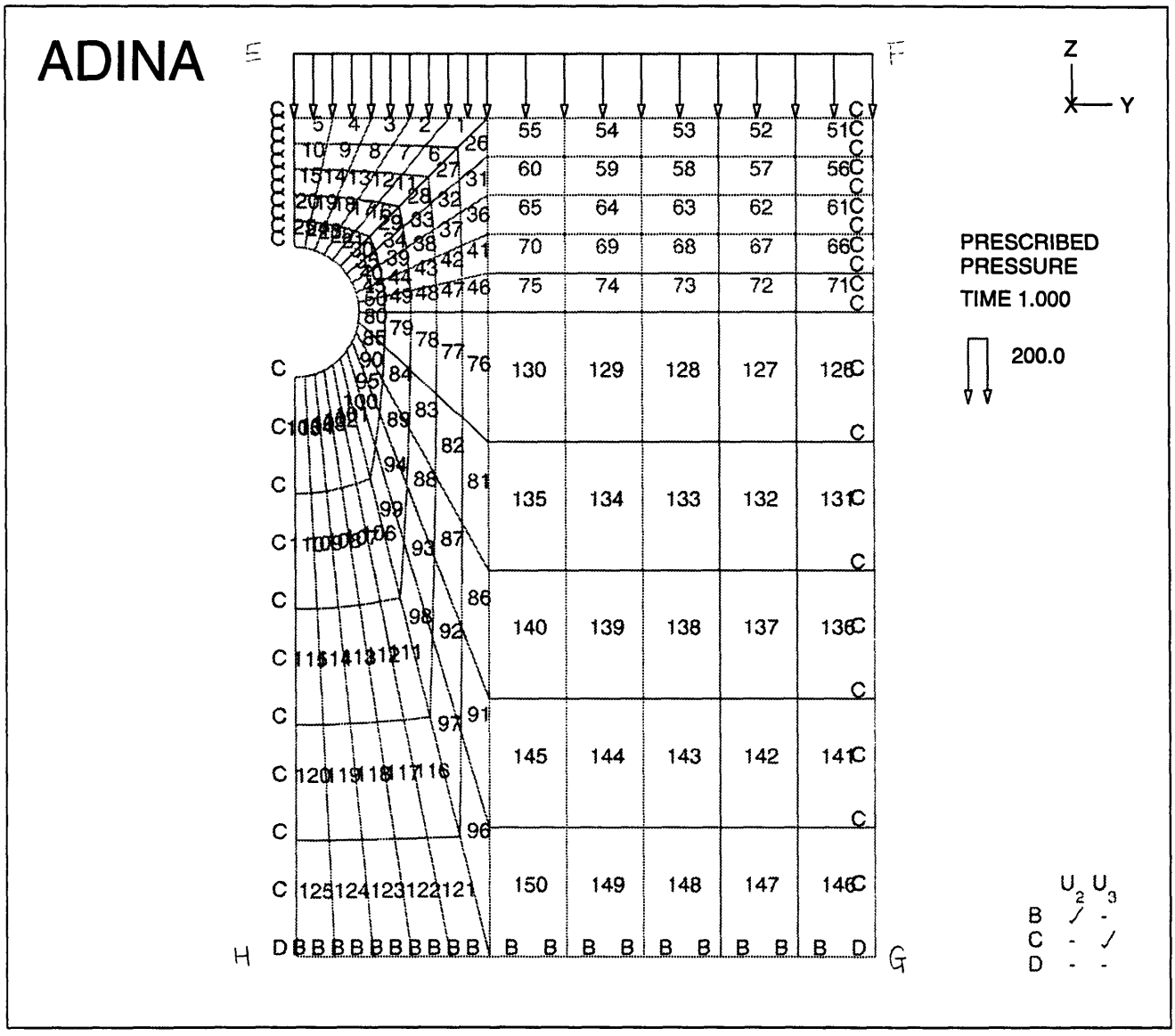

Figure 4-16 The Global Geometry and FEM Mesh for a Circular Tube

(Cover = 2 m)

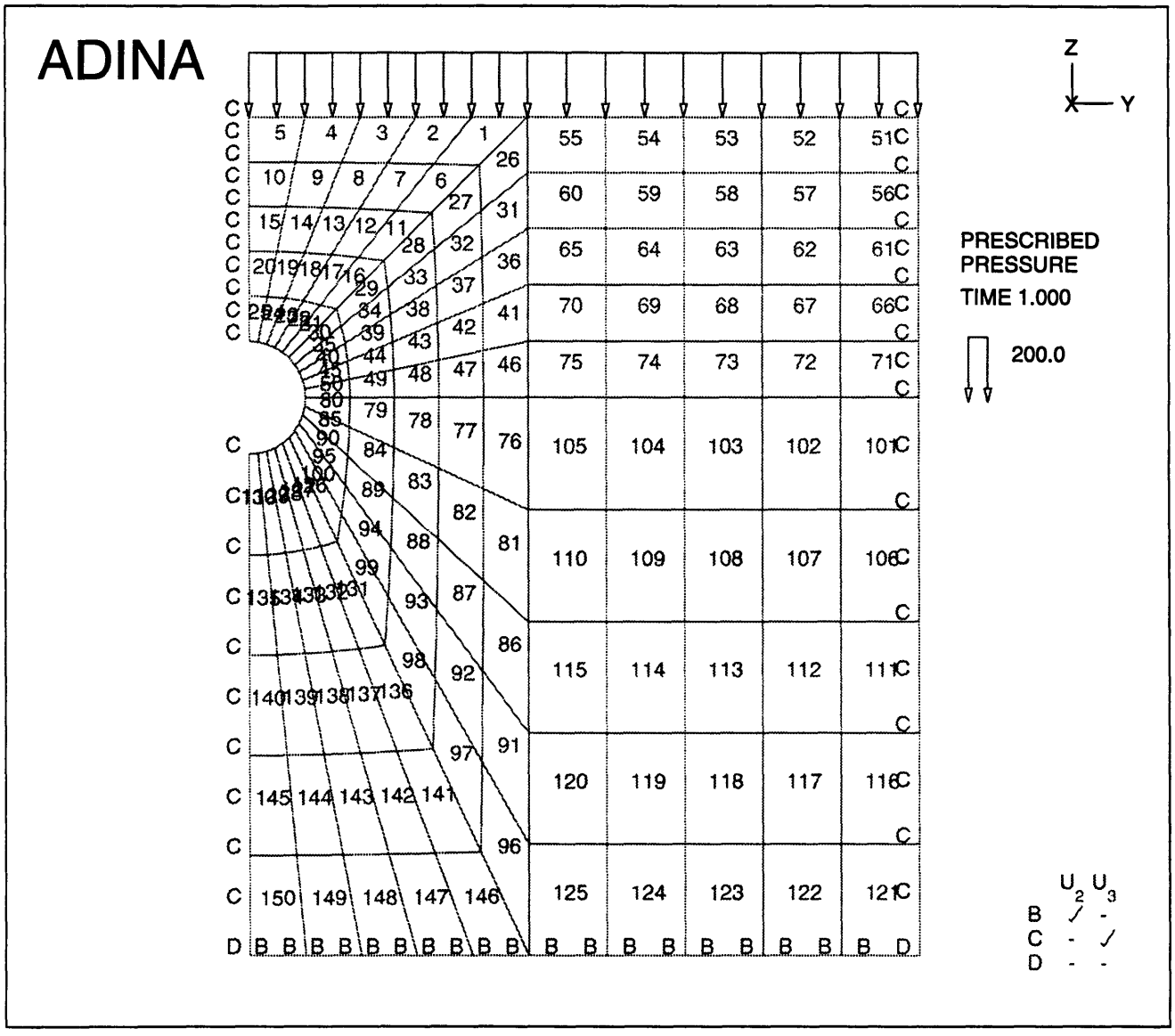

Figure 4-17 The Global Geometry and FEM Mesh for a Circular Tube

(Cover = 4 m)

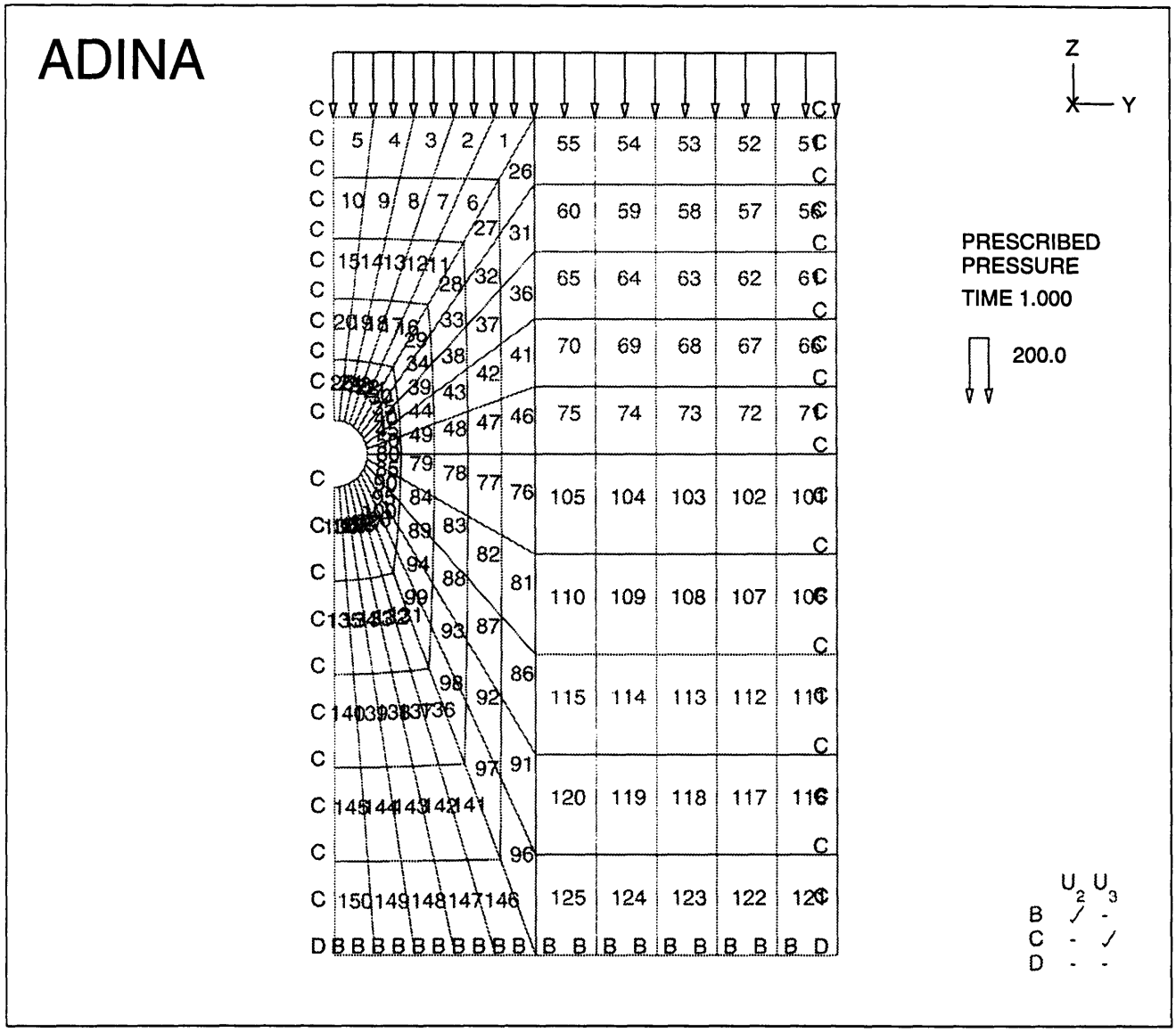

Figure 4-18 The Global Geometry and FEM Mesh for a Circular Tube

(Cover = 9 m)

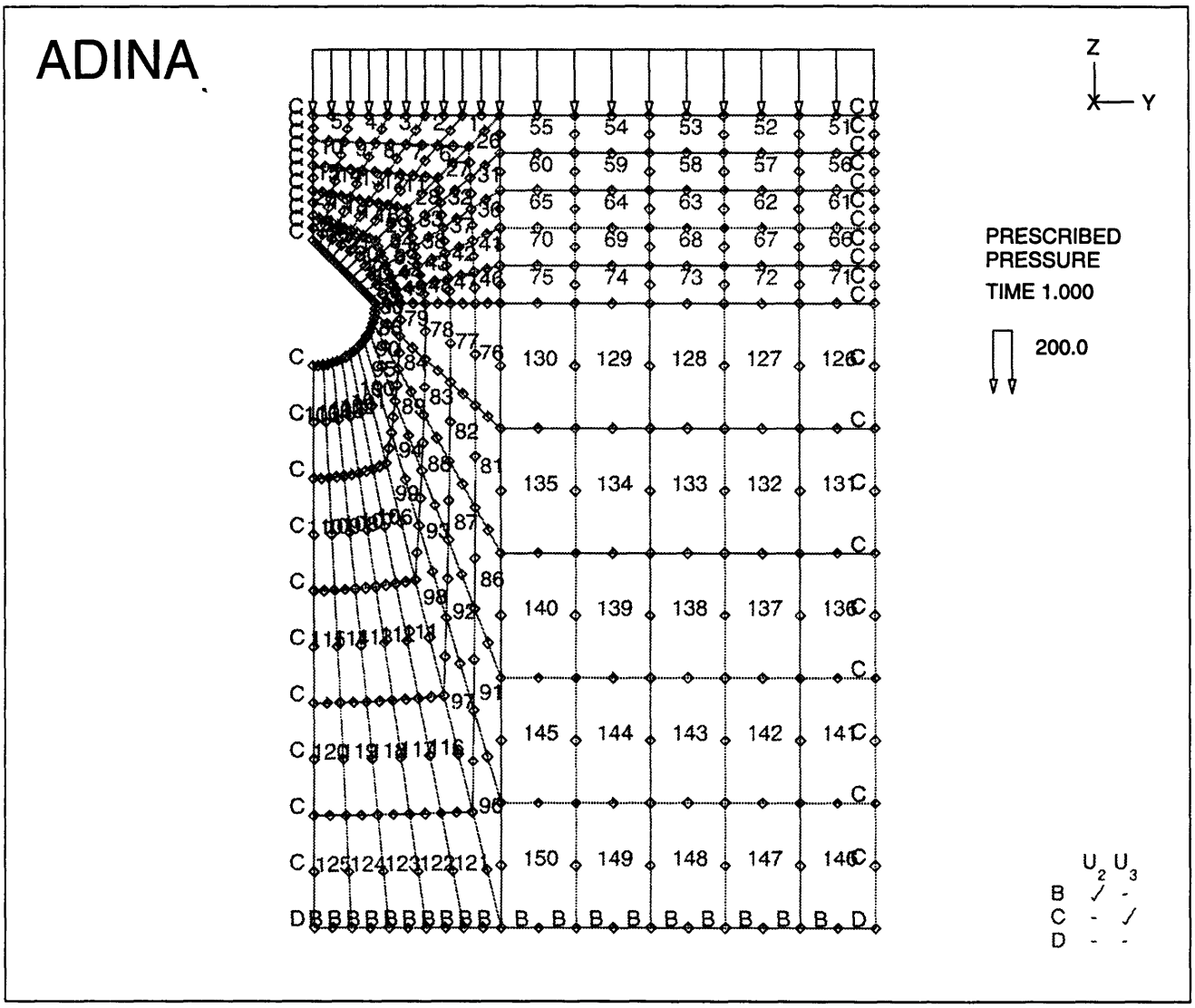

Figure 4-19 The Global Geometry and FEM Mesh for a Triangular Tube

(Cover = 2 m)

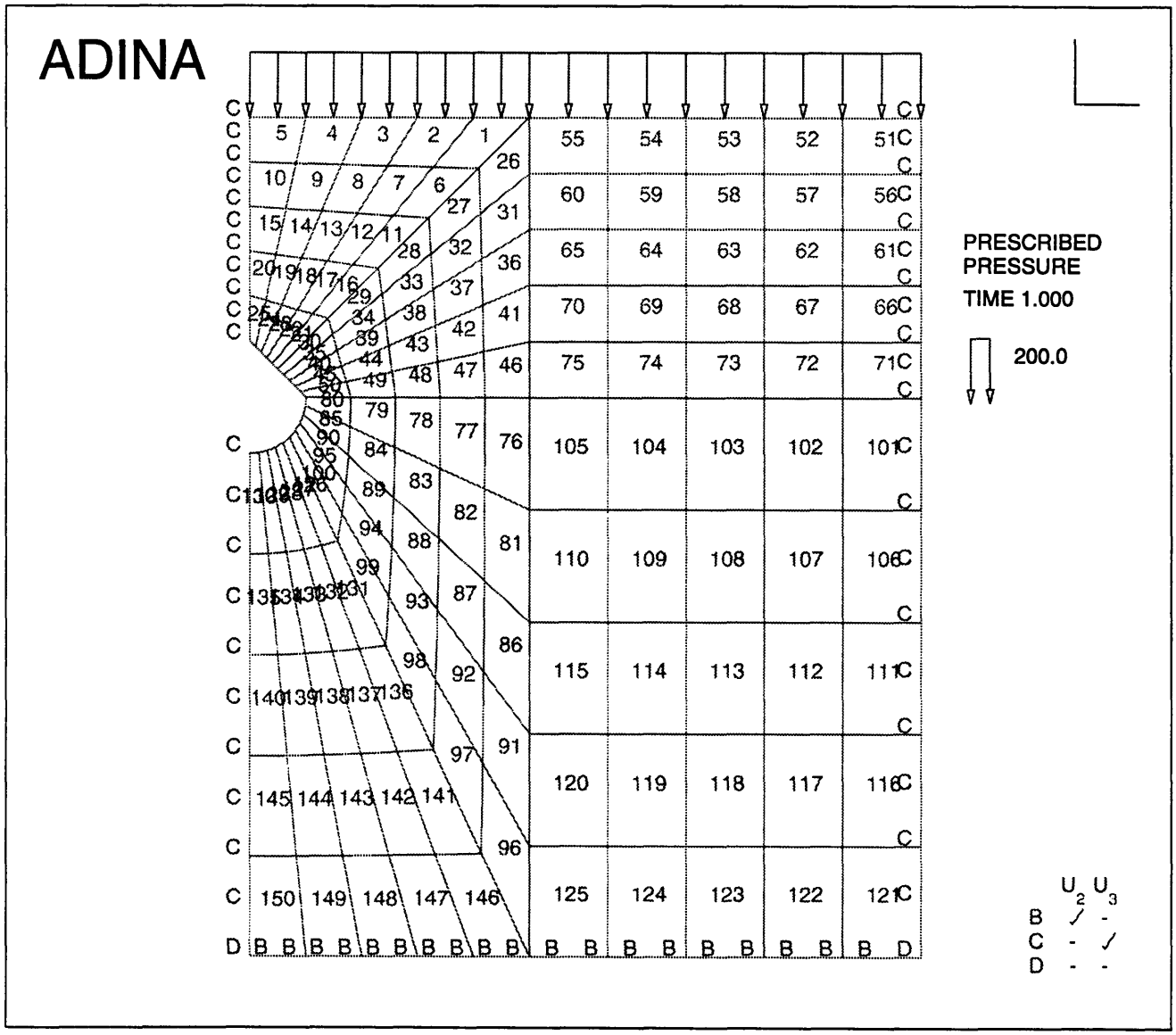

Figure 4-20 The Global Geometry and FEM Mesh for a Triangular Tube

(Cover = 4 m)

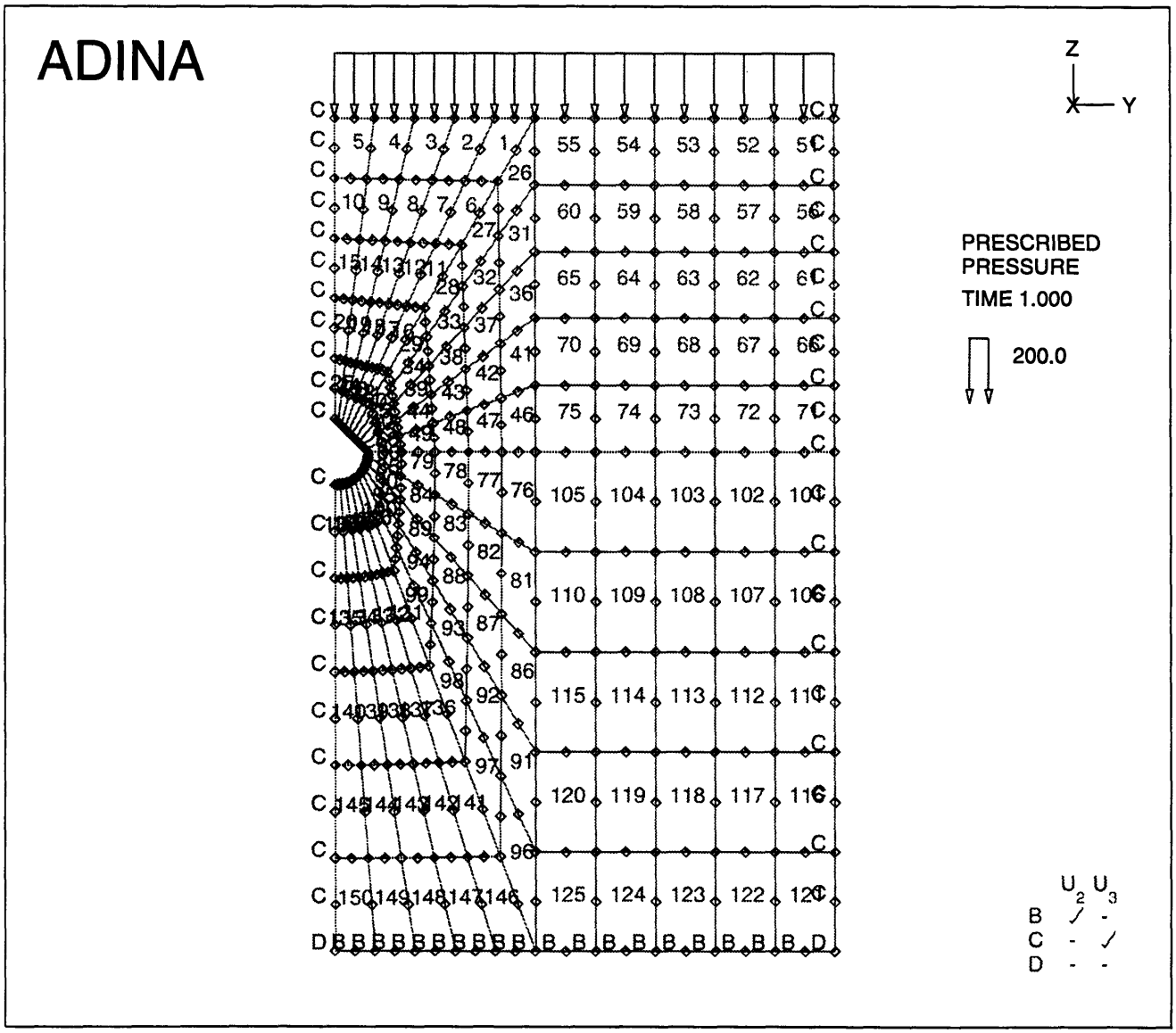

Figure 4-21 The Global Geometry and FEM Mesh for a Triangular Tube

(Cover = 9m)

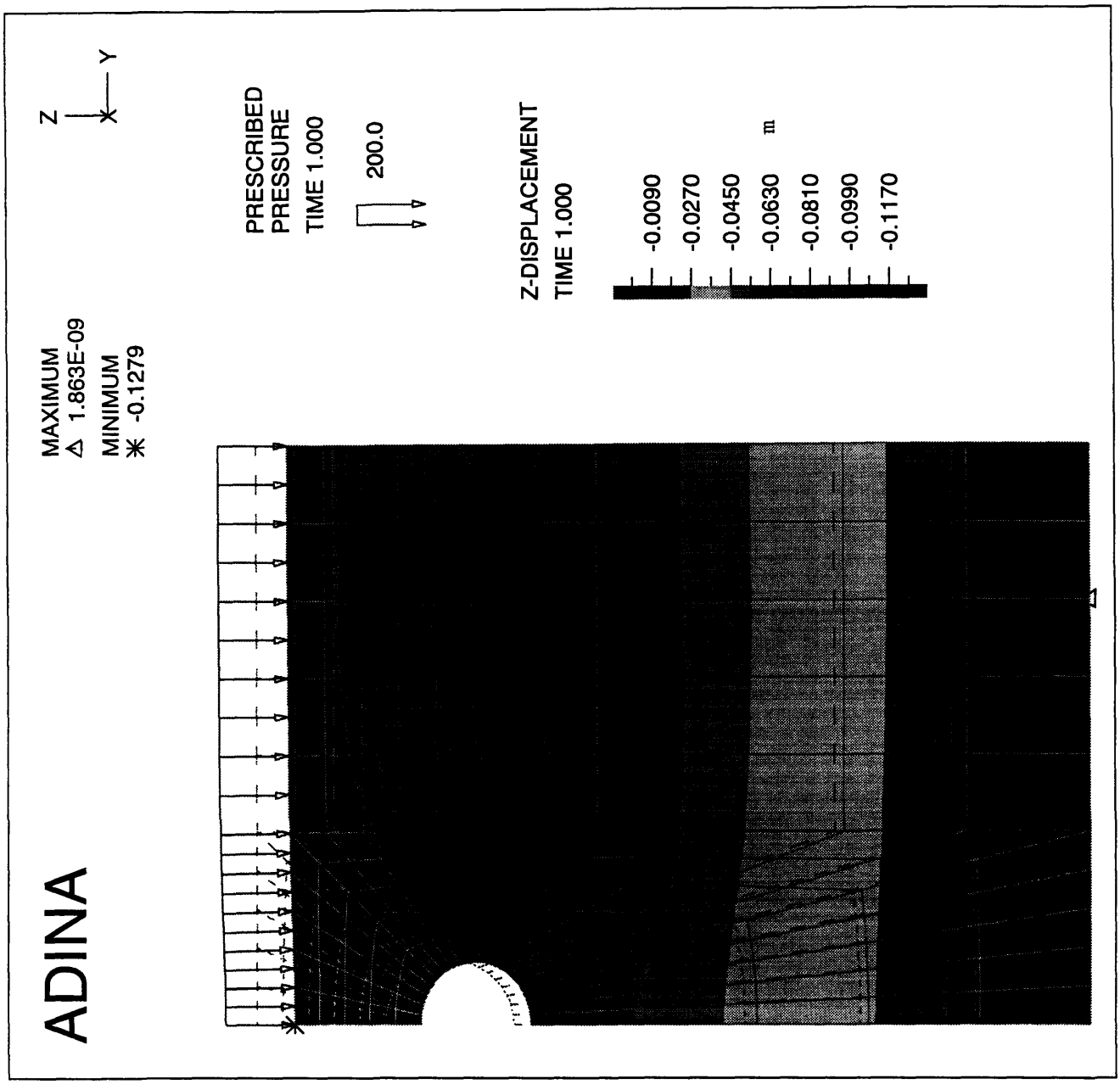

Figure 4-22 The Ground Settlement for a Circular Tube (Cover = 2 m)

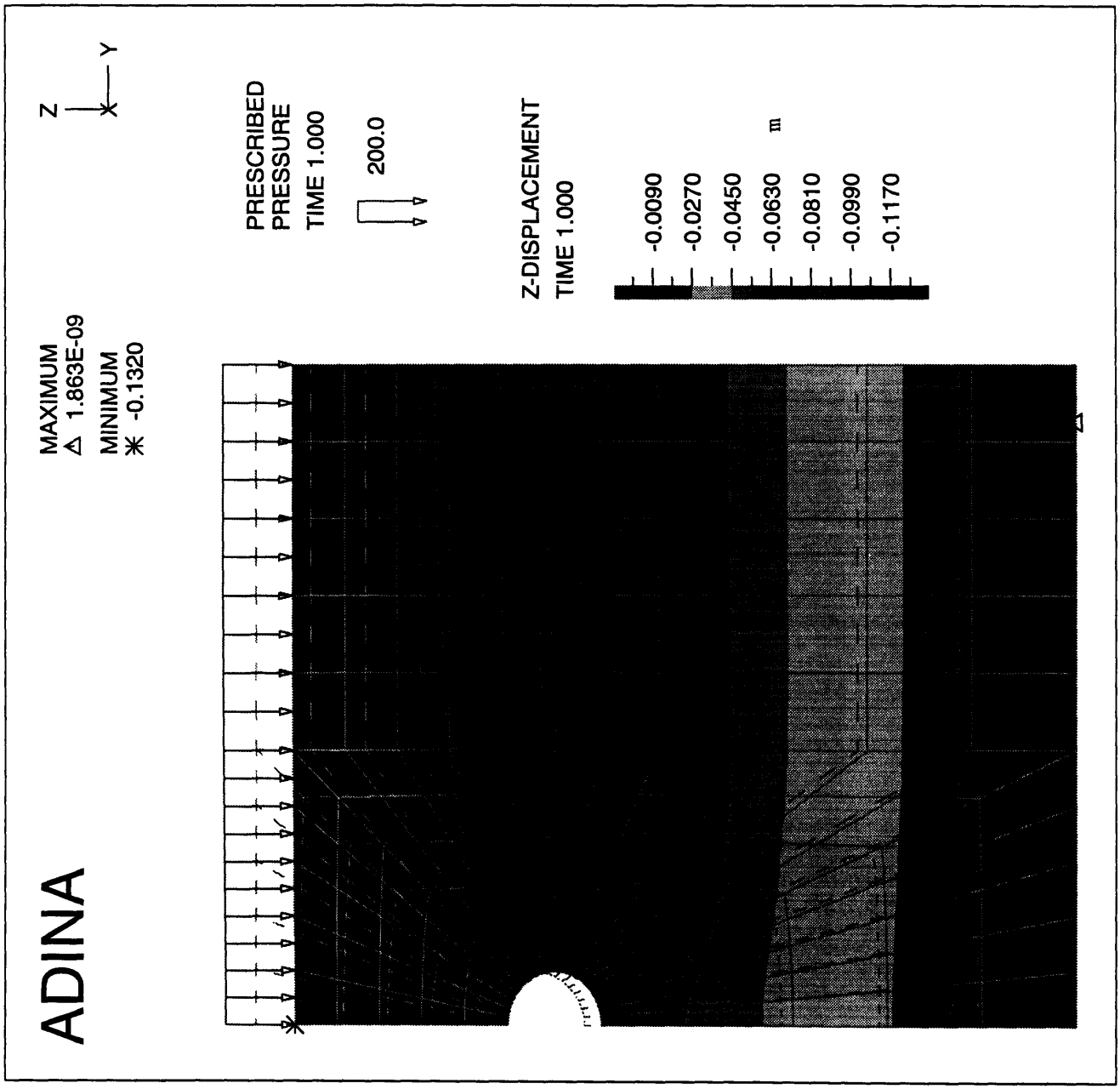

Figure 4-23 The Ground Settlement for a Circular Tube (Cover = 4 m)

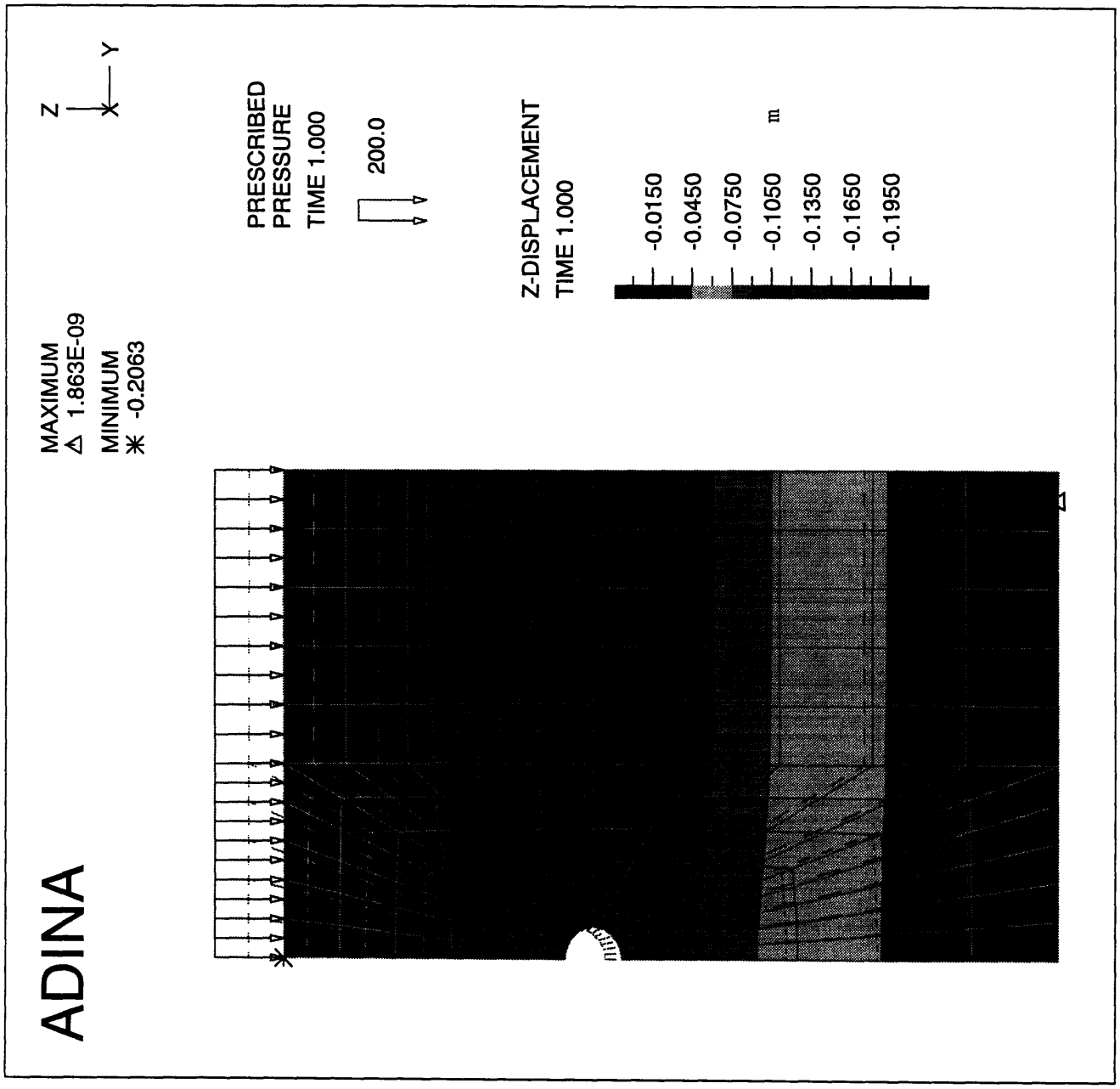

Figure 4-24 The Ground Settlement for a Circular Tube (Cover = 9 m)

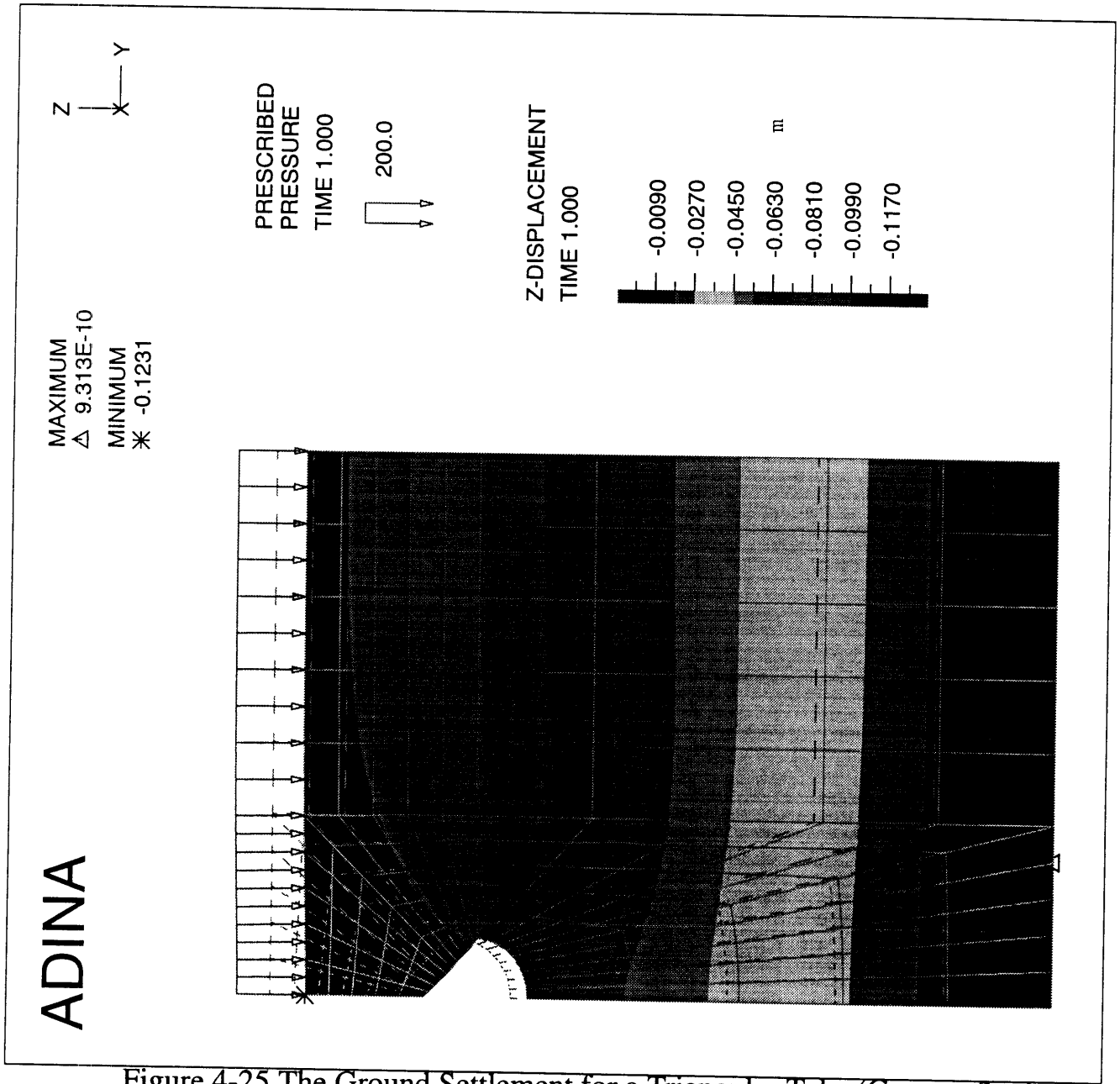

Figure 4-25 The Ground Settlement for a Triangular Tube (Cover = 2 m)

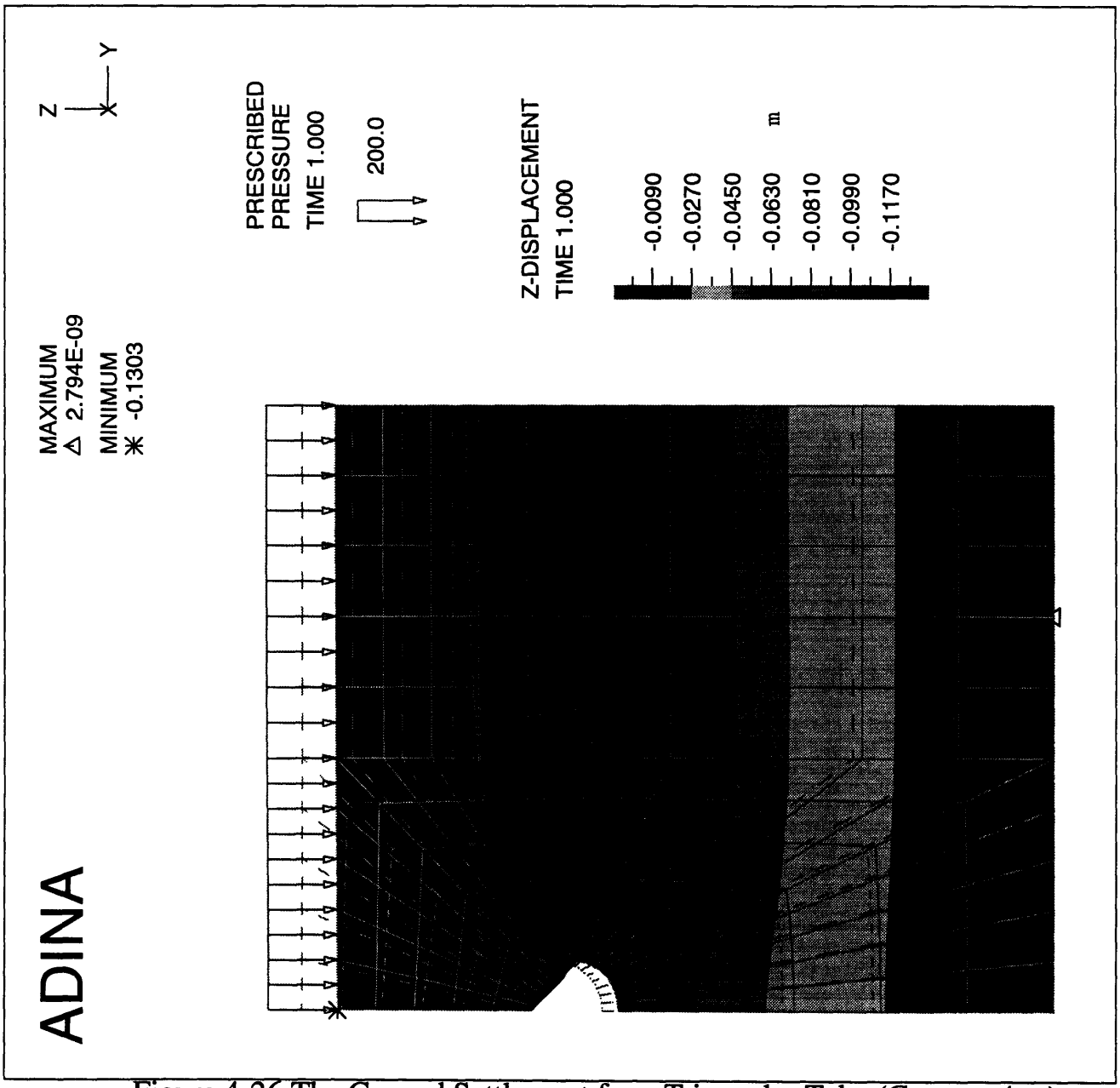

Figure 4-26 The Ground Settlement for a Triangular Tube (Cover = 4 m)

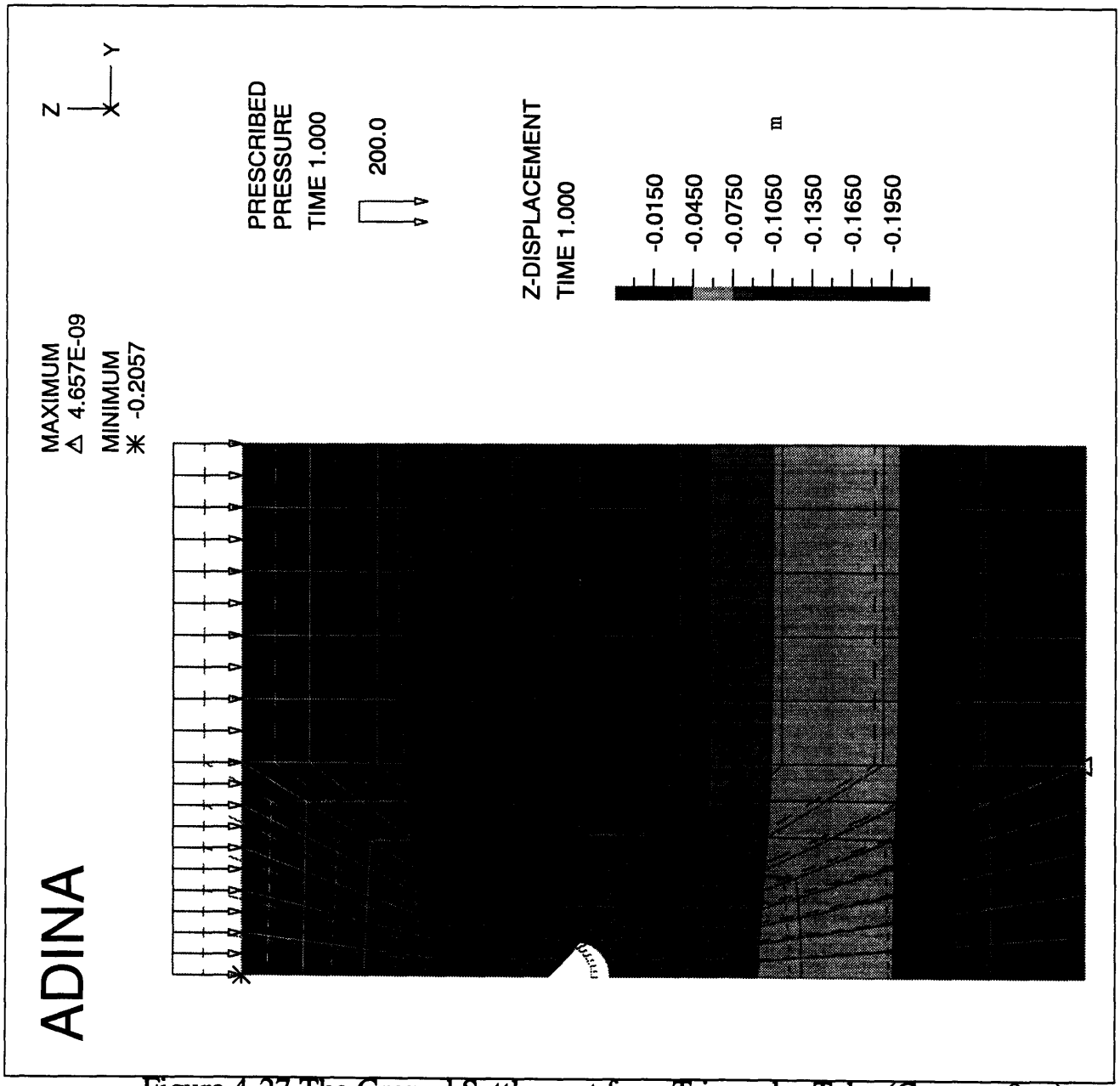

Figure 4-27 The Ground Settlement for a Triangular Tube (Cover = 9 m)

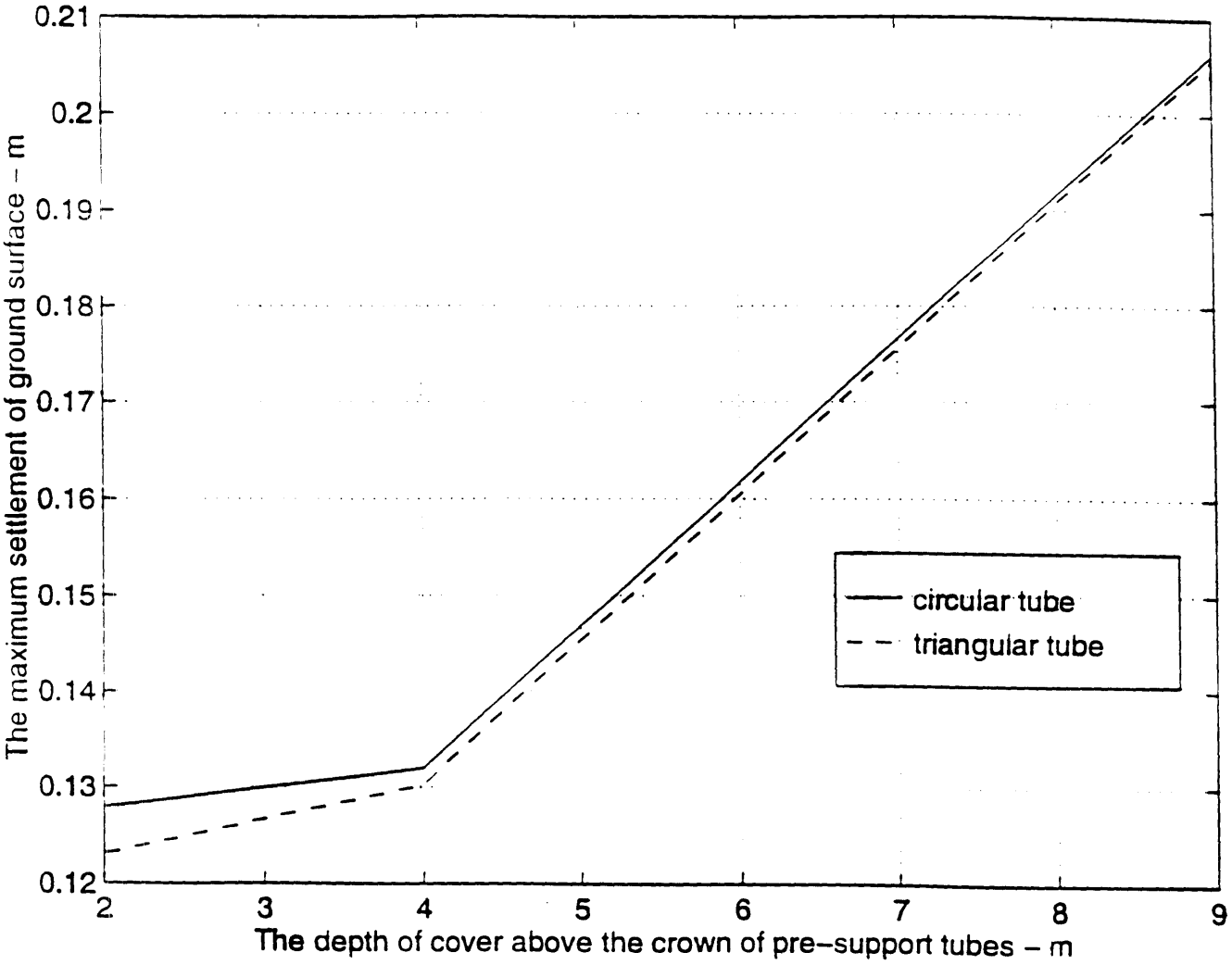

Figure 4-28 Summary of Results from Figures 4-22 to 4-27

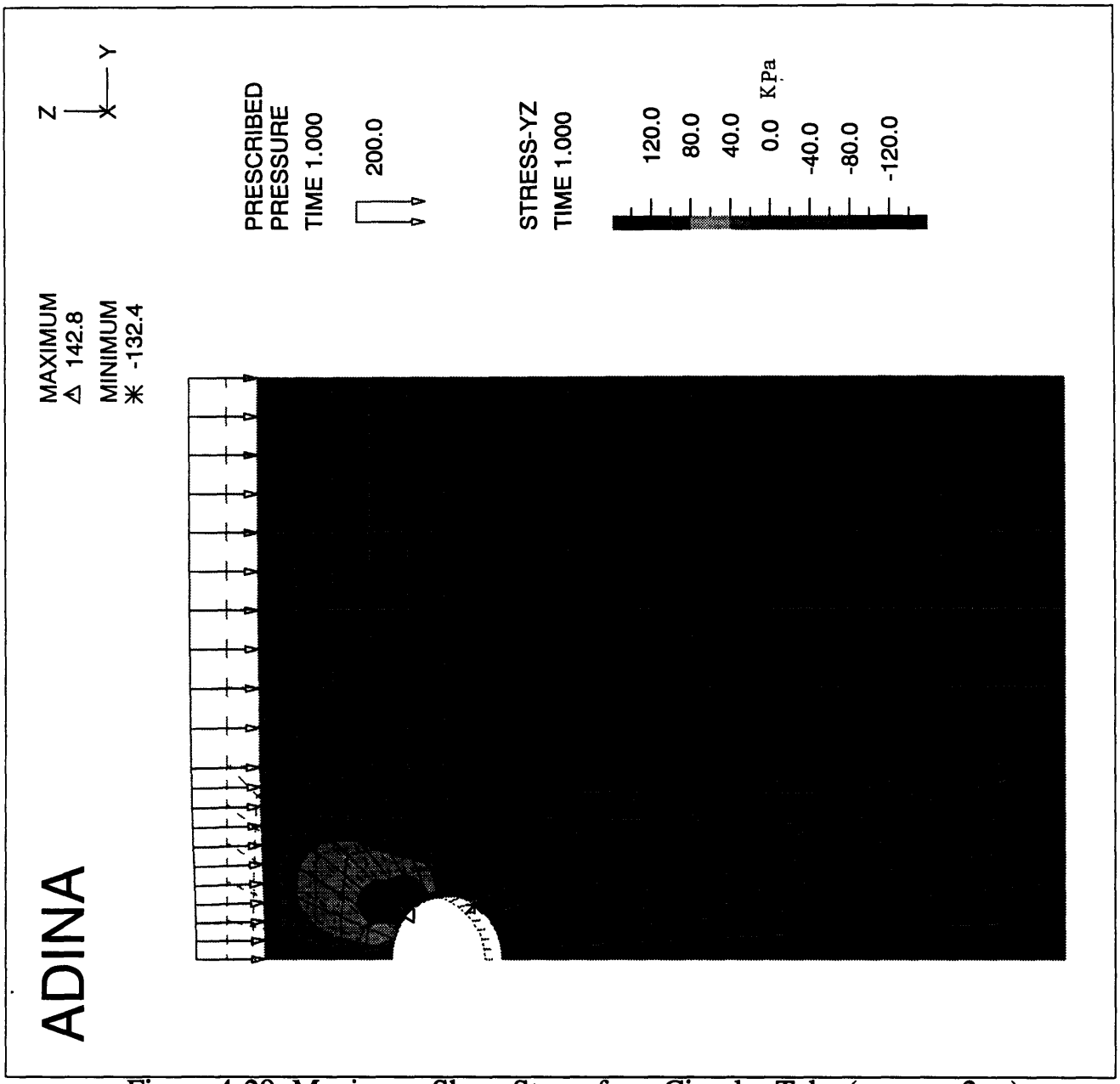

Figure 4-29 Maximum Shear Stress for a Circular Tube (cover = 2 m)

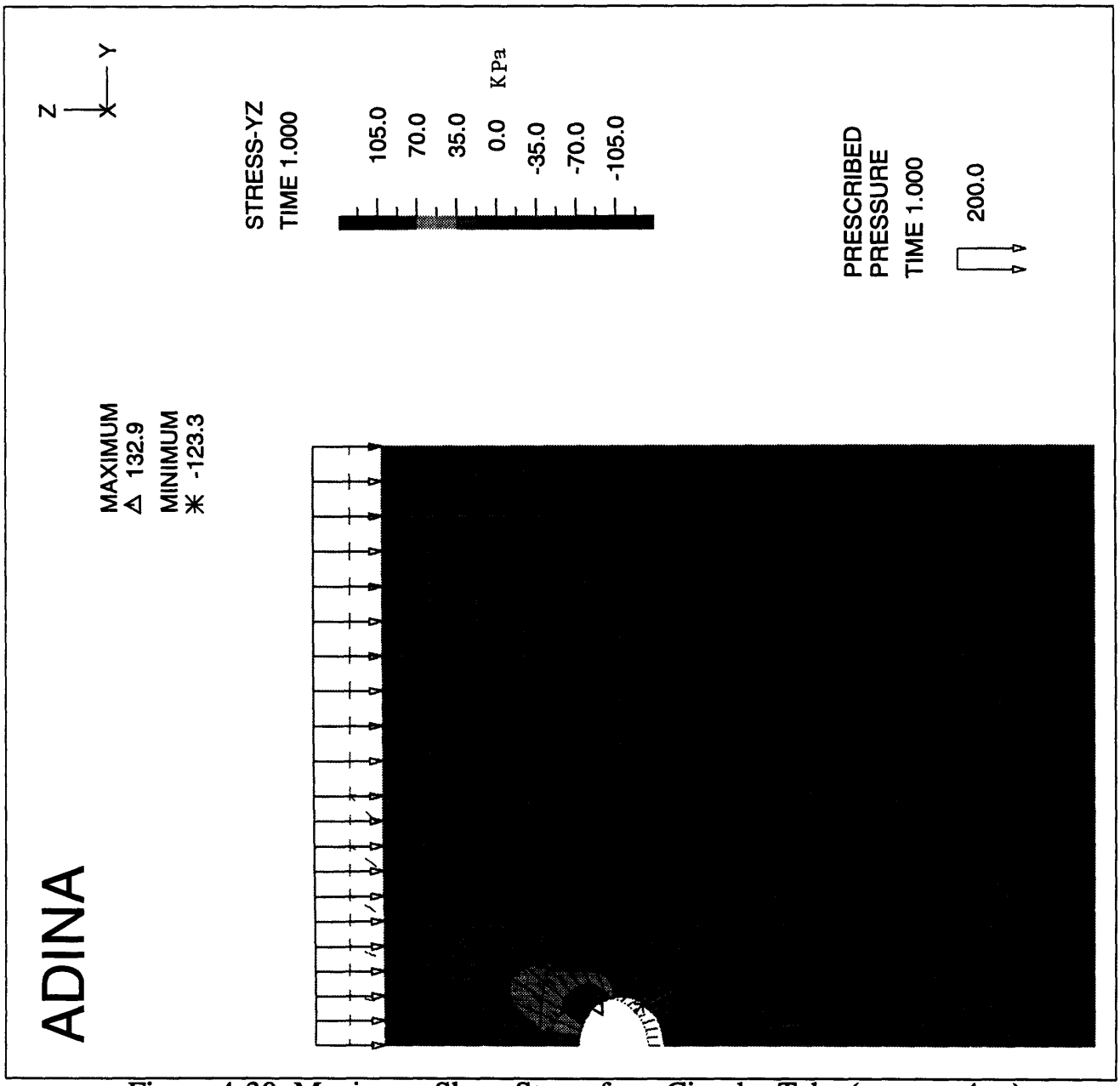

Figure 4-30 Maximum Shear Stress for a Circular Tube (cover = 4 m)

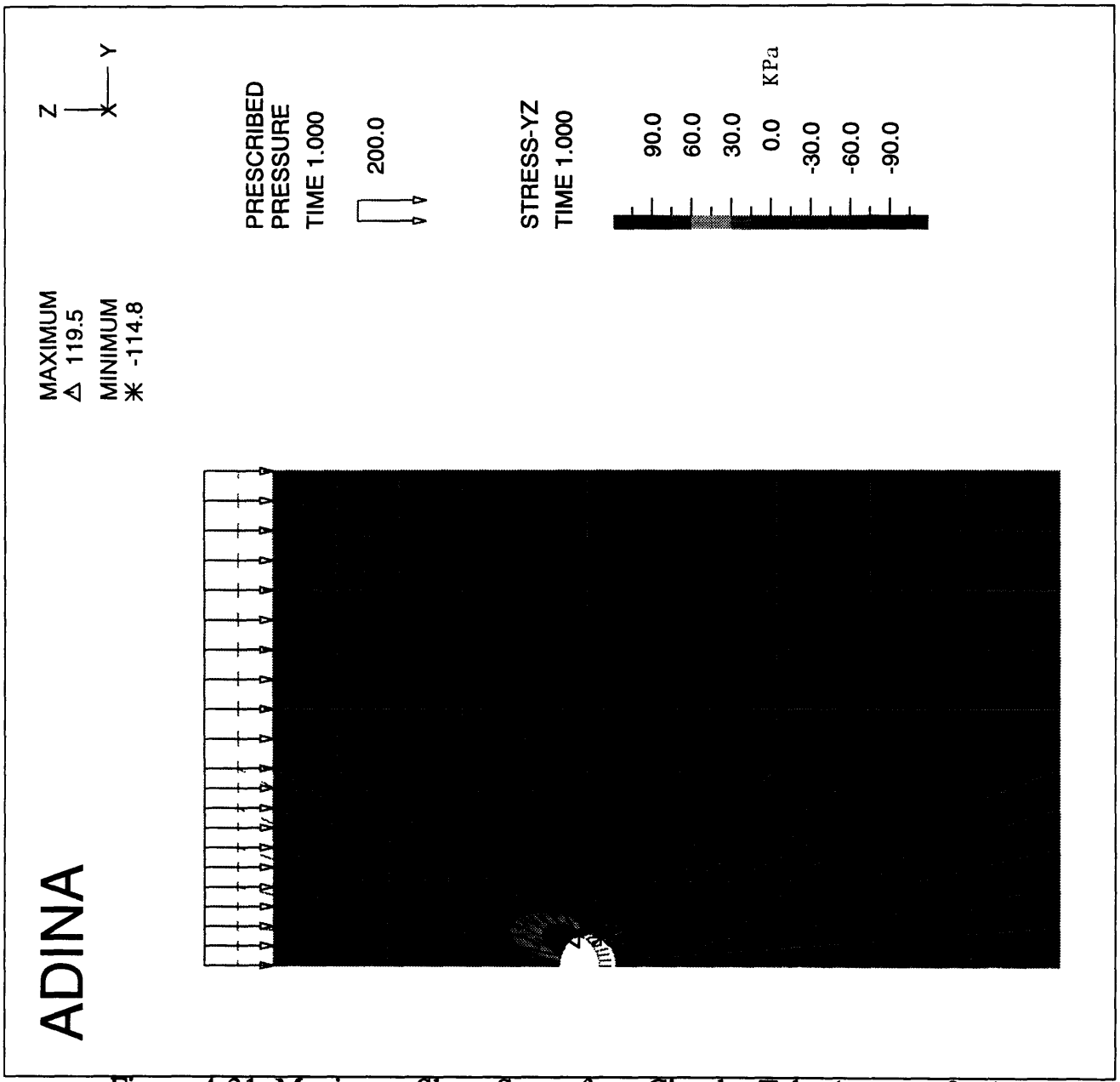

Figure 4-31 Maximum Shear Stress for a Circular Tube (cover = 9 m)

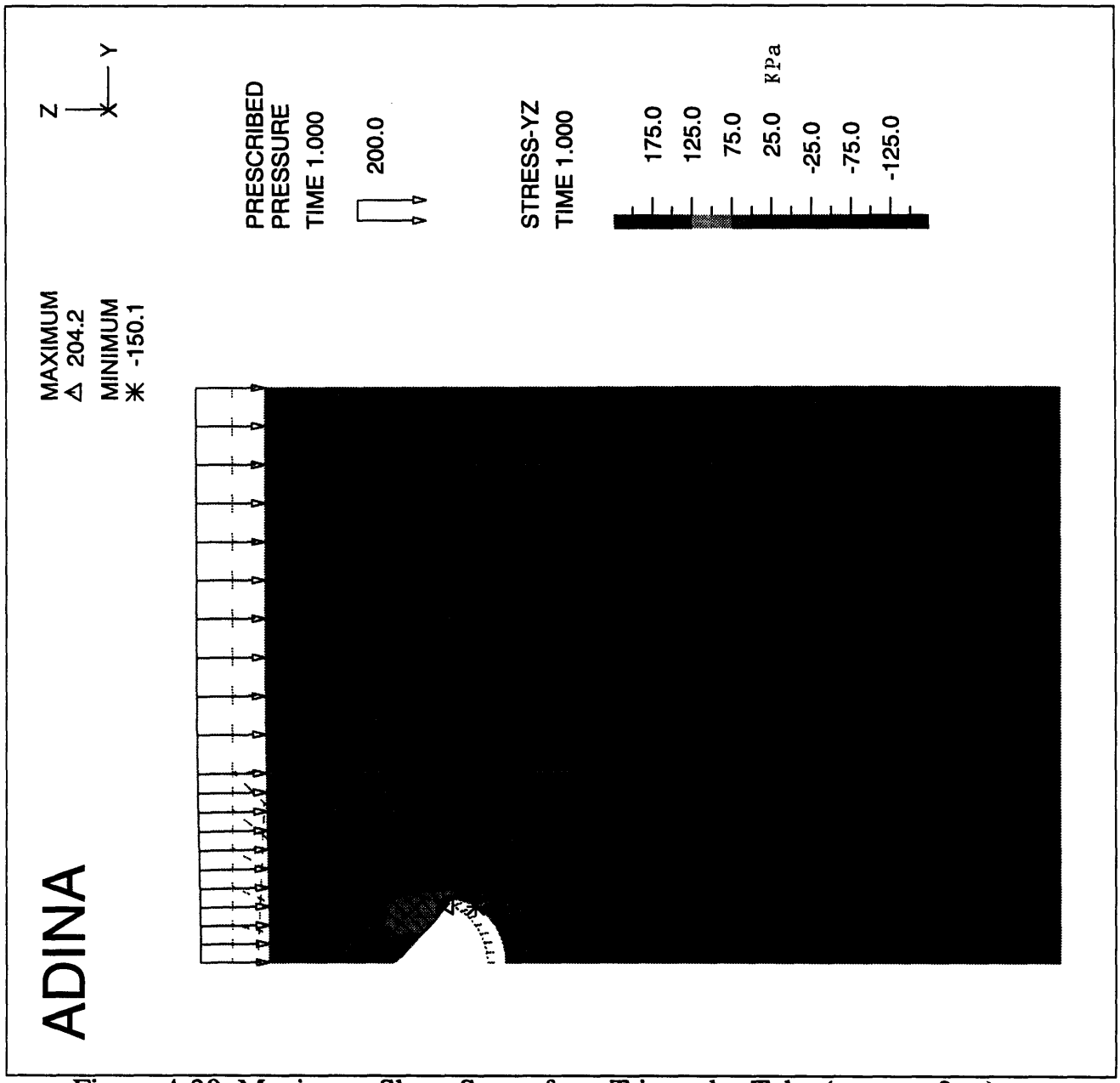

Figure 4-30 Maximum Shear Stress for a Triangular Tube (cover = 2 m)

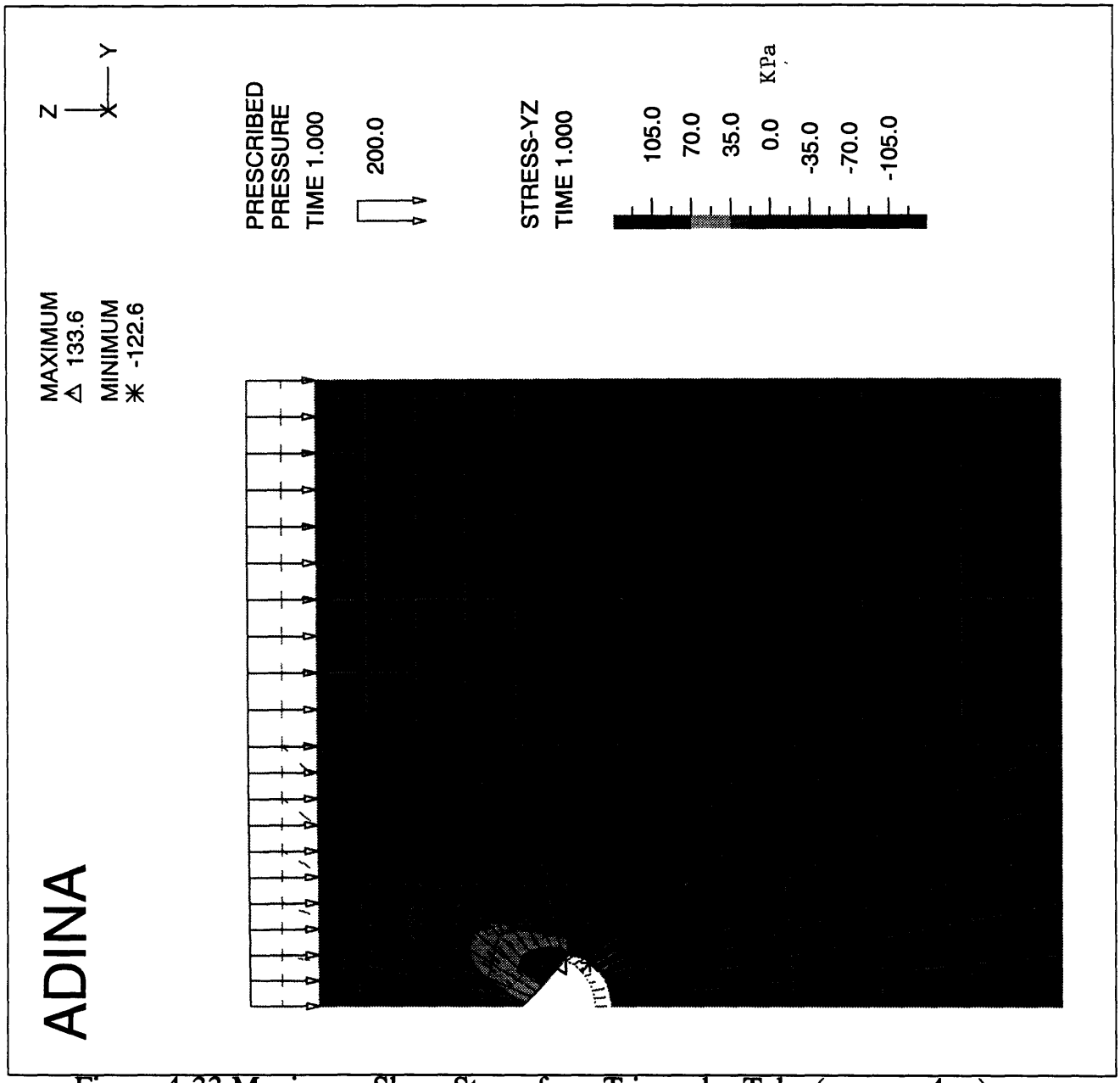

Figure 4-33 Maximum Shear Stress for a Triangular Tube (cover = 4 m)

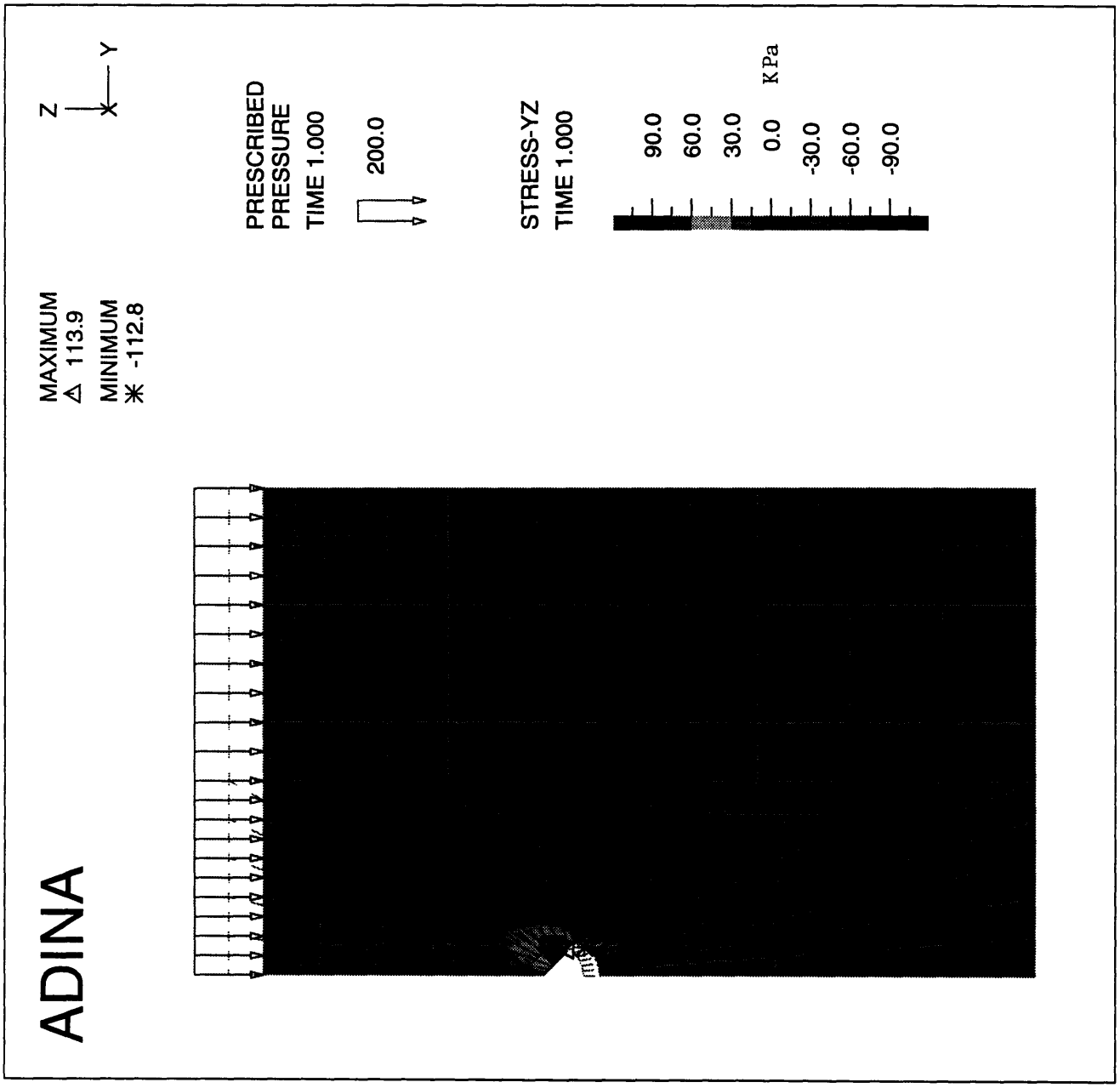

4-34 Maximum Shear Stress for a Triangular Tube (cover = 9 m)

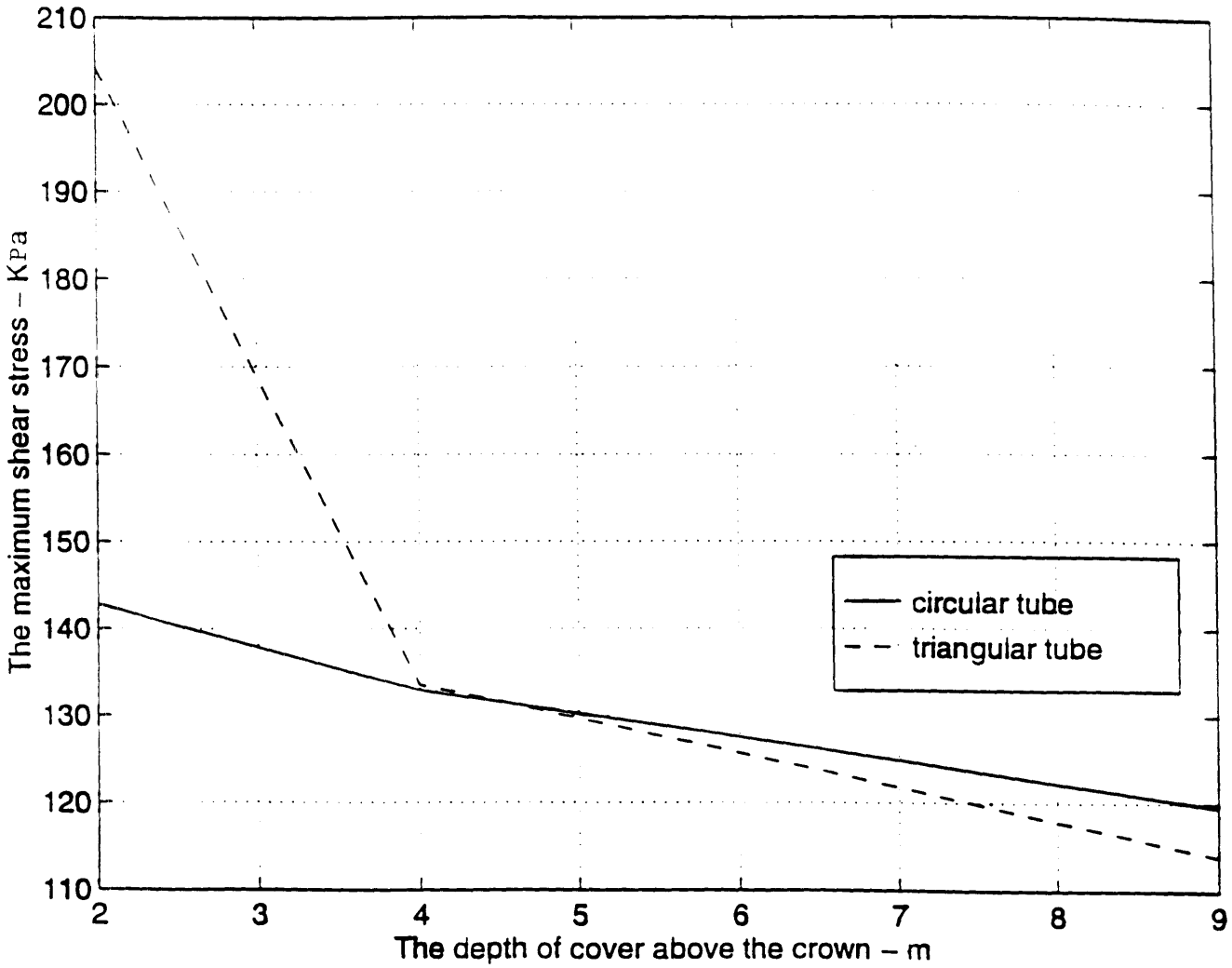

Figure 4-35 Summary of Results from Figures 4-29 to 4-34

Table 4-1 The settlements of Circular and Triangular Tubes			
The Depths of Cover	Circular Tube	Triangiar Tube	The Different Settlements
2 m	12.79 cm	12.31 cm	0.48 cm
4 m	13.20 cm	13.03 cm	0.17 cm
9 m	20.63 cm	20.57 cm	0.06 cm

Table 4-2 The Max. Shear Stresses of Circular and Triangular Tubes			
The Depths of Cover	Circular Tube	Trianglar Tube	The Different Max. Shear Stresses
2 m	142.8 KPa	204.2 KPa	61.4 KPa
4 m	132.9 KPa	133.6 KPa	0.7 KPa
9 m	119.5 KPa	113.9 KPa	5.6 KPa

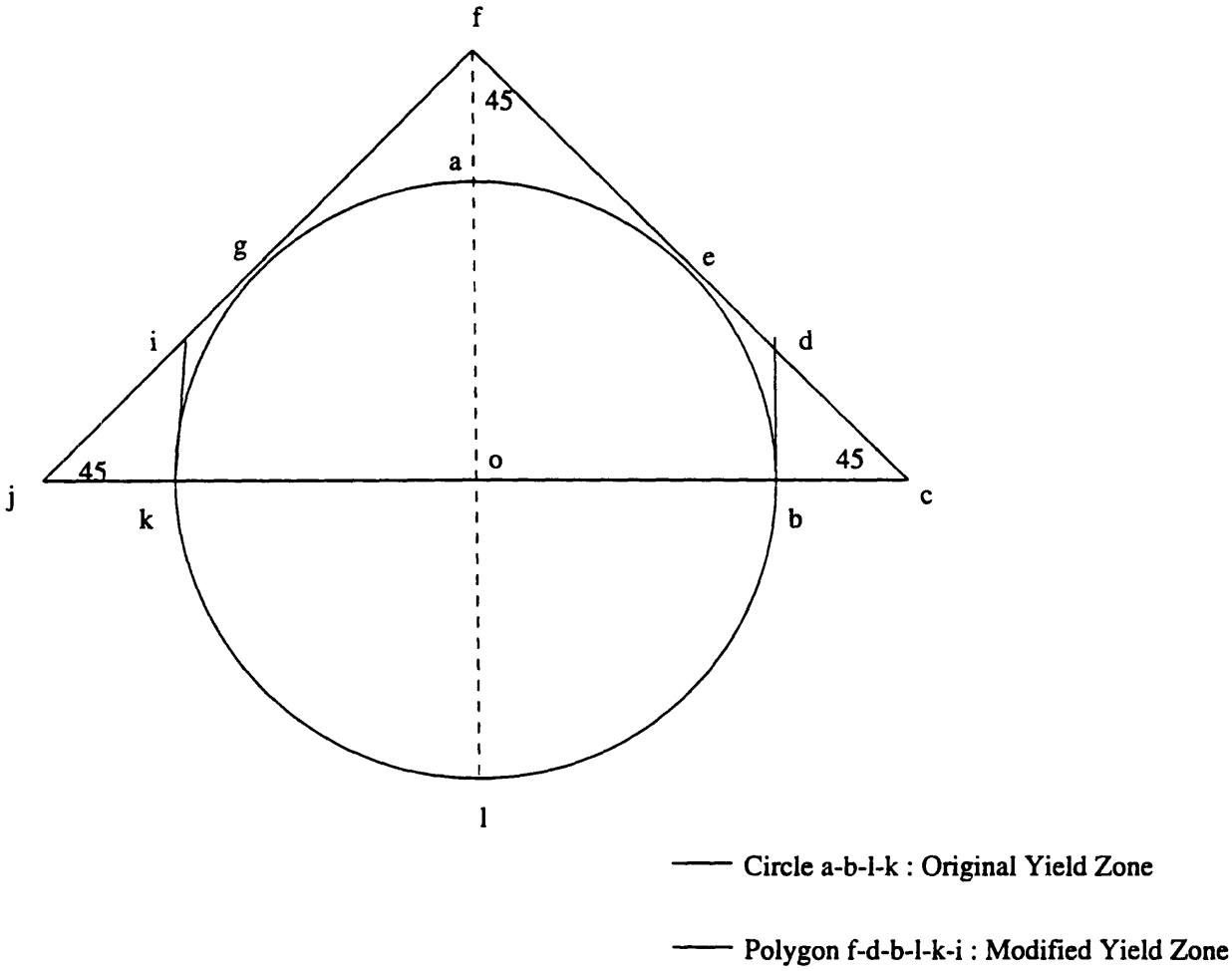

Figure 4-36 The Modified Yield Zone of Circular Opening in Uniform Soil

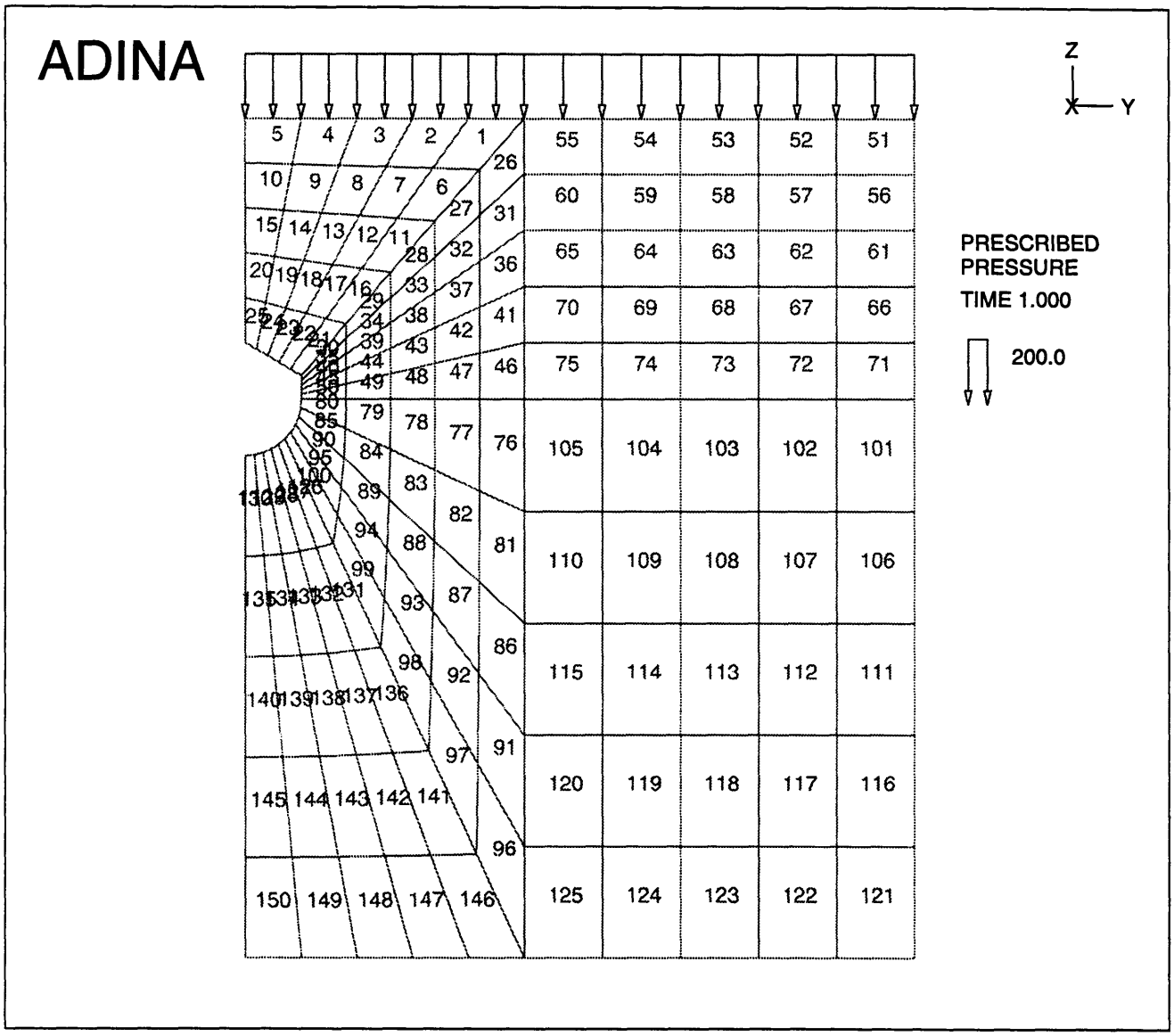

Figure 4-37 The Global Geometry and FEM Mesh for the Modified Model

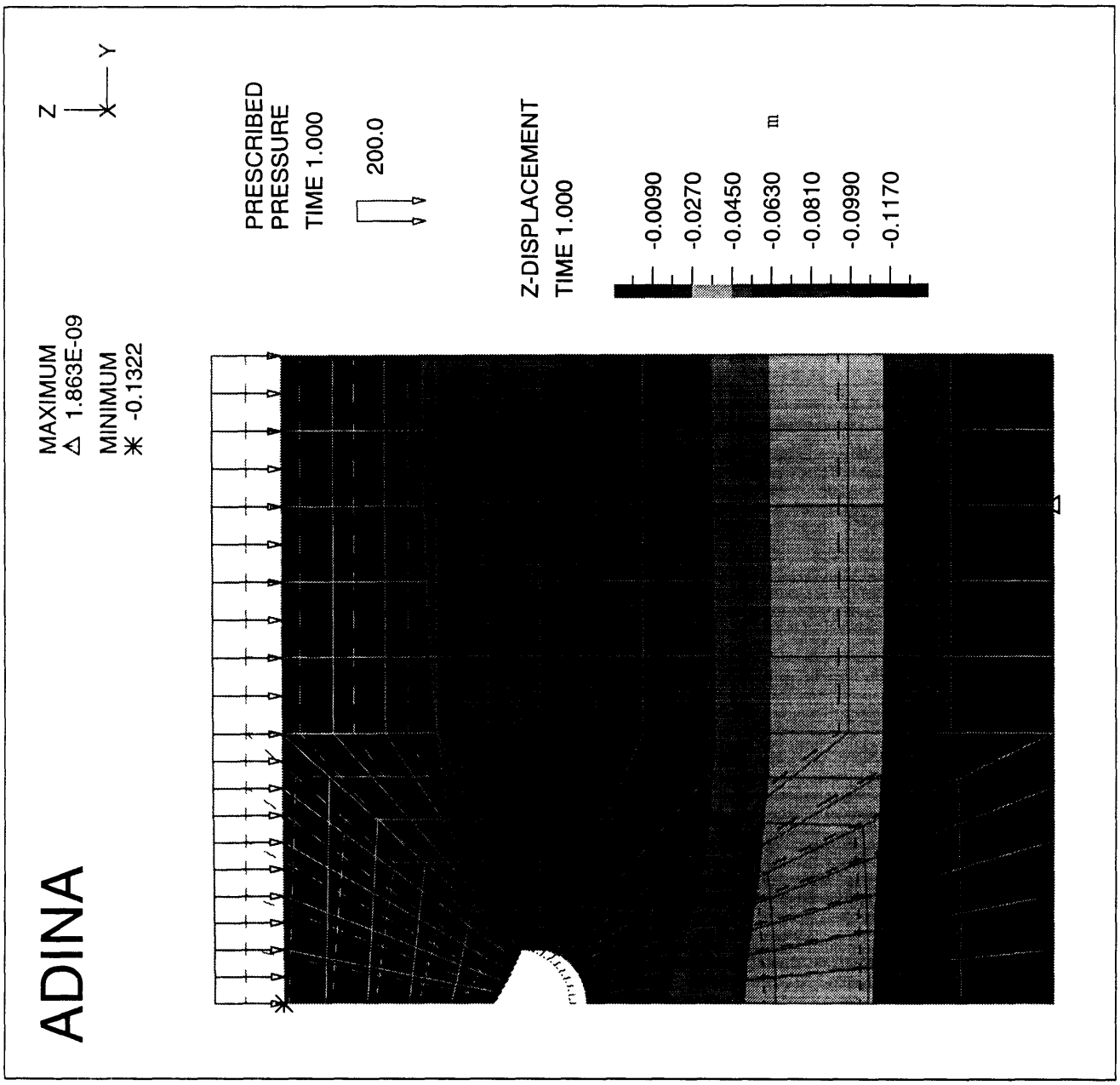

Figure 4-38 The Settlement for a Modified Model

Chapter 5.Conclusion and Recommendations for Future Research

5.1 Conclusion

The development of arching has not been well understood so far. It, however, plays a significant role in engineering design. For economic reasons, it is cost-effective for geotechnical engineers to take into account the effect of arching in the design of structural supports. The ground adjacent to a structure, for example, can cause the subterranean structure to have a much greater load-carrying capacity than an identical, yet unburied, structure. On the other hand, the arching effect can sometimes cause the buried structure to have less load-carrying capacity than an unburied identical structure, which may result in the collapse of the constructed object. The safety issue hence makes the effect of arching a major concern for engineers.

The development of arching can be roughly divided into four different stages. The first stage is an original triangle, and the other stages are different combinations of two triangles. One triangle has a flatter slope than the original one; and the other has a steeper slope than the original one.

The Mohr Failure Envelope is used to explain the different stages of arching. It explains quite well the edges of the above triangular combinations, but explains poorly the points of the intersections of the two triangles. The Mohr-Coulomb Failure Envelope, on the other hand, explains the behavior well for all the regions.

By clearly categorizing the different stages of arching, using the Mohr Failure Envelope and the Mohr-Coulomb Failure Envelope, further understanding of the development of arching can be reached.

No matter how deep or shallow a tunnel is to be built, an appropriate consideration is needed to prevent potential collapse. It should be noted that the formation of triangular arching needs a certain depth of cover above it. As a result, if a deep tunnel is being built in sandy soil, some displacement of the above soil can be beneficial to the tunnel structure, for example, making the soil produce its maximum strength. However, to build a shallow tunnel, reducing the displacement of

the soil is the best way to prevent the settlement at the ground surface, which is especially crucial if the tunnel is being build in a city.

Transforming the traditional horizontal pre-supporting circular tube into the new triangular design minimizes the yield zones of the opening, and the settlement of the ground surface will decrease. Both the empirical explanation and the F.E.M. method prove that the triangular pre-support tubes can reduce the ground surface settlement better than the traditional circular pre-support tubes.

5.2 Recommendations for Future Research

There are a number of areas concerning the arching effect where further research is needed. Some of them are summarized below:

1. The directions of the major principal stresses during the transformation between different stages of arching are not known. In the present analysis, the directions of major principal stresses are assumed to be horizontal. Evans (1983) has argued that major principal stresses are horizontal when the triangular prism forms. It is unclear, though, how these directions change during the transformation between different arching stages.
2. The triangular tubes can also produce greater inter-locking effects by changing the lower portion of the tube into a circular shape. It remains unclear that what kind of shape is an optimal one. Again, all the connection points (Figure 4-17) need to keep an arc shape to reduce the stress concentration.
3. The 'Error Curve' method for settlement prediction was originally obtained from the natural caverns, or tunnels which do not have reinforcement and pressure support. Therefore, a reduction factor for the calculated settlements with modern construction technology is required. The reduction factor will change according to different excavation technologies and soil types.

BIBLOGRAPHY

Allgood, J. R., and Herrmann, H. G. (1969), "Static Behaviorof Buired Reinforced Concrete Model Cylinders', US Naval Civil Engineering Lab.,Tech. Rep. R606.

Atkinson, J. H., E.T. Brown, and D.M. Potts (1975), "Collapse of Shallow Unlined Tunnels in Dense Sand", Tunnels and Tunneling, Vol. 7, No 3, pp 81-87.

Atkinson, J. H.,and D.M. Potts (1975),"A Note on Associated Field Solutions for Boundary Value Problems in a Variable ϕ - Variable υ Soil", Geotechnique, Vol. 25, pp. 379-384.

Atkinson, J. H.,and D.M. Potts (1977)," Stability of a Shallow Circular Tunnel in Cohesionless Soil", Geotechnique 27, No. 2, pp. 203-215.

Attewell, P. B. (1977), "Ground Movements Caused by Tunneling in Soil". Proc. Int. Conf. Large Ground Movs. and Structure. Cardiff, U.K. 812-948. Pentech Press, London.

Attewell, P. B., Yeates, j. & Selby, A. R. (1986), Soil Movements Induced by Tunneling and Their Effects on Pipelines and Structures. Chapman and Hall, New York.

Bickel, John o. & Kusel, T. R. (1982), "Tunnel Engineering Handbook". Van Nostrand Reinhold Company Inc., New York.

Bulson, P. S. (1985), "Buried Structures - Static and Dynamic Strength", Chapman and Hall, London New York.

Clough, G. W. & Schmidt, B. (1981), "Design and Performance of Excavation and Tunnels in Soft Clay", Soft Clay Engineering. Chap. 8 569-634. Eds. E. W. Brand & R. P. Brenner. Elsevier, New York.

Darling, Peter (1993), " Jacking under Singapore's Busiest Street", Tunnels and Tunneling, Pactific rim issue, Summer, pp. 19-23.

Duddeck Heinz (1988), "Guidelines for the Design of Tunnels", Tunnelling and Underground Space Technology, Vol. 3, No. 3, pp 237-249.

El-Nahhas, F., El-Kadi, F., Ahmed, A. (1992), "Interaction of Tunnel Linings and Soft Ground", Tunnelling and Underground Space Technology, Vol. 7, No. 1, pp 33-43.

Einstein, H. H., Schwartz, C. W., Steiner, W., Baligh, M. M., Levitt, R. E. (1980), Improved Design For Tunnel Supports, Final Report of University Research, U. S. Department of Transportation.

Engesser, Fr. (1882), " Ueber Den Erdduck gegen innere Stüzwande (Tunnelwande)", Deutsche Bauzeitung, No. 16, pp. 91-93.

Fukuchi, G. (1991), " The Present and Future of Mechanized Tunnel Works in Soft Ground", Tunnelling and Underground Space Technology, Vol. 6, No. 22, pp 175-183.

Halts, Robert D., Kovacs, William D., An Introduction to Geotechnical Engineering, Apprentice-Hall, Jew Jersey, 1981

Hough, B. K. (1957), Basic Soils Engineering. The Ronald Press Co., New York.

Lambe, T. W. and Whitman, R. V. (1969), Soil Mechanics. John Wiley and Sons, New York.

Larson, D. G. (1992), "A Laboratory Investigation of Load Transfer in Reinforced Soil", Ph.D. Thesis of Civil Engineering, M.I.T..

Lunardi, P. (1991), "Cellular Arch Technique For Large Span Station Cavern", Tunnels and Tunneling, November, pp. 23-26.

Madan, M. M. (1991), "An Analytical Approach to Tunnel Construction", Tunnels and Tunneling, May, pp. 71-74.

Meyerhof, G. G. (1970), Some Research on Underground Flexible Arches, Proc. Conf. on Subway Construction, Budapest.

Munn, J. F., Carre, G. L. and Kennedy, T. E. (1970), Failure of Footing-Supported Buried Steel Arches Loaded Statically, US Army Waterways Experiment Station, Misc. paper N-70-2.

Parker, H. W. (1992), "Concept and Construction of the Mount Barker Ridge Tunnel", Tunnels and Tunneling, North American Issue, Autumn, pp. 15-16.

Peck, R. B. (1969), "Deep Excavations and Tunneling in Soft Ground", State of the art report, in 7 Th. In. Conf. On Soil Mechanics and Foundation Engry. Mexico City.

Pender, M. J. (1980), "Elastic Solutions for a Deep Circular Tunnel", Technical Notes, September.

Rogers C. D. F. & Yonan, S. J. S.(1992), "Experimental Study of a Jacked Pipeline in Sand", Tunnels and Tunneling, June, pp. 35-38.

Sebasteiano Pelizza and Daniele Peila (1993), "Soil and Rock Reinforcements in Tunneling", Tunneling and Underground Space Technology, Vol. 8, No. 3, pp. 357-372.

Soliman, E., Duddeck, H., & Ahrens, H. (1993), "Two and Three Dimensional Analysis of

Closely Spaced Double-Tube Tunnels", Tunneling and Underground Space Technology, Vol. 8, No. 1, pp. 13-18.

Stein, Dietrich, Möllers Klemens, and Bielecki Rolf (1989), Microtunnelling - Installation and Renewal of Norman-Size Supply and Sewage Lines by the Trenchless Construction Method, Ernst & Sohn Verlag für Architecktur und technische Wissenschaften, Berlin.

Stone, K. J. L. (1988), "Modeling of Rapture Development in Soils", Ph. D. Dissertation, Wolfson College, Cambriduge University.

Stone, K. J. L. (1992),"Effect of Dilatancy and Particle Size Observed in Model Tests on Sand", Soils and Foundations, Vol. 32, No. 4, pp. 43-47.

Tarkoy, peter (1991), "Appropriate Support Selection", Tunnels and Tunneling, October,pp. 42-45.

Wallis Shani (1992), "Micro Assistance for Macro Undertaking In Atlanta", Tunnels and Tunnelling, January, pp 39-42.

Watson, Kathy (1992), "Micro Goes French", Tunnels and Tunneling, May, pp. 37-40.

APPENDIX A

The Computer Program Used for Empirical Comparison between the Circular and the Triangular Tubes

```
 * Function to Calculate the Surface Settlement by Peck's Error Curve */

 * Shu-Sheng Chen */

#include <stdio.h>
#include <math.h>
#include <stdlib.h>

 * Declare the prototypes of function */
double *settlement(double hc,double tr,double sr,int np,double rl, double rr,double
void re_out(double *a,FILE *f,int np );


void main()
{
int np,type, type1;
double hc,tr,sr,rl,rr,q,k1,k2,dwt, *b;
FILE *f1;
char str[20];

printf("Please Choose the below Type of Tubes \n");
printf("  1. Tringular Tube.  n");
printf("  2. Circular Tube.  n" );
scanf("%d",&type);
if ( type != 1 && type != 2){
  printf(" You Have a Wrong Choose \n");
  exit(-1);
}

printf("Please Choose the soil type  \n");
printf("  1. Cohesive Soil. \n");
printf("  2. Granular soil. \n" );

scanf("%d",&type1);
if ( type1 != 1 && type1 != 2 ){
  printf(" You Have a Wrong Choose \n");
  exit(-1);
}
else if ( type1 == 1){
  k1=0.005;
  k2=0.025;
}
else if ( type1 == 2){
  k1=0.02;
  k2=0.05;
}


printf(" Please Key in the Length of the Cover in Meters \n");
scanf("%lf",&hc);
printf(" hc = %f \n",hc);

printf(" Please Key in the Radius of the Main Tunnel in Meters \n");
scanf("%lf",&tr);
printf(" tr = %f \n",tr);

printf(" Please Key in the Radius of the Pre-Supporting Tube in Meters \n");
scanf("%lf",&sr);
printf(" sr = %f \n",sr);

printf(" Please Key in the Number of Surface Data Pt. in Odd Integer Number \n");
scanf("%d",&np);
printf(" np  = %d \n",np);

printf(" Please Key in the Left Range of Surface Settlement for Calculating in meter
```

```
scanf("%lf",&rl);
printf(" rl = %f \n",rl);

printf(" Please Key in the Right  Range of Surface Settlement for Calculating in met

scanf("%lf",&rr);
printf(" rr = %f \n",rr);

printf(" Please Key in the Friction Angler of Soil in Degree \n");
scanf("%lf",&q);
printf(" q = %f \n",q);

printf("Please Key in How Far the Design Water Table Away from Ground Surface \n");
scanf("%lf",&dwt);
printf(" dwt = %f \n",dwt);
if ( hc >= dwt){
  printf(" This case is not suitable for using presupporting tube \n");
  exit(-1);
}

printf(" Please Enter the Name of the Output file \n");
scanf ("%s", str);
f1 = fopen (str, "w");
 * check the open is successful or not */
if (f1 == NULL){
  printf("error in opening %s",str);
  exit(-1);
}
b=settlement(hc,tr,sr,np,rl,rr,q,type,k1,k2,dwt);
re_out(b,f1,np);

}

/* Function to calculate the settlement */
double *settlement(double hc,double tr,double sr, int np,double rl, double rr,
  double q, int type, double k1, double k2, double dwt)
  {
double dx=0.0, *b, h1=0.0, max_s1=0.0, max_s2=0.0, x1=0.0, x2=0.0, y=0.0, q1=0.0;
double lt; /* The Rightmost Presupporting Tube for Design */
int i=0, j=0;


b = malloc((3*np)*sizeof(double));
if ( b== NULL)
  exit(-1);

dx=(rr-rl)/(np-1);
q1=q*3.1416/180;
for (j=0; j<np; j++){
  *(b+3*j)=0.0;
  *(b+3*j+1)=0.0;
  *(b+3*j+2)=0.0;
}

lt=sqrt(pow((tr+1),2.0)-pow((hc+tr-dwt),2));
x1= -lt;


for (h1=dwt ;x1 <= (-tr/2); h1 -= (2*sr)){

  if (type == 1){
    max_s1 = 0.4/h1*k1*1000;
    max_s2 = 0.4/h1*k2*1000;
  }
  else {
    max_s1 = 0.8/(h1)/(sin(2*q1))*k1*1000;
```

```
    max_s2 = 0.8/(h1)/(sin(2*q1))*k2*1000;
  }


  if ( (tr+1) > (hc+tr-h1)) && (tr != 0.0)
    x1 = (-1.0)*sqrt(pow((tr+1),2.0)-pow((hc+tr-h1),2));

  else
    x1 = 99999.9;/* conside only one main tunnel & no supporting tube */

  for ( x2= r1,j=0; x2 <= (rr+0.01); x2 += dx ,j++){
    *(b+3*j)= x2;
    *(b+3*j+1) += (max_s1)*(exp(-x2*x2/2));
    *(b+3*j+2) += (max_s2)*(exp(-x2*x2/2));
  }
}


for ( ; (x1 > (-tr/2)) && (x1 <= (tr/2 )) ; x1 += (2*sr)){
  y=sqrt(pow((tr+1),2.0)-pow(x1,2));
  h1= hc + tr - y;

 if (type == 1){
    max_s1 = 0.4/h1*k1*1000;
    max_s2 = 0.4/h1*k2*1000;
  }
  else {
    max_s1 = 0.8/(h1)/(sin(2*q1))*k1*1000;
    max_s2 = 0.8/(h1)/(sin(2*q1))*k2*1000;
  }


  for ( x2= r1,i=0; x2 <= (rr+0.01); x2 += dx,i++ ){
    *(b+3*i)= x2;
    *(b+3*i+1) += (max_s1)*(exp(-x2*x2/2));
    *(b+3*i+2) += (max_s2)*(exp(-x2*x2/2));
  }
}

y=sqrt(pow((tr+1),2.0)-pow((tr/2),2));
h1= hc + tr - y;


for ( ; (x1 >= (tr/2 - 0.01)) && (x1 <= (lt+0.01)); h1 += (2*sr)){
  x1=sqrt(pow((tr+1),2.0)-pow((hc +tr -h1),2));

 if (type == 1){
    max_s1 = 0.4/h1*k1*1000;
    max_s2 = 0.4/h1*k2*1000;
  }
  else {
    max_s1 = 0.8/(h1)/(sin(2*q1))*k1*1000;
    max_s2 = 0.8/(h1)/(sin(2*q1))*k2*1000;
  }


  for ( x2= r1,i=0; x2 <= (rr+0.01); x2 += dx,i++ ){

    *(b+3*i)= x2;
    *(b+3*i+1) += (max_s1)*(exp(-x2*x2/2));
    *(b+3*i+2) += (max_s2)*(exp(-x2*x2/2));

  }
}

return(b);
```

```
 * Function to Output Data for Drawing Figures *
void re_out(double *b,FILE *f,int np )
{
int i,test;

    fprintf(f,"a = [ \n");

    for (i=0; i<np;i++)
      {
        test=fprintf(f," %f   %f   %f \n",*(b+3*i),*(b+3*i+1),*(b+3*i+2));
        if (test < 0)
          printf(" error in file write \n");
      }
        fprintf(f," ]; \n");

return;
}
```

```
Script started on Mon May 15 14:25:42 1995
athena% a.out
Please Choose the below Type of Tubes
  1. Tringular Tube.
  2. Circular Tube.
1
Please Choose the soil type
  1. Cohesive Soil.
  2. Granular soil.
2
 Please Key in the Length of the Cover in Meters
5
 hc = 4.000000
 Please Key in the Radius of the Main Tunnel in Meters
8
 tr = 8.000000
 Please Key in the Radius of the Pre-Supporting Tube in Meters
1
 sr = 1.000000
 Please Key in the Number of Surface Data Pt. in Odd Integer Number
23
 np  = 23
 Please Key in the Left Range of Surface Settlement for Calculating in meters
-20
 rl = -20.000000
 Please Key in the Right  Range of Surface Settlement for Calculating in meters
20
 rr = 20.000000
 Please Key in the Friction Angler of Soil in Degree
40
 q = 40.000000
Please Key in How Far the Design Water Table Away from Ground Surface
9
 dwt = 9.000000
 Please Enter the Name of the Output file
a1.m
athena% more a1.m
 [H [Ka = [  [K
 [K -20.000000   0.000000   0.000000  [K
 [K -18.181818   0.000000   0.000000  [K
 [K -16.363636   0.000000   0.000000  [K
 [K -14.545455   0.000000   0.000000  [K
 [K -12.727273   0.000000   0.000000  [K
 [K -10.909091   0.000000   0.000000  [K
 [K -9.090909   0.000000   0.000000  [K
 [K -7.272727   0.000000   0.000000  [K
 [K -5.454545   0.000002   0.000005  [K
 [K -3.636364   0.008470   0.021174  [K
 [K -1.818182   1.206116   3.015289  [K
 [K 0.000000   6.298413   15.746032  [K
 [K 1.818182   1.206116   3.015289  [K
 [K 3.636364   0.008470   0.021174  [K
 [K 5.454545   0.000002   0.000005  [K
 [K 7.272727   0.000000   0.000000  [K
 [K 9.090909   0.000000   0.000000  [K
 [K 10.909091   0.000000   0.000000  [K
 [K 12.727273   0.000000   0.000000  [K
 [K 14.545455   0.000000   0.000000  [K
 [K 16.363636   0.000000   0.000000  [K
 [K 18.181818   0.000000   0.000000  [K
 [H [Km2[illegible]--([illegible]ss [illegible] c[illegible]e. 'q' to quit.] [m [J
 [K ];  [K
 [Jathena% a.out
Please Choose the below Type of Tubes
  1. Tringular Tube.
  2. Circular Tube.
```

```
2
Please Choose the soil type
  1. Cohesive Soil.
  2. Granular soil.
2
 Please Key in the Length of the Cover in Meters
4
 hc = 4.000000
 Please Key in the Radius of the Main Tunnel in Meters
8
 tr = 8.000000
 Please Key in the Radius of the Pre-Supporting Tube in Meters
1
 sr = 1.000000
 Please Key in the Number of Surface Data Pt. in Odd Integer Number
23
 np  = 23
 Please Key in the Left Range of Surface Settlement for Calculating in meters
-20
 rl = -20.000000
 Please Key in the Right  Range of Surface Settlement for Calculating in meters
20
 rr = 20.000000
 Please Key in the Friction Angler of Soil in Degree
40
 q = 40.000000
Please Key in How Far the Design Water Table Away from Ground Surface
9
 dwt = 9.000000
 Please Enter the Name of the Output file
a2.m
athena% more a2.m
 [H [Ka = [  [K
 [K -20.000000   0.000000   0.000000  [K
 [K -18.181818   0.000000   0.000000  [K
 [K -16.363636   0.000000   0.000000  [K
 [K -14.545455   0.000000   0.000000  [K
 [K -12.727273   0.000000   0.000000  [K
 [K -10.909091   0.000000   0.000000  [K
 [K -9.090909   0.000000   0.000000  [K
 [K -7.272727   0.000000   0.000000  [K
 [K -5.454545   0.000004   0.000011  [K
 [K -3.636364   0.017200   0.043001  [K
 [K -1.818182   2.449443   6.123607  [K
 [K 0.000000   12.791144   31.977861  [K
 [K 1.818182   2.449443   6.123607  [K
 [K 3.636364   0.017200   0.043001  [K
 [K 5.454545   0.000004   0.000011  [K
 [K 7.272727   0.000000   0.000000  [K
 [K 9.090909   0.000000   0.000000  [K
 [K 10.909091   0.000000   0.000000  [K
 [K 12.727273   0.000000   0.000000  [K
 [K 14.545455   0.000000   0.000000  [K
 [K 16.363636   0.000000   0.000000  [K
 [K 18.181818   0.000000   0.000000  [K
 [H [Km2QK00H008--(95800000ss 8p000000 c0HtiHue. 'q' to quit.] [m [J
 [K ];  [K
 [Jathena% exit
athena%
script done on Mon May 15 14:28:22 1995
```